STUDY OF ABNORMAL GRAIN GROWTH IN BETA ANNEALED TI-6AL-4V FORGINGS

THESIS

Lee R. Morris, Captain, USAF

AFIT-ENY-MS-18-M-310

DEPARTMENT OF THE AIR FORCE
AIR UNIVERSITY

AIR FORCE INSTITUTE OF TECHNOLOGY

Wright-Patterson Air Force Base, Ohio

AFIT-ENY-MS-18-M-310

STUDY OF ABNORMAL GRAIN GROWTH IN BETA ANNEALED TI-6AL-4V FORGINGS

THESIS

Presented to the Faculty

Department of Aeronautical Engineering

Graduate School of Engineering and Management

Air Force Institute of Technology

Air University

Air Education and Training Command

in Partial Fulfillment of the Requirements for the

Degree of Master of Science in Aeronautical Engineering

Lee R. Morris, B.S.A.E.

Captain, USAF

March 8, 2018

AFIT-ENY-MS-18-M-310

STUDY OF ABNORMAL GRAIN GROWTH IN BETA ANNEALED TI-6AL-4V FORGINGS

Lee R. Morris, B.S.A.E.
Captain, USAF

Committee Membership:

Maj Ryan O'Hara, PhD
Chair

Dr. Anthony Palazotto
Member

Dr. Sheldon Semiatin
Member

Dr. Ryan Morrissey
Member

Abstract

Beta annealed Ti-6Al-4V has been used extensively in current aerospace platforms due to properties such as high strength to weight ratio. Recent inspections during aircraft production have revealed regions of excessive grain sizes, resulting in quarantined parts and excessive time spent on root cause analysis and risk mitigation efforts. Uncertainty surrounding these parts has led to increased costs and may cause future aircraft production delays. Part manufacturers have intermittently reported problems with abnormal grain growth in these alloys for years, but to date no supplier has been able to determine the source of this microstructural phenomenon. Leveraging common Finite Element Method (FEM) software, sidepressing and upsetting forging processes are simulated to predict internal strain and temperature results for use in identifying regions of localizations effecting grain development. Results were used to guide forging tests in an attempt to reproduce abnormal grain growth in the material. Microscopy and image analysis were used to quantify effects of forging parameters on successful development of coarse grains in sidepressing and upsetting forgings. This work seeks to directly support Air Force Research Laboratory (AFRL)'s Materials and Manufacturing Directorate in determining cause of this ongoing issue.

Acknowledgments

First and foremost, the author would like to thank his fiancé, Ali, for her unwaivering support throughout this endeavor. She has endured and encouraged me on this journey from the beginning, and without her this experience would have been a struggle. Additionally, my family's support and encouragement has been instrumental in my success over the years and throughout my educational career. They have always believed in me and pushed me to be the best person I can be.

This research would not have been possible without the help and support of a variety of people. My advisor's Maj. O'Hara, Dr. Semiatin, and Dr. Morrissey have helped me through my first major academic research undertaking. Without their guidance this research would not have come to fruition. Many AFIT personnel have been instrumental in this work. Jamie Smith and his team of lab technicians were always available and ready to help with any task. Furthermore, Brian Crabtree and his team of machinist provided countless manhours of precision and expert machining in support on this work. Many personnel from AFRL/RX were also critical to the success of this work. The personnel of the Materials Integrity Branch and the Metals Division provided open access to their laboratory equipment and supplies. Additionally, the lab technicians Adam Long and Tommy Cissel provided years of metallography experience in the assistance of specimen preparation for this research.

Each and every person was essential to this research. I am grateful to everyones assistance and to have been able to work with so many great people. Thank you!

Lee R. Morris

Table of Contents

Page

Page

List of Figures

List of Tables

List of Acronyms

AFIT Air Force Institute of Technology

AFRL Air Force Research Laboratory

AGG Abnormal Grain Growth

ASTM American Society for Testing and Materials

BCC Body-Centered Cubic

DEFORM Design Environment for Forming

EDM Electrical Discharge Machining

ELI Extra Low Interstitial

FEM Finite Element Method

GUI Graphical User Interface

HCP Hexagonal Close-Packed

HF Hydrofluoric Acid

SEM Scanning Electron Microscope

SFTC Scientific Forming Technologies Corporations

List of Symbols

$\bar{\epsilon}$	Effective Strain
$\bar{l}$	Mean Lineal Intercept at Image Magnification
$\bar{l}_o$	Mean Lineal Intercept at 1x Magnification
d	Grain Diameter(Size)
d_v	Volume-Weighted Grain Size
G	ASTM Grain Size Number
M	Image Magnification
M_b	1x Magnification
V_i	The Volume of Grains Corresponding to the Grain Size d_i
V_T	The Total Volume of Material

STUDY OF ABNORMAL GRAIN GROWTH IN BETA ANNEALED TI-6AL-4V FORGINGS

I. INTRODUCTION

1.1 Background

Advanced aircraft use β annealed Ti-6Al-4V for critical structural components due to its high strength-to-weight ratio. β annealed Ti-6Al-4V is a titanium alloy used regularly in the aerospace industry. Its popularity stems from its balance of strength, ductility, fatigue, and fracture properties [1]. For instance, titanium has a higher specific strength to weight ratio than most metallic materials and high temp creep resistance up to around 450°C. The material also has a high fatigue resistance in corrosive environments and good corrosive resistance in welding applications [2].

The properties of titanium are strongly affected by its thermomechanical history to include temperature/heat treatment and the method, nature, and magnitude of deformation. [2, 3]. β annealed titanium forgings for aircraft components typically receive their material characteristics from four processes, as depicted in Figure 1.1 [1]. Initially the material is homogenized to create a uniform microstructure [1]. Next, a deformation process forms the material into a desired shape [1]. Temperature is then maintained above the β phase temperature so recrystallization will occur [1]. Finally, the material is β annealed to attain desired material properties[1]. Ti-6Al-4V is considered to be one of the most difficult materials to forge due to its narrow processing windows of time and temperature to produce components with controlled microstructure and desired mechanical properties [4].

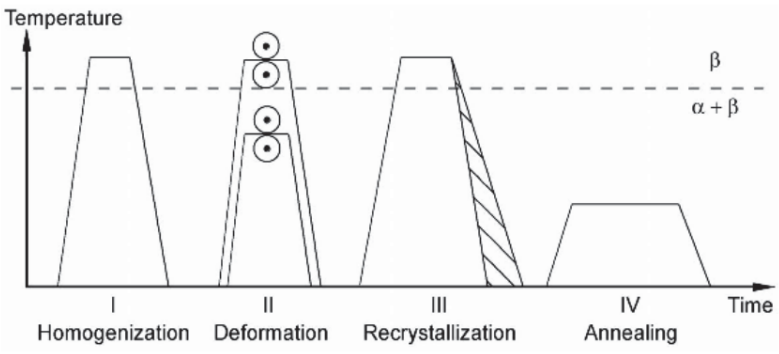

Figure 1.1. Typical processing route for Ti-6Al-4V lamellar microstructure[1]

Titanium is a two phase material where its crystalline structure is sensitive to temperature. As Ti-6Al-4V increases from ambient temperature, it exists in the α phase where the microstructure maintains a specific shape. When the material is raised above the β transus temperature, it transforms to a β phase microstructure with a different crystalline shape and properties [1]. The β transus refers to the temperature where titanium changes from α to β phase. β annealed Ti-6Al-4V is desired in critical aerospace applications due to its strong transformed microstructure [5].

Abnormal Grain Growth (AGG) associated with the microstructural characteristics of Ti-6Al-4V has been noted to develop during the production of β annealed titanium forgings. When the material is annealed above the β transus temperature and then cooled, the microstructure returns to the α phase, but α grains develop in prior β grains. The microstructural characteristic, AGG, refers to the abnormally developed prior β grains. The cause of this microstructural phenomenon is not well understood and little guidance exists to control its development. Furthermore, the true affects of these characteristics on the material are not well defined and cause concern with structurally significant components.

1.2 Problem

Grain sizes are defined by grain boundaries within a material, which are interfaces between different microstructural orientations. It is generally stated that strength of an alloy increases with decreasing grain size [6]. Recent inspections during aerospace aircraft production processes have revealed regions of excessive grain sizes that exceed production specification requirements.

The inspections have waisted countless resources to include: quarantined part replacement, excessive time on analysis, and risk mitigation efforts by multiple organizations. Uncertainty surrounding effected part performance has led to increased costs and aircraft production delays. Titanium parts manufacturers have intermittently reported problems with AGG Ti-6Al-4V for years However, no supplier has yet determined the source or cause.

In the Air Force, most titanium structural components are thin with detailed webs and ribs. To reduce the number of required forgings and resources used, each part is designed to be forged as few times as possible. This way minimal post machining is required before the part goes into service. However, large deformation is necessary to achieve the desired shape in few steps. The problem with large deformation is that it generates deformation heat in the material. The addition of this heat into a forging already close to β transus temperature may result in the material being pre-expoosed to β transus temperature prior to annealing. The effects of this temperature generation on microstructure during forging are not yet well understood.

Maintenance hours, resources, and missions will continue to be affected by AGG without a preventative solution. Until parameters and processes resulting in grain size variation in titanium are well documented, the aerospace industries will continue to be plagued by uncontrolled microstructure.

1.3 Research Questions and Objectives

The overall objective of this research is to identify critical forging process parameters and their tolerances that result in the development of AGG in β annealed Ti-6Al-4V forgings. This objective will encourage updates to titanium forging process standards used in industry to prevent the development of abnormal grain size in future aerospace structural components.

Several questions were defined to guide research of this topic. These questions include:

- What process parameters of fundamental forging operations contribute most to the development of AGG in β annealed Ti-6Al-4V?
- Which forging operation is most likely to develop AGG?
- For each forging operation, what are the parameters that lead to AGG?

1.4 Justification

Identifying the cause of AGG is a financial motivator for the military to reduce maintenance hours and cost caused by inspection and replacement of structural components. This research is required to gain an understanding of the forging parameters leading to AGG in β annealed Ti-6Al-4V forgings. These results will be used to spear head future testing to further understand the impact on affected titanium component material properties.

1.5 Scope

The titanium alloy industry is largely dependent on the aerospace industry due to its demand for high strength and low weight materials [1]. This research may

have far reaching impacts to other industries as titanium alloy production becomes increasingly economical. Determining the parameters leading to AGG in Ti-6Al-4V is important in establishing and revising titanium forging and manufacturing standards.

This research seeks to analyze forging parameters to identify tolerances that result in AGG. The scope of this research includes computational forging simulations and experimental forging tests used to replicate AGG.

Together, computational and experimental tests will be used to investigate forging parameters affecting fundamental idealized processes used in most material deformations. The processes investigated include upsetting and sidepressing forgings. An upsetting forging is the axial compression, while sidepressing is a lateral compression of a cylinder of material. These operations are significant as they represent common generalized plane strain and axial stress processes used in many forging plans.

1.6 Assumptions

Based on the four step forging process for creating β annealed Ti-6Al-4V, AGG is assumed to occur after the homogenization process. This assumption is required to limit the scope of this research. Currently, Air Force Research Laboratory (AFRL) does not have reason to believe that material work prior to forging is responsible for the development of AGG. AFRL investigations into material supply, forging production, and heat treatment have not revealed deviations from industry standards. For this reason, material identified with AGG is assumed to originally meet material standards prior to forging. These assumptions will allow for narrowed and specific research.

1.7 Approach

This research is divided into two major parts, computer Finite Element Method (FEM) simulations and physical forging tests. The goal of using FEM simulations is to create FEM models that represent the basic forging processes of upsetting and sidepressing operations. These simulations allow for more extensive parameter analysis than through experimental forging tests alone. Forging tests with metallurgical evaluation of the specimens will also be conducted to compare against the simulation's predictions. Additionally, the tests will be used to show correlations of forging process inputs to the formation of AGG.

Simulations representative of forging processes were created to allow a wide range of parameters to be altered and tested. Parameters that appear to influence effective strain, strain rate, and temperature within the material as it is forged may indicate regions prone to developing large grain size. Forging parameters suspected of affecting these state variables include ram speed (speed of the forging press), initial material temperature, and reduction in height of the material. A test matrix was created to outline possible tests based on these parameters and was restricted within the forging capabilities available. The insights gained from simulations were used to guide the decisions for experimental testing.

Each test was simulated via Design Environment for Forming (DEFORM), a FEM software designed to simulate forging process. Post processing allowed state variables to be evaluated at each step of the forging. Simulations that predicted regions of high strain or increased temperature relative to the surrounding material were flagged for closer analysis. Forging experimental test conditions were produced from the simulations that appeared most likely to predict large grain size.

Forging tests were conducted based on the tests specified from simulations and included separate tests for each operation. Following each test, the material was

sectioned, cut, and etched so the internal material, grain size, and microstructure could be evaluated. Etching a material involves applying an acid to the surface of interest to remove particles between grains to enhance the visual appearance of grain boundaries. Grain size was measured over the material for comparison to determine if AGG developed. The results of each test were compiled and used to determine the parameters with the most effect on AGG.

1.8 Materials/Equipment/Support

Both the Air Force Institute of Technology (AFIT) and the AFRL provided resources and personnel used to conduct this research. The AFRL provided the expertise of Dr. Sheldon Semiatin, AFRL material technical advisor, and Joe Brown, the forging press lab technician. Additionally, AFRL provided their hydraulic forging press, heating furnace, Ti-6Al-4V bar stock, and other required equipment for forging operations. AFIT provided their Scanning Electron Microscope (SEM), DEFORM FEM software, computers for simulation, and equipment required to section and etch titanium. DEFORM training was also coordinated by AFIT through Scientific Forming Technologies Corporation in Columbus, Ohio.

II. BACKGROUND

2.1 Chapter Overview

The goal of this chapter is to explore relevant topics relating to grain size in β annealed Ti-6Al-4V forgings. The first topic for discussion is titanium. It forms the core of this thesis and without it many of the aircraft used today would not exist. The next topic covers material forgings and their significance to titanium and the aerospace industry. This subsection also evaluates the idealized forging operations used to represent forgings in industry. Finally, Finite Element Method (FEM) and forging simulations are discussed in the last subsection. FEM is used extensively in this thesis and deserves evaluation as its relates to titanium, forging, and grain size. These topics will provide a foundation for the research discussed hereafter.

2.2 Titanium

Titanium is the fourth most abundant structural metal on earth, following aluminum, iron, and magnesium [1], [7]. It also has the highest strength to density ratio of all known metals, but is only used in limited applications due to high price. In fact, titanium is named after the Titans of Greek mythology[7]. The Titans were hated by their father and held in captivity in the earth's crust [7]. Such is Titanium, as the element does not naturally exist in pure form [7]. The high price is partially from extraction from $TiCl_4$ by use of a magnesium reducing agent via the Kroll's process [7]. One of the primary markets driving titanium alloy production is the aerospace industry [8]. Such demand comes from requirements for aircraft to be both light weight and strong to endure flight.

The most widely used titanium alloy in the U.S. and in the aerospace industry is Ti-6Al-4V [1]. This alloy contains six percent Aluminum and four percent Vanadium

by weight and is the reason for the Ti-6Al-4V designation. This titanium alloy first debuted in the U.S. in 1954 and has only grown in popularity [1], [8]. Between the years 1990 to 1994 it accounted for almost 56% of the U.S. titanium market [1]. Despite the development of other titanium alloys, Ti-6Al-4V is still the alloy of choice for much of the aerospace industry. This is primarily because of its excellent balance of mechanical properties, but also because it is the most intensively developed and tested titanium alloy [7].

2.2.1 Basic Properties

Titanium is desirable for use on aircraft because it has excellent strength-to-weight ratio, corrosion resistance, creep resistance, fatigue strength, and weldability [2]. Additionally its specific strength is higher than most metallic materials up to between 400-500°C [8]. A generalized value of titaniums density is $4.5\,\frac{\mathrm{g}}{\mathrm{cm}^3}$ which is notably lower than both iron and nickel based metals around $7.9\,\frac{\mathrm{g}}{\mathrm{cm}^3}$ and $8.9\,\frac{\mathrm{g}}{\mathrm{cm}^3}$ respectively, but slightly higher than aluminum at $2.7\,\frac{\mathrm{g}}{\mathrm{cm}^3}$ [1]. Titaniums yield stress level is around 1000 MPa and is comparable to iron and nickel metals, but aluminums yield stress is much less at about 500 MPa [1].

Similarly, titanium has excellent corrosion resistance due to its high reactivity to oxygen. When it is exposed to oxygen it immediately reacts and forms a stable oxide surface layer, which can resist corrosion in extreme environments [1]. Unfortunately, this is also a major reason for increased materials cost[1]. During production and melting it must be immersed in a vacuum and inert gas to prevent excessive exposure to oxygen to maintain its desired material properties. When in powder form, the material reactive in oxygen rich environments and can spontaneously combust.

2.2.2 Microstructure

Allotropy is a key concept in the research of titanium, forgings, and grain size. It is the property of some elements to take two or more different microstructural forms [7]. The different forms are caused by temperature which force chemical bonds between metallic atoms to change/re-arrange. The formation of atoms in a metal is called a crystalline lattice structure and is used to define microstructures [9].

Pure metals are crystalline solids whose atoms are packed together closely in a repeating pattern [9]. A single representative grouping of these patterns can be defined as a unit and used to define the atomic structure of the metal [9]. The center of each atom within a unit is called a lattice point [9]. A crystalline lattice structure is therefore a unit of lattice points used to define the microstructure of a crystalline solid [9]. Allotropic metals have two or more types of crystalline lattice structures that can be formed at different temperatures and are called phases. Titanium's two phases are shown in Figure 2.1.

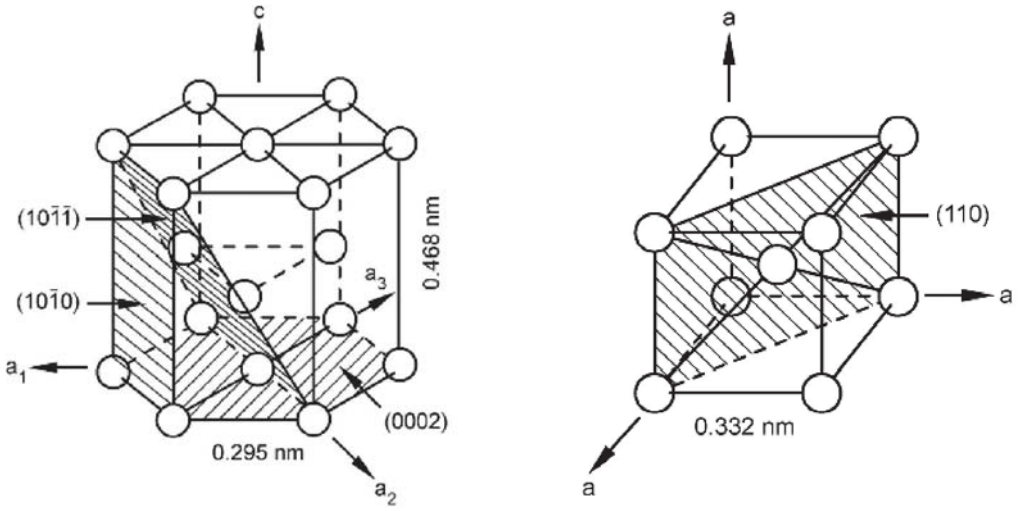

(a) Hexagonal Close-Packed (HCP)[1] **(b) Body-Centered Cubic (BCC)** [1]

Figure 2.1. The two crystalline lattice structures of Titanium representing the α and β phases. A) HCP crystal unit cell of α structure. B) BCC crystal unit cell of β phase structure

Pure titanium has two allotropic phases that transform at approximately 882°C (1619.6°F) [1, 8, 10]. The first phase is called the α phase and exists when titanium is below 882°C [1]. The α phase is a HCP crystal material structure with three slip systems [1]. The α phase is difficult to deform because of its low crystal symmetry and limited number of deformation modes from crystallographic slip or twinning [5]. According to von-Mises criterion, at least five independent slip systems are required for homogeneous plastic deformations of metals. The limited ductility from HCP is the result of additional deformation on secondary slip systems as well as possible mechanical twinning. An example of this structure is shown in Figure 2.1a with the three slip systems shaded in grey.

The second phase is called the β phase and is a BCC microstructure [1]. An example of this phase structure is shown in Figure 2.1b and exists predominately when titanium is above 882°C[1]. The phase transformation temperature is also called β transus because microstructure transitions to β phase. Additionally, this phase deforms easier due to more (12) slip systems.

The exact β transus temperature depends on the purity of titanium and is therefore a function of interstitial and substitutional elements in the metal [1]. Interstitial elements are impurities such as hydrogen, oxygen, nitrogen, and carbon that are small enough to fit between normal crystalline lattice structures [1]. In contrast, substitutional elements replace atom locations within a crystalline structure when they are similar in size. Both interstitial and substitutional elements can be used to develop varying types of metal alloys.

2.2.3 Alloys

Metal alloys are composed of a primary metallic element to which other elements are added. When developing parts for a product the metal components are rarely in

pure form. Other elements are added to create a material with specific mechanical properties. Metals containing additional elements are referred to as alloys because they do not represent a pure form of the metal. Each metal has unique alloying properties and can accept specific elements.

Titanium alloying elements are classified into α and β stabilizing categories [8]. The element is considered α stabilizing if it increases the β transus temperature above 882°C and β stabilizing if it decreases the temperature [1]. Schematic diagrams showing the effects of α stabilizing elements and β stabilizing elements is shown in Figure 2.2. The primary alloy evaluated in this research is Ti-6Al-4V and will be the focus of this subsection.

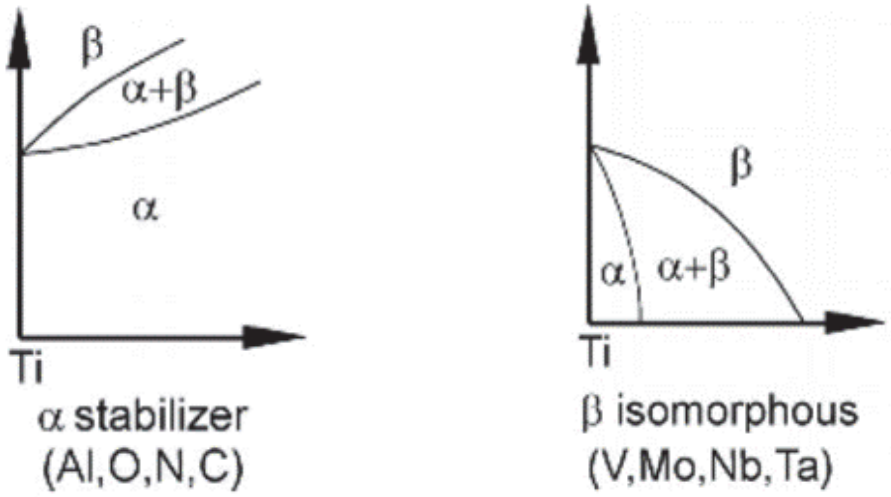

(a) Effect of α stabilizers[1] **(b) Effect of β stabilizers** [1]

Figure 2.2. Schematic diagrams depicting the effect of α and β stabilizing elements on β transus temperature. X-axis shows increasing quantities of α or β stabilizing elements. The Y-axis represents the phase of the alloy with increasing temperature.

Common α stabilizing elements include Aluminum, Oxygen, Nitrogen, and Carbon [1]. Aluminum is the most popular substitutional α stabilizing element in titanium because it is the only one that raises the β transus temperature and has large solubility in both phases [1]. The transition temperature increases from 882°C to about 1000°C and forms an α+β two phase region when six percent Aluminum is

added [1]. However, it is usually restricted to six percent to prevent Ti_3Al precipitates from forming in the α phase [1].

β stabilizing elements are divided into two categories, isomorphous elements and eutectoid forming elements [1]. β isomorphous elements contain the same microstructural crystalline form while β eutectoid elements have a minimum phase transformation temperature between liquid and solid states. The most common β isomorphous elements include Vanadium, Molybdenum, and Niobium [1]. In many alloys, the β phase can be partially stabilized at lower temps, and the equilibrium volume fractions of α and β can vary with temperature when using proper quantities of these elements [1, 5]. Common β eutectoid elements include Chromium, Iron, and Silicon [1]. Vanadium is the β stabilizing element used in Ti-6Al-4V. Fifteen percent is the maximum soluble quantity of Vanadium and lowers the $\alpha + \beta$ two phase from 882°C to about 700°C [1]. However, the maximum solid soluble quantity of Vanadium in the α phase is three percent at 680°C [1].

The Ti-6Al-4V alloy is classified as an $\alpha + \beta$ alloy due to the two-phase region created by the alloying elements [1]. The β transus temperature of this alloy exists at about 993°C and about 975°C for the Extra Low Interstitial (ELI) form [1]. In general, this alloy has a great balance of strength, ductility, fatigue, and fracture properties, but only maintains them up to about 300°C [1]. Also notable is that the microstructure and mechanical properties are sensitive to the material's thermomechanical processing history [3]. The effects of thermomechanical processing are discusses later in Section 2.3.6.

2.3 Forging

Many types of metal shaping processes exist for producing structural aircraft components. Forging is the primary process used for shaping moderate to large size

titanium components. The ability to control microstructure and mechanical properties while still producing large, reproducible components makes it favorable over other processes [7]. Specifically, forging is a non-isothermal bulk metal working process where high temperature material is placed between two metal dies that apply pressure to plasticly deform it to a new shape [11]. Non-isothermal forging refers to temperature fluctuations within the material during the deformation process instead of maintaining steady-state material temperature. This is important because changes in temperature have significant effects on material deformation. Regardless, titanium forgings require large forging presses due to its high strength and flow stresses [1]. Drop/steam hammers, mechanical screw, and hydraulic presses are preferred methods to apply the required forces [1]. Fast mechanical and hammer presses are less appropriate due to their high deformation rates and increased risk of cracking and overheating the workpiece [7]. Hydraulic press forgings are typically preferred when the titanium requires tight control of the forging parameters [1].

Aircraft structure and component forgings are produced over multiple steps. The number of steps is dependent on the size and complexity of the forging and workability of material. Each step is documented and collected in a forging production plan [1]. The first step is plotting/roughing, where a preform is pressed into a workpiece with the desired shape for the first rough forging/blocker step [1]. Plotting is an upsetting operation where a small cylindrical billet of material(preform) is axially pressed to create a larger diameter workpiece [1]. A blocker type forging die may be used in the next step to form irregular shapes by creating non-uniform cross-sections of the material to create an impression closer to the desired final shape [1]. All steps include a specific workpiece temperature to reduce material flow stress and produce desired material properties. Important design considerations for forgings include: temperature, degree of deformation, rate of deformation, friction conditions, tooling

temperature, transfer times, microstructure, and deformation history of the starting material [7].

2.3.1 Titanium in Forgings

Although forging is popular for manufacturing titanium components, the crystal structure of the α phase and dependence of flow stress on temperature make it challenging to form [11]. Ti-6Al-4V is usually forged in the $\alpha + \beta$ phase but in some instances, forging in the β phase may be desired for damage tolerant parts [1].

Hot forming titanium is recommended between about 860-980° C in order to produce crack-free forgings [8, 7]. At this temperature a large volume fraction of BCC β structure and the basal plane of HCP disappears to further ease deformation [7]. As β phase increases and α decreases, an increasing number of slip systems exist to decrease the required load for plastic deformation. In this forging regime hydraulic presses are typically preferred in order to achieve moderate and controlled deformation gradients [8].

It is more difficult to achieve and regulate the internal quality of titanium than it is to form into a shape. Additionally, microstructure is more important as it controls the final mechanical properties of the part. Ti-6Al-4V hot deformations are difficult to forge due to narrow processing windows of time and temperature for producing components with controlled microstructure and improved mechanical properties [4]. Other challenges to forging include titanium's high reactivity to oxygen, low thermal conductivity, and high heat capacity [2]. When exposed to high temperatures, titanium develops a brittle oxide layer that must be removed from the material. It is called an α case and does not have the same properties as the rest of the material. Low thermal conductivity means low heat transfer between titanium and other materials it contacts. The material also has high heat capacity. Together with high

heat capactiy, these can result locally generated heat that does not dissipate quickly during forging. In particular, these factors can lead to the localization of heat during deformation and significant dependence of plastic flow resistance on strain rate [2]. Furthermore, due to the allotropic nature of titanium, the determination of temperature distributions in deformation zones during forging is important because of their effect on material properties and structures. By controlling the thermomechanical state of the material during deformation it is possible to control the properties of the product [2].

2.3.2 Forging Operations

Forgings are split into two categories, open and closed die [12]. In open die forgings the material is not constrained laterally by the forging die [1, 12]. Instead, the lateral flow of material is controlled by the total reduction in workpiece height, frictional boundary conditions, and heat transfer between workpiece and die [12]. Two idealized and common open die forging examples evaluated in this thesis include upsetting and sidepressing [8]. Figure 2.3 depicts an idealized sidepressing and upsetting forging layout.

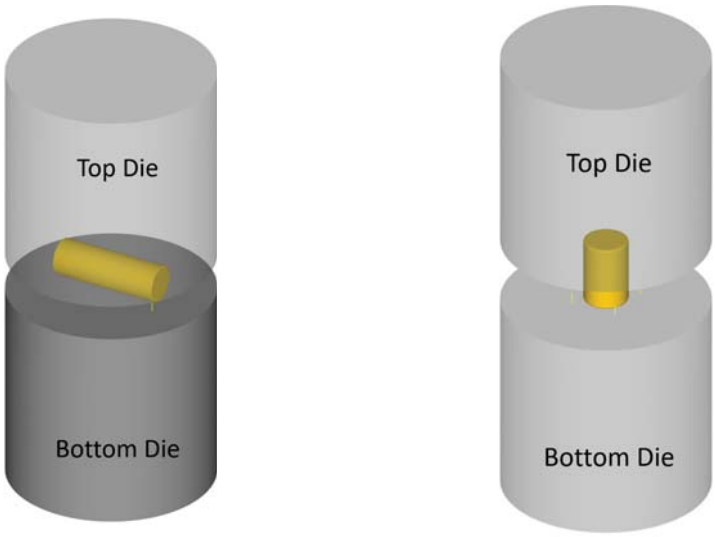

(a) Sidepressing Forging **(b) Upsetting Forging**

Figure 2.3. Two diagrams depicting the layout of idealized sidepressing and upsetting forgings.

Upsetting is the axial compression of a cylinder between two flat die while sidepressing is the compression of a round bar or cylinder along the lateral surface. Alternatively, closed die forgings constrain material laterally by die shape [1, 12]. Closed die impart a defined shape onto the workpiece [12]. Lateral metal flow is controlled similarly to an open die forging but with material constrained by die shape. Closed die forgings are generally more difficult to model and predict, but once created they are easier to control material flow and microstructure [1].

2.3.3 Forging Workability

A material's properties directly affect material flow during deformation. Each alloy is different and must be evaluated with regard to a specific forging process to prevent excessive strain or deformation. This evaluation characterizes the workability of a material. Figure 2.4 depicts a chart comparing different material workability, flow strength and die filling capacity. Ti-6Al-4V has moderate flow strength with good forgeability when compared to other materials[12].

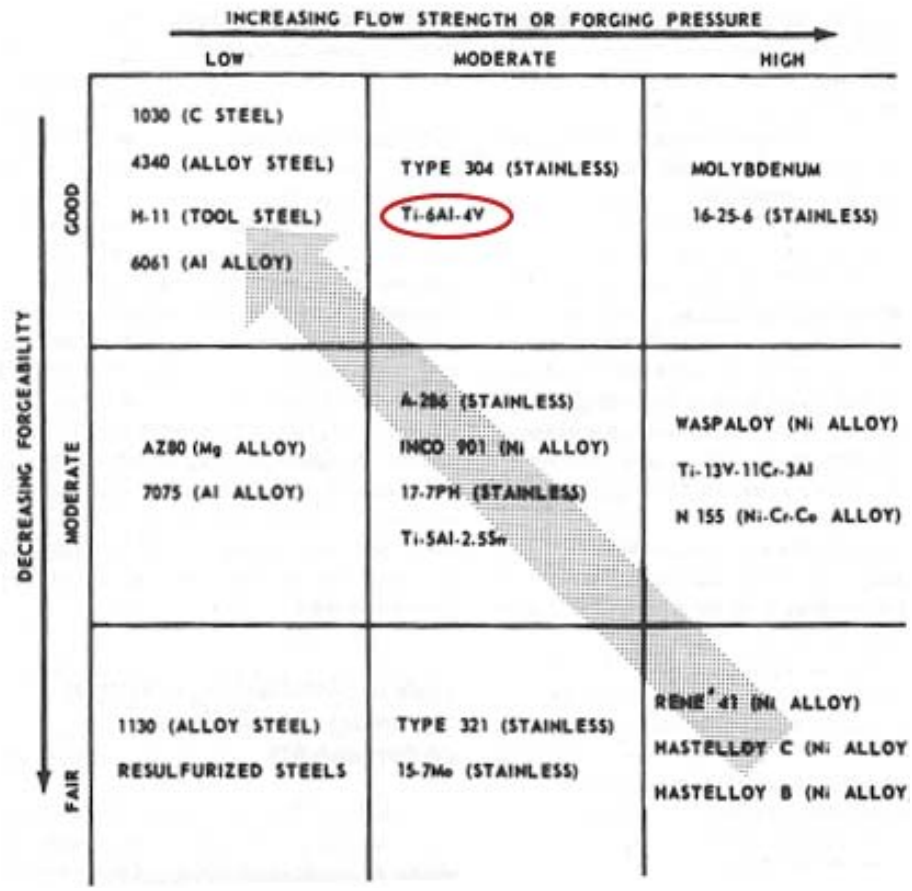

Figure 2.4. A comparison of the interactions of workability, flow strength, and die filling capacity of different materials in forgings [12]. The shaded arrow indicates increasing ease of die filling. Ti-6Al-4V is identified in red.

The term workability refers to the determination of flow stresses and total working loads in a metal forming process [12]. Flow stress is considered a function of strain, strain rate, temperature, and microstructure [13]. Temperature can cause either strain softening or hardening in flow behavior, and different cooling rates can effect microstructure and flow stress [13]. Workability characteristics determine equipment utilization and dictate thermomechanical processes that control the microstructure of the material for its specific application [12]. Workability is directly related to a materials forgeability.

Forgeability is determined primarily by a material's structure, properties, and

process conditions [12]. Material structure variables include grain/phase structure, texture, and crystal structure [12]. Material properties include temperatures, flow stresses, and physical properties [12]. Material temperature effects include melting point, recrystallization, and phase changes [12]. Flow stresses are determined by variations in strain, strain rate, and temperature [12]. Physical properties are measurements such as density, specific heat, and thermal conductivity. The flow behavior and mechanical properties of Ti-6Al-4V can be significantly affected by initial microstructure, deformation temperature, and deformation rates [4].

One of the most important process variable for forgeability and workability is forming temperature [12]. The Ti-6Al-4V's high diffusion coefficient at high temperatures in the BCC β phase leads to better ductility and ease of deformation than in other phases [4]. In the β phase there is a higher volume fraction of BCC structure, which lowers flow stress because more slip systems are available than HCP structures in the α phase [4]. Therefore, forging in the α/β phase makes processing more difficult, yet produces better combination of strength and toughness [4].

Strain also plays a large role in flow stress. An increase in flow stress at high strain rates can be attributed to the high volume fraction of dislocations impeding movement resulting in a resistance to plastic deformation [4]. Low strain rates maintained at a high temperature, however, cause less significant variation of flow stress making it a better forming process [14].

2.3.4 Forging Defects

Many forging defects can occur if forgeability and workability parameters are not adequately controlled. Forgings can be classified by temperature such as cold and hot/warm forming or by isothermal and non-isothermal. Each regime has its own set of defects, but typically non-isothermal forgings have greater variations in

quality [13]. Temperature changes in non-isothermal forgings, and therefore, produces variability in microstructure. Processing windows and material chilling have large effects on variability because of heat transfer from the material. This research focuses on hot forgings, which have two classes of workability defects, fracture and flow-localization [12]. Shear banding, which results from heat transfer effects, is a form of flow-localization.

Workability problems from flow-localization controlled failures are common and associated with material chilled zones and shear bands [12, 15]. In most metals, flow stress is dependent on temperature during deformation [15]. Chilled zones can form from large heat transfer between a hot workpiece and much cooler die and environment [12, 8]. This heat transfer effect is often referred to as die chill. The result is a chilled workpiece leading to increased flow stress during deformation. The amount or extent of chilling is a function of the interface heat transfer coefficient, deformation rate, and initial temperature [15]. Additionally, chilling combined with friction can influence metal flow patterns, forming loads, and the development of metal flow defects [15]. Shear bands, which are regions of intense localized high deformation, are one such defect, and can form between chilled zones [12, 16].

Additional defects can arise when the core material temperature increases despite die chill. During forging this phenomena results from deformation energy release effects [8]. The material naturally resists deformation, which gives rise to flow stress. Titanium is forged close to β transus and may exceed this temperature depending on the deformation rate and flow stress. Flow softening behavior has been observed at fast strain rates in titanium forgings and may indicate the generation of deformation heat [14]. The results of local β temperature and flow softening during forging is not clear, but would likely result in mixed microstructure and may degrade the desired properties of the material.

Defects can be adequately prevented by selection and control of working temperature, strain rate, reduction in workpiece, and stress state [11]. These regions can be observed in a material after forging and during optical examination when the surface is polished and etched.

2.3.5 Workability Tests

Workability tests are developed to investigate the cause of forging defects. They can be used to evaluate the interactions of material properties and process variables that result in flow localization [12]. Two common forging tests include non-isothermal upsetting and sidepressing tests [12]. Each leverages fundamental forging operations to study heat transfer effects on flow localization [12].

The easiest test is the nonisothermal upsetting test where a cylindrical workpiece rests axially and is compressed between flat parallel die. A standard layout of this test is shown in Figure 2.3b. The workpiece geometry, die temperatures, die speed, lubrication, and workpiece dwell time are test variables [12]. Heat transfer is critical for evaluation and is a function of the densities and thermal properties of the workpiece and die, initial temperatures, deformation rate, and heat transfer coefficients [12]. If flow localization exists it will form axisymmetric chill zones, which can have detrimental effects on material flow. [12]. More defects are likely to occur if the workpiece cools too much.

In non-isothermal sidepressing tests a cylindrical workpiece resting on side is pressed between flat parallel die [12]. A diagram of this forging test layout is shown in Figure 2.3a. This test is similar to upsetting except flow localization occurs through shear banding [12]. An absence of chill zones in this test is the result of less initial contact area for heat transfer. Additionally, this test is a plane strain operation where shearing can occur [12]. An example of shear banding is shown in Figure 2.5

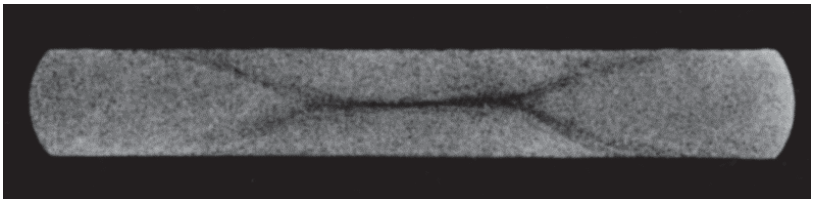

Figure 2.5. An example of shear bands in a sidepressing forging[11].

Temperature has a significant effect on the appearance of shear bands. When the workpiece is below β transus, shear bands appear with increasing reduction of workpiece height [12]. However, when temperatures exceed β transus, flow stress is small and shear bands are less likely to occur [12] [13]. Long deformation times may influence workpiece temperature and increase flow stress resulting in shear bands [12].

In both tests several specimens are required to be pressed at a variety of workpiece temperatures, die temperatures, and die speeds [12]. The tests are used to determine flow stresses as a function of strain, strain rate, and temperature [16] [11]. Additionally, they can be used to evaluate contact time as a parameter in forging process control [13]. As workpiece is in contact with die, the material cools and increases flow stress. The amount of chilling in the workpiece is a function of the interface heat-transfer coefficient, the deformation rate, and the initial temperature [15] [13]. The variation of these parameters may result in simultaneously occurring phase transformations from β to $\alpha+\beta$ regions and vice versa in the workpiece due to large variations of temperature changes and cooling rates [13]. As a result, the distribution of phases throughout the workpiece is non-uniform and differs throughout the specimen.

In one study by Shean Lee et al., workability of Ti-6Al-4V forgings were evaluated by deformation profiles. The study evaluated flow stress as a function of two parameters, temperature sensitivity and deformation index [13]. Temperature sensitivity indicates flow stress depends on temperature [13]. A large sensitivity means a larger stress variation during temperature change, which is an intrinsic property of the material [13]. Deformation index indicates the effect of process parameters and

workpiece geometry on deformation [13]. This mechanism is related to the forging conditions of which temperature through the forging processes is important, such as transfer, contact, and dwell time [13]. If deformation index is large, then a significant non-uniform deformation pattern will occur [13]. This study showed that large temperature sensitivity will result in severe local non-uniform deformation, and a large deformation index will produce severe global non-uniform deformation [13].

2.3.6 Thermal Processing

After forging, titanium is typically thermally processed by annealing and/or aging to attain desired final mechanical properties. These processes change the microstructure and precipitation states of the β component by raising the temperature for a specified period of time [8]. The temperature achieved and rate the material is cooled also effects the microstructure and material properties.

β annealing is often used in α/β titanium to develop transformed β microstructure for fracture critical aerospace applications [5]. It is typically performed 50-75° C above β transus temperature with heating time kept to a minimum to prevent excessive grain growth [8]. Rapid and slow periods of grain growth have been observed during heating and vary noticeably between different lots of identical alloys [5]. After heat treatment, grain size should be on the order of 500-600μm [1][8].

Heat treatment of titanium typically occurs in an inert gas to prevent the absorbtion of oxygen into the surface of the material [17]. If it is not treated in a controlled atmosphere, oxygen and nitrogen will be absorbed at the surface, stabilize the α grains, and form a hard brittle layer called an alpha case [17]. An example of α case occuring in Ti-6Al-4V is shown in Figure 2.6[17]. This case must be removed prior to the part entering service [17].

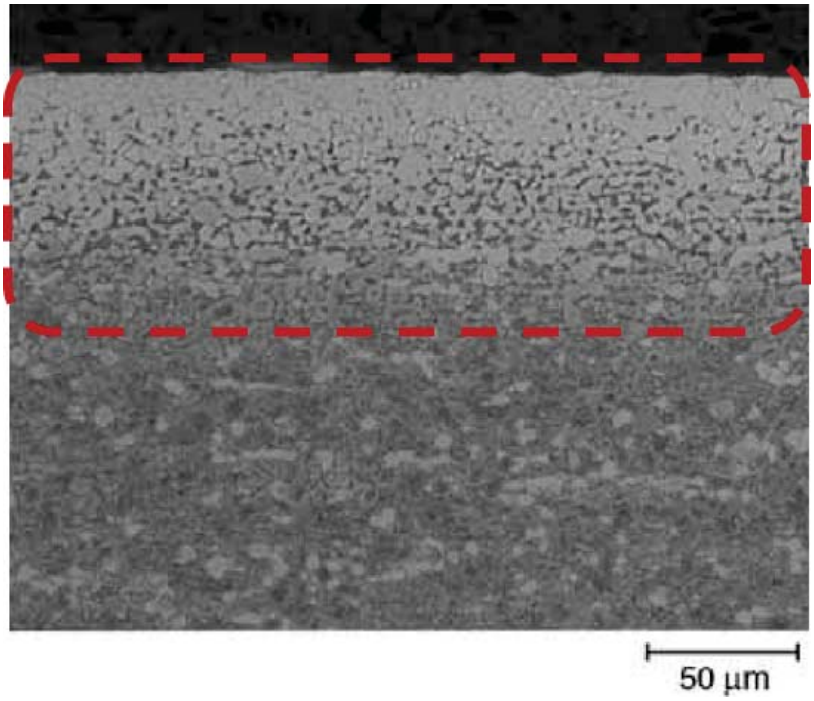

Figure 2.6. Representative α case on Ti-6Al-4V after exposure to 885 °C for 90 minutes[17]. The α case region is enclosed by the red dashed rectangle.

2.3.7 Annealing and Grain Growth

During forging and thermal processing, titanium microstructure, to include grain size and shape, changes as a result of thermomechanical mechanisms. Annealing is the thermomechanical process of interest used in conjunction with forging to attain the desired mechanical properties for aerospace application. Annealing is composed of three microstructural changes to include recovery, recrystallization, and grain growth and is used to release deformation energy stored in the material[18].

Recrystallization is defined as the formation and migration of high angle grain boundaries driven by the stored energy from deformation[18]. In contrast, recovery is defined as the release of stored energy from processes that do not require the movement of high angle grain boundaries, and typically involoves the rearrangement of dislocations to lower energy levels[18]. Both microstructural changes occur at high temperatures and result in the creation of strain free grains[2, 19].

Dynamic recrystallization can sometimes occur during forging when the material is hot enough. Recrystallization can be described in terms of nucleation frequency and growth rate and is a function of strain, strain rate, temperature, and initial grain size [2, 19].

The final mechanism is grain growth or coarsening which occurs from the migration of grain boundaries present prior to annealing [19]. It can occur in deformed material, but specifically refers to the increase in grain size that results from annealing after recrystallization [19]. Normal grain growth results from the disappearance of the smallest grains causing the microstructure to uniformly coarsen [10, 18]. Knowledge of the microstructure at one point in time and the time dependent evolution of mean grain size allows for a complete description of the evolving microstructure. Abnormal Grain Growth (AGG) can also occur and is considered secondary recrystallization [10]. It is characterized by the growth of a small number of grains at a rate greater than that of the mean grain size[20, 18]. Grain size distribution depends on time and larger abnormal grains consuming smaller ones [10]. The comparison of large grains to the average grain size of a specimen will be used in this research to determine the development of AGG from conducted forging trials.

Burke and Turnball suggested a list of seven subjective laws of recrystallization for metals that also include grain growth [19].

1. A minimum deformation exists to cause recrystallization
2. The smaller the degree of deformation, the higher is the temperature required to cause recrystallization.
3. Increasing annealing time decreases temperature necessary for recrystallization
4. Final grain size depends on deformation and annealing temperature. Small grains are caused by greater deformation and lower annealing temperature.

5. Larger original grain size requires greater cold deformation to give equivalent recrystallization temperature and time.

6. The amount of cold work required to give equivalent deformation hardening increases with increasing working temperature.

7. Continued heating after recrystallization causes grain size to increase

The laws of recrystallization can be used as a guide to predicting grain growth in simulations. They include relationships that can be used to help understand the development of grains when evaluating grain growth. After material is forged in this research, it will be β annealed based on industry processes. The process will remain standard for each specimen to limit variation in grain growth caused by annealing temperature and duration.

2.4 Titanium Characterization and Metallography

Many methods exist for evaluating metals and their internal structures and properties. Light microscopy is primarily used for characterizing grain size of titanium specimen. Microscopy is the process of using microscopes to study objects and metal that are not otherwise visible to the human eye.

To view metals with a microscope the surface of interest must be prepared properly. In most instances, a material will need to be sectioned/cut to expose an internal surface desired for inspection. From this point, a distortion free surface is required for characterization of the metal [1]. The metal must be polished to achieve the desired finish. For titanium, this can be accomplished mechanically or electrolytically [1].

Surface preparation for this thesis was accomplished using mechanical polishing, which includes two major stages. The first stage is preliminary polishing and uses either coarse diamond paste with kerosene, coarse alumina in a water slurry, or silicon

carbide paper [1]. The second stage is final polishing, which uses either fine diamond paste or fine alumina in a slurry of water and dilute Hydrofluoric Acid (HF) [1]. When titanium is polished it can smear and the HF acid removes the smeared metal from the surface [1]. Smeared metal obscures the microstructure of metal and can create misleading appearances [1].

After the metal has been polished, it can be viewed with a microscope. An optional step is to use an etchant on the polished surface to more easily see grain size and grain boundaries. An etchant is typically an acid that is applied to the polished surface of the metal to highlight or increase contrast between specific microstructural characteristics. Etchants work by corroding away specific features of the material.

In titanium, Kroll's etch or an oxalic acid strain etch are often used [1]. The composition of Kroll's etchant is 95% H_2O, 3% HNO_3, 2% HF or 95% H_2O, 4% HNO_3, and 1% HF [1]. Kroll's etchant is used with a swab on the metal surface until it becomes less reflective [1]. The composition of oxalic acid stain etchant is equal parts of aqueous 10% oxalic acid and 1% aqueous HF solution [1]. The oxalic acid etch is used by immersing the specimen in the etchant until it appears cloudy [1]. In actuality, there are many variations of titanium etchants and all use small percentages of HF acid, often below five percent of the solution. HF acid is a very dangerous acid and is the acting solute in the solution. In all cases of etchants, when the specimen is finished, it is rinsed with water and dried with a jet of nitrogen to avoid scratching the surface.

The specimen is now prepared for optical analysis or microscopy. Aside from evaluating the resulting microstructure, it is also significant to accurately determine the average grain size of the material to compare against the size of any abnormal grains. The standard for determining average grain size comes from American Society for Testing and Materials (ASTM) and is ASTM E-112-13 "Standard Test Methods

for Determining Average Grain Size" [21]. Three methods to determine grain size are described in the standard and include comparison, planimetric, and intercept methods[22]. When used with computational assistance, the intercept method reduces error and increases measurement efficiencies compared to the other methods [22]. It involves overlaying lines on an optical image of microstructure and measuring the distance between intercepts created by grain boundaries. An average is calculated from the intercept lengths and used to determine a predefined ASTM grain size number referenced from the standard [22]. The methodology for using this procedure is further defined in Section 3.8.2.

2.4.1 Grains and Morphology

Similar to other metals, titanium is a polycrystalline material composed of grains differing in size and orientation. They are the formation of many crystal lattices into a single crystalline structure and their interfaces are called grain boundaries. Since titanium is an allotropic material, it can have two phases of grains, α and β. The shape and size of each phase is heavily reliant on the material's thermomechanical processing. The variety of grains that can form as a result of the α/β transformation allows for variation in microstructure and adaptation to desired applications [8].

Grain microstructures are categorized between α and β phases and several types exist depending on the temperature, degree of deformation, and cooling rate of the material [8]. These types include globular/equiaxed, or primary α, Widmanstätten, bi-modal, basketweave, martensitic, and bi-lamellar [8]. In this research, forgings will be conducted at near β transus temperatures for hot working. Following the forging operations, the specimen will be β annealed above the β transus. For this reason, the description of microstructures will follow this process.

Preform microstructure is important because it has significant influence on hot

deformation behavior [23]. Transformed β microstructure is unstable during hot deformation and shows flow softening before steady state [23]. The term transformed β is sometimes used to describe grains that were β phase at time of heat treatment, but have developed an α structure within the grain during cooling [8]. In the α/β hot working regime microstructure also undergoes strain dependent spheroidization, which occurs by shearing of lamellae followed by globularization of the microstructure [23]. Globularization refers to the development of a spherical morphology, while lamellar grains appear acicular. An example of lamellar and globular grains are shown in Figure 2.7. $\alpha + \beta$ preform microstructure is the most common [23]. Images showing examples of transformed β and lamellar microstructure is shown in Figure 2.7 [17].

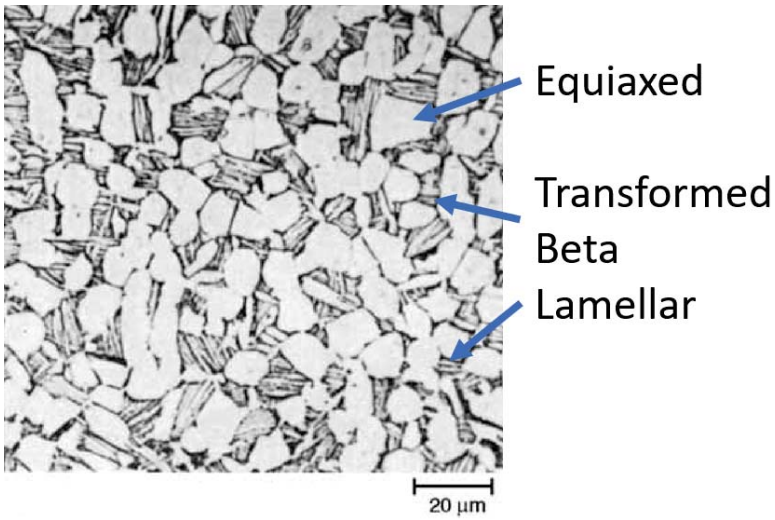

Figure 2.7. Solution treated 1 hour at 955 °C Ti-6Al-4V forging, air cooled, and β annealed 2 hours at 705 °C. Equiaxed (globular) α grains are light, transformed β is dark, lamellar α exists within transformed β[17]. The overall microstructure is referred to a bi-modal due to the combination of equiaxed and transformed β grains.

Primary α grains form through nucleation and growth during recrystallization from $\alpha + \beta$ regime working operations and remnants may remain through subsequent heat treatment [8] [7]. Its morphology can vary from elongated plates in lightly worked material to equiaxed globular morphology in heavily worked material [8]. Globular

or bimodal α formation can occur depending on cooling rates from high regions of the α+β phase field [8] [7].

Irrespective of initial microstructure, when titanium exceeds the β transus temperature during heat treatment, the grains change from α (HCP) to β (BCC) structure. During cooling following heat treatment, diffusion controlled phase transformation occurs [13]. When the material cools from a high temperature, the phase will change according to the equilibrium of free energy [13]. In this transformation, α lamellae grains form in prior β grains via nucleation and growth from along the grain boundaries [8]. These transformed or prior β grains, also known as secondary α, have varying morphology depending on the cooling rate and composition of the material. Increasing cooling rate increases α nucleation rate in β grain boundaries [8]. This enhances the formation and growth of α lamellae in prior beta grains [8]. Examples of the effect of fast and slow cooling rates on lamellar size is shown in Figure 2.8.

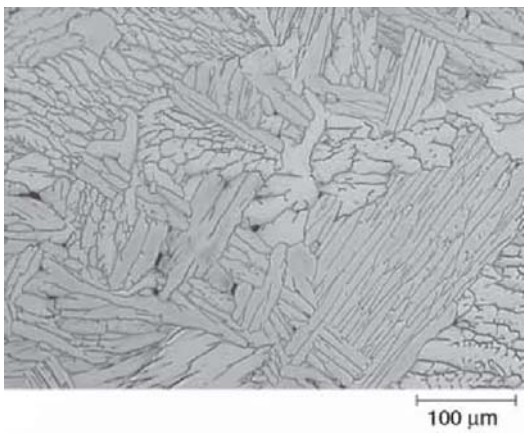

(a) Coarse Lamellar Grains[17].

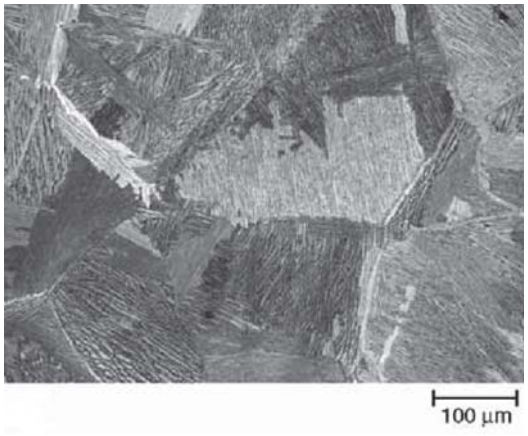

(b) Fine Lamellar Grains[17].

Figure 2.8. The images depict two Ti-6Al-4V specimen heated to different temperatures and furnace cooled. Cooling rate effects the size of lamellar grains. A) is β annealed at 1040 °C and furnace cooled representing slow cooling rate and coarse lamellar grains. B) is β annealed at 1050 °C and furnaced cooled representing fast cooling rate and fine lamellar grains.[17].

The orientation of the lamellae is related to the parent β structure [5]. The single close-packed plane within the α HCP structure is parallel to one of six close-packed

planes in the β BCC structure [5]. Also, one of the three close-packed directions in the basal plane of the α structure is parallel to one of the two close-packed directions lying within the specific close-packed plane in the β structure [5]. As a result, when a β grain returns to α phase, it transforms into colonies of lamellae having one of 12 (six·two) possible alpha phase orientations [5] [7]. Each colony has their own orientation within the prior β grain and forms from the prior β grain boundary [5].

The length and width of the α lamellae variants are determined by the cooling rate [8]. Under the β transus, time and temperature diffusion processes are slow [7]. Quenching from β phase transforms β grains by a diffusionless process into fine, needle-like martensitic α structures [7] [8]. When not quenching, a fast cooling rate leads to fine lamellar α structure within prior β grains [8]. This structure often contains overlapping lamellae of differing orientations and is commonly referred to as a basketweave or Widmanstätten microstructure. A representative image of Widmanstätten grain shape is shown in Figure 2.9.

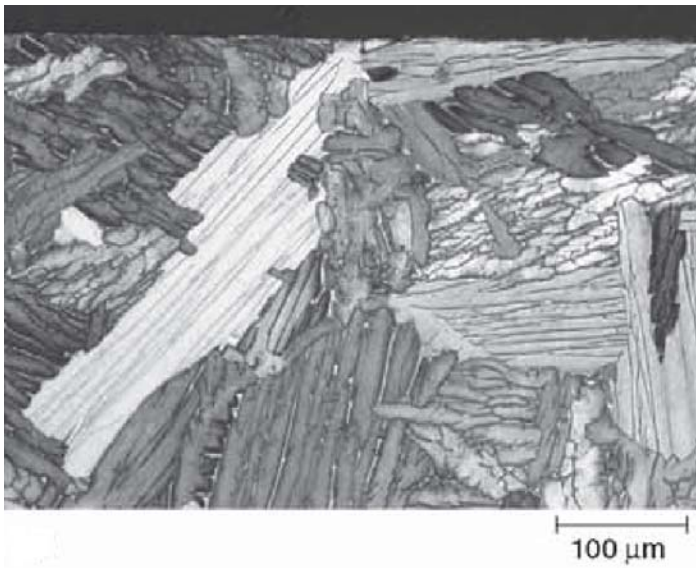

Figure 2.9. Ti-6Al-4V β annealed at1040 °C **and furnace cooled. The resulting image is representative of Widmanstätten structure [17].**

Slower cooling rates lead to more coarse lamellae and the formation of aligned α

lamellae in colonies [8]. Finally, slow cooling from above transus transforms β into globular α [8]. Under certain conditions, α grains can take the shape of long, wide grains called plates produced along preferred plains in the prior β matrix [17]. These plates can take on jagged appearances and be further defined as serrated α [17]. A representative image of plate-like α is shown in Figure 2.10[17].

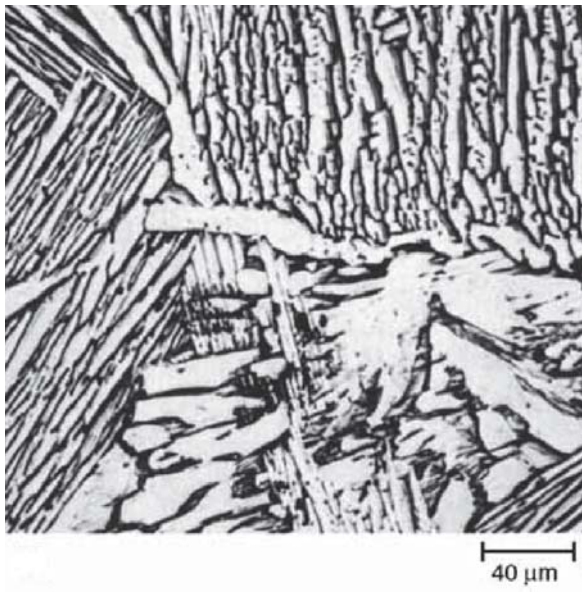

Figure 2.10. Ti-6Al-4V bar, held for one hour at1065 °C **and furnace cooled. The resulting grain shape is representative of plate-like α (light) with intergranular β (dark). [17]**

The yield strength of an alloy should increase with decreasing grain size [6]. α colony size is one of the most important parameters in determining mechanical properties because small grain size improves yield strength, ductility, and crack propagation resistance [8]. Furthermore, microstructure grain types have varying effects on mechanical properties. Fine scale platelets/lamellae grains increase strength and ductility and slow crack nucleation [7]. In contrast, coarse grains are more resistant to creep and fatigue crack growth [7]. Equiaxed grains have high ductility and fatigue strength [7]. As a result, bimodal grains have a balance of equiaxed and lamellar properties [7].

2.5 Finite Element Method

Workability tests have been used for many years to identify causes of forging defects within materials. These deterministic tests have allowed manufacturers to design against undesirable material properties. Unfortunately, they require many iterations and resources before solutions are identified. FEM presents an alternative to forging large quantities of material for results and is used extensively in this research.

FEM uses mathematical models to describe mechanical systems [24]. Simplifying assumptions are generally required, but the models can reasonably describe the behavior of specific systems. Typically they contain differential equations and are very challenging to derive solutions [24]. High performance computers are often required to solve these models. FEM is becoming more desirable with increasing access to high performance computers. They have allowed many numerical solution techniques to be developed and applied to find approximate solutions to engineering problems [24]. FEM is one technique that requires the division of a problem into sub domains called finite elements [24]. Therefore, the problem consists of many finite elements that can be solved and used towards the overall simulation. In the case of this research, forging and heat treatment operations are designed and solved using FEM.

2.5.1 DEFORM

In this research, Design Environment for Forming (DEFORM), produced by Scientific Forming Technologies Corporations (SFTC), is the FEM software used to simulate the forging workability tests on titanium. DEFORM is a FEM based process simulation system designed to analyze forming and heat treatment processes. This software is designed specifically for deformation simulations and is commonly used in the forging industry as a way to improve die design, die filling, microstructure control, and other industry based forging and heat treatment processes. The application and

use in industry, as well as to forming operations, is a primary reason DEFORM is used as the FEM solver in this research. A goal of this research is not only to use FEM to evaluate the effects of forging parameters on AGG, but also to use it as a means to predict AGG. Developing a method to predict AGG using existing industry tools will create a means for industry to immediately implement control AGG in Ti-6Al-4V forgings.

The software includes both 2D and 3D, auto-meshing and re-meshing, and post processing capabilities, in addition to many other tools not used in this research [25]. The primary Graphical User Interface (GUI) in DEFORM allows the user to develop combined forming operations including heat transfer and deformation processes. The processes used to develop the simulations in this research include transfer and dwell operations, followed by forming and cooling operations. DEFORM also includes a robust materials database for common materials used in industry[25]. Ti-6Al-4V is included as a default material and contains material properties and flow stress data compiled from a variety of sources [25]. Data was collected by a series of isothermal hot compression tests used to determine flow stress at specific temperatures for the material tested. In forming processes, plastic flow data is fundamental to DEFORM simulations[25]. It governs deformation and flow behavior of the object undergoing permanent deformation [25]. In the simulation, flow stress from deformation is given as a function of plastic strain, strain rate, and temperature. The data generated from the isothermal hot compression tests is used to determine these parameters at any step of deformation in the forging simulation. These parameters are used extensively in this research to predict AGG and prevents the need to develop a constitutive equation for these forging simulations [25].

2.5.2 Simulation Inputs

A robust simulation tool is useless without appropriate inputs and parameters to create a simulation with usable results. Many of the inputs used in this software are specifically from material properties. The values required to simulate a workability test include material heat transfer coefficient, material emissivity, shear friction coefficient, transfer and resting times, environmental temperatures, and the forging die temperatures.

The material heat transfer coefficient is designated by the variable "h" and is used to describe the heat transfer between two objects. For Ti-6Al-4V this value was gathered from two articles investigating heat transfer and was determined to be approximately $20\frac{KW}{m^2K}$ on H13 steel die [13] [15] [26]. Emissivity of a material is the ratio of heat emitted by that material and heat emitted by a perfect blackbody at the same temperature [27] [28]. A value of 0.67 was used for this alloy and chosen as a representative value based on data presented by Titanium Metals Corporation and recommendations received from Dr. S.L. Semiatan of Air Force Research Laboratory (AFRL) [29]. Higher levels of emissivity around 0.6 to 0.8 are generally associated with oxidized metals, while polished metals are lower in a range of 0.1 to 0.3 [27],[29].

Friction must also be considered between the workpiece and die. A shear friction constant is reasonable for this simulation due to the small amount of relative movement between the two surfaces. Constant shear friction is used for bulk-forming simulations and is defined by $f_s = m \cdot k$ where f_s is the frictional stress, k is the shear yield stress, and m is the frictional factor [30]. Therefore, friction is a function of yield stress of the forged material [28]. The frictional factor is largely based on forging temperature and lubrication used between the die and workpiece. One Ti-6Al-4V ring compression test performed at 50 percent reduction in height with glass lubricant by Zhu et al. found that the friction coefficient could be on the order of

about 0.35 [31]. The SFTC default friction factor of 0.3 for a lubricated hot forging was used because of its similarity to this study. [28].

The remaining inputs including transfer time, resting time, environmental temperature, and die temperatures were chosen based on measurements from the forging facility. Average transfer time measured for previous forgings at the AFRL forging press is about 5 seconds. The average resting time on the bottom die is approximately 12 seconds. Finally, it is estimated that the environmental temperature remains about 21.1°C in the forging bay and the dies are heated to about 37.7°C.

2.5.3 Mesh

Generating a mesh is essential to developing a successful simulation. One key attribute of DEFORM is its robust auto-mesh package. This software streamlines simulation processes and allows very large and complex models to be simulated using reasonable computing technology [32]. A mesh is a small block or shape defined over a computer generated geometry. Each block contains a specific area of material that uses a defined relationship to model the material's response. A block can also be called an element and is composed of nodes. More elements in a mesh, represent smaller amounts of material within an element. Having a large number of elements refines the mesh and produces a more accurate simulation. Unfortunately, due to the increased number of elements, there are more equations and interactions the computer must solve. This effect can dramatically increase the computational time required to solve a simulation. Many types of meshes and element shapes exist to optimize simulations. Additionally, they can be represented in two or three dimensions depending on the complexity of the model.

In this thesis both two and three dimension simulations were designed. Both will have very different simulation complexities and require varying amounts of compu-

tational time. As a result, most simulations in the thesis will be two dimensional because they are less complex and require less computational time. This means a smaller mesh for the simulation and fewer elements and nodes. The 3D simulations will be much more complicated and require a mesh containing an order of magnitude more of elements and nodes.

The exact size of each mesh and the simulation step ratio required for the model is dependent on material size and complexity of the simulation. Ultimately a convergence study of critical parameters is required to ensure the simulation is converging and not becoming unstable. Although mesh size is determined through convergence, the step ratio can be estimated using a mesh ratio that relates size of the specimen to time [27]. Ideally, the largest step ratio possible while maintaining simulation stability is desired [27]. This ultimately reduces the computational time for the simulation while still producing good results [27]. This ratio states a reasonable mesh ratio will be less than or equal to 0.5. The ratio is defined by $M = \frac{\kappa * \tau}{\varepsilon^2}$, where $\kappa = 1$, ε is 1/6th the thickness of material, and τ is the time step [27]. By defining the mesh ratio to 0.5, it is possible to estimate the largest acceptable step ratio for the simulation.

2.6 Summary

In summary, Ti-6Al-4V is a widely used titanium alloy in the aerospace industry for its high strength-to-weight ratio and corrosion resistance. This material is commonly forged to produce structural components despite requiring tight forging process control. This alloy is sensitive to temperature variations during forging and can easily develop material defects if not controlled properly. Workability tests are commonly used to evaluate material defects caused by forging processes and offer a method to determine process restrictions required for Ti-6Al-4V. The use of FEM software, DEFORM, allows many workability test simulations to be modeled before

actually using resources to produce tests. Chapter 3 will outline the methodology used to develop the workability tests, simulations, and forgings for this alloy.

III. RESEARCH METHODOLOGY

3.1 Chapter Overview

A methodology was devised leveraging the research from Chapter II and applying it to the motivation of this thesis. The overall purpose is to identify forging parameters and their affect in developing large grain size in β annealed Ti-6Al-4V forgings. The investigation was divided into three major components to include Finite Element Method (FEM) analysis, forging tests, and metal microscopy. FEM was used to test many different forging parameters to select specific tests that would most likely result in Abnormal Grain Growth (AGG) while also limiting the amount of resources used. Titanium is expensive, and so are the resources required to forge and process it into measurable specimen. The following chapter will explore the theory, procedures, and materials required to produce representative simulations, conduct forging tests, and prepare and analyze Ti-6Al-4V microstructure. An overview of the chapter is shown below in Figure 3.1.

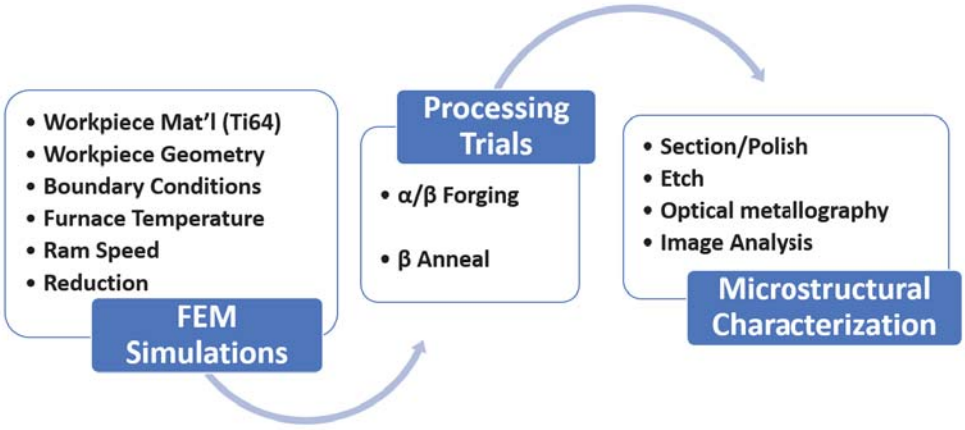

Figure 3.1. The methodology is divided into three major components, FEM, Forging Trials, and Microstructural Characterization.

3.2 Theory

The FEM software, Design Environment for Forming (DEFORM), was used in the first portion of the investigation to simulate forgings. Computational simulations allow users to iterate and simulate many variables of a representative mechanical process with only a computer. Iteration allows forging variables to be compared and narrowed to those likely to result in large grain development. The methodology for FEM in this investigation includes developing simulations representative of the desired forging process, validating them against physical tests, and using them to predict the results of physical tests. The forging processes represented in this research were based on the workability tests described in Section 2.3.5. Both sidepressing and upsetting forgings were simulated in order to test axial and plane strain processes. These tests represent fundamental open die forgings used within forging production plants in industry. Simulating them will provide general insight into fundamental forging processes.

Today's computational simulations visually mimic mechanical operations, but never provide complete or correct results. In the words of statistician George Box, "All models are wrong, but some are useful." It is this rule of thumb that requires a level of validation to any simulation or model used to predict a response. Physical forgings will be used in this investigation to validate the FEM simulations. By comparing the simulations to actual forgings it is possible to further refine the simulation to produce more realistic results. Finally, the results guide the selection of parameters for use when forgings are conducted. Materials are typically limited and restrict the number of tests or forgings available. Simulations allow an unrestricted number of predictions and are used to narrow the selection of tests.

Large grain size in Ti-6Al-4V results from a combination of deformation temperature, strain, strain rate, and heat treatment [4]. Forging speed and reduction in

height of the material contribute directly to strain and strain rate. Typically, lower temperature forgings experience greater internal strain when forged because material resists deformation when cool. It is also noted in Section 2.2.2 that α phase titanium resists deformation more than β phase because it only has three slip systems. On the other hand, when material is forged quickly it produces internal heat generated through deformation. This happens from material resisting deformation, and being forced to deform at a quick rate. It would seem lower forging temperature and fast forging speed would produce regions of internal locally high strain. This may raise internal temperature to β transus thereby pre-exposing the material to β phase. If pre-exposed, the material might experience local transformations that might grow larger than average during heat treatment. By using FEM it is possible to capture these parameter interactions through simulation comparisons.

Using simulations to vary forging speed, reduction in height, and furnace temperature will assist in comparing tests most likely to produce large grain size. Forging temperature, strain, strain rate, and material flow profiles can be compared to identify regions of interest. Any localization that results can be analyzed to determine potential relevance to grain growth. Information gathered through simulations will guide forging tests, and be used as feedback to improve simulations and further guide understanding of grain growth.

Metallography must be performed after forgings tests in order to evaluate microstructure. The purpose of forging tests is to demonstrate an ability to produce and control grain development in titanium outside of computational simulations. The material must be sectioned, polished, and etched to observe internal microstructure using optical microscopy. Photographic analysis software can then quantify average grain size and distribution. Only then will the effect of forging parameters on grain growth of titanium be clear.

3.3 Materials and Equipment

Many resources are required to conduct an investigation of titanium grain growth. The Air Force Institute of Technology (AFIT) has provided the FEM software, DEFORM, for forging simulations. The software required a computer with minimum four cores, 16 gigabytes of random access memory, and a sizable hard drive for two dimensional analysis. For three dimensional analysis, 20 cores, 128 gigabytes are recommended. Additionally, they have provided optical analysis tools to evaluate grain size and ratios. Primarily, these tools included a Zeiss inverted optical microscope with automatic stage and photo stitching capability. Photo-analysis of grain images was accomplished using various imaging packages available in MATLAB. Additionally, the AFIT model shop provided machining expertise when required. Common machining requests included wire Electrical Discharge Machining (EDM) sectioning of forging workpiece, heat treatment of specimen, and milling/surface grinding of α case oxide layer from specimen. A selection of specimens were also sent to Winston Heat Treating in order to heat treat to typical industry standards in vacuum with nitrogen quench.

The Air Force Research Laboratory (AFRL) Materials and Manufacturing Directorate provided the majority of forging and polishing resources for this investigation. A 1-ton hydraulic forging press and a heating furnace were used to conduct forging operations. They also provided the Ti-6Al-4V cylindrical workpieces for sidepressing and upsetting tests. The lab's polishing equipment was used to achieve 1μm surface finishes and Hydrofluoric Acid (HF) was provided to surface etch the samples to optically reveal grain boundaries.

3.4 Simulation Development

A useful model for simulation of Ti-6Al-4V forgings was required to predict forging results to conduct a design of experiments analysis on forging variables. Results from a previously validated three dimensional sidepressing model and its associated physical forgings were used as a baseline for the development of simulations in this research. Replicated simulations were compared in two and three dimensions and then updated with parameters more representative of the forging process in this research. A design of experiments was then executed with the new simulation using a combination of two and three dimension versions. The development of two dimensional simulations was essential due to initial computational limitations. Approximately a 90% reduction in computational time was realized by using two dimensional simulations prior to receiving an updated computer. The results of these simulations were later used to guide physical forging tests by developing predictions for AGG.

Validating simulations is necessary before using them for research. This section shows simulations in this work reasonably represent Ti-6Al-4V sidepressing forgings and previous simulations on this topic. These simulations can be used with a degree of confidence when simulating additional forging processes of the same material.

A sidepressing simulation was baselined to previous Ti-6Al-4V sidepressing tests and simulations to develop a validated FEM simulation for this thesis. A baseline model, done under contract work by AFRL, developed a validated simulation using DEFORM as the FEM solver and compared the results to a series of Ti-6Al-4V sidepressing forgings. A working simulation for this thesis was successfully created by comparing outputs with the baseline.

The baseline consisted of developing three sidepressing simulations using DEFORM and validating them against forgings with the same process parameters. A depiction of this simulation is shown in Figure 3.2

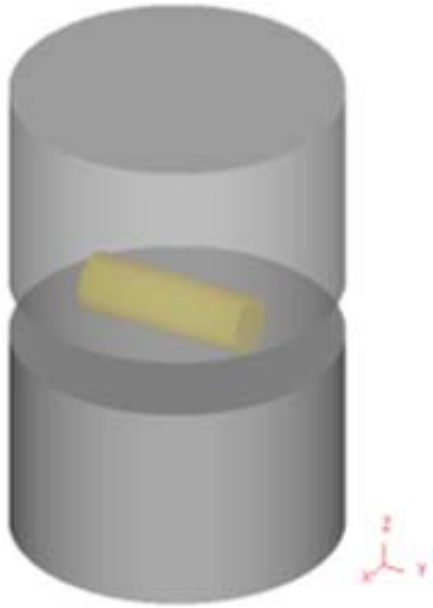

Figure 3.2. Baseline sidepressing simulation layout validated through forging tests.

The simulation was designed to represent a sidepressing forging, where a cylindrical workpiece was removed from a furnace, transported to the forging press, placed on the bottom die, and pressed. Simulations were created based on this test in order to validate the FEM results. Three simulations were developed due to uncertainty regarding heat transfer and friction between the workpiece and dies. Key parameter specifications used in the baseline work are shown in Table 3.1

Table 3.1. Baseline Simulation Inputs

Parameter	**Input**
Transfer Time	3s
Resting Time	7s
Environmental Temperature	21.1 °C (70°F) during Transfer Time
Environmental Temperature	37.78 °C (100°F) during Resting and Forging
Workpiece Temperature	954.44 °C (1750°F)
Die Temperature	37.78 °C (100°F)
Radiation Emissivity	0.6
Die Velocity	1524 $\frac{\text{mm}}{\text{min}}$ (60$\frac{in}{min}$)
Flow Stress and Thermal Data	DEFORM Ti-6Al-4V Data
Billet Corner Radius	1.59 mm (0.0625 in)
Billet Diameter	63.50 mm (2.5 in)
Billet Length	190.50 mm (7.5 in)
Die Diameter	355.60 mm (14 in)
Die Stroke	43.82 mm (1.725 in)
Forging Number	8820
Number of Elements	100,000
Friction Coefficients(m)	0.40, 0.30, 0.25
Heat Transfer Coefficient(h)	0.0050, 0.0025, 0.0020 BTU/s/in^2/°F

The baseline simulation begins by representing the workpiece being removed from the furnace at 954.44 °C in an environment that is 21.1 °C. It will take the workpiece three seconds to be transported from the furnace to press where it will rest seven additional seconds before forging begins. The ambient air temperature at the press will be 37.78 °C with dies being the same temperature. When the forging begins, the upper die will move in a negative "z" direction at 1524$\frac{mm}{min}$. The press will continue until it has reached a die stroke of 43.82 mm at which time the simulation will end.

Access to forging parameters allowed very close reproduction of baseline simulations. The simulation developed as a baseline for this thesis used the exact inputs as Table 3.1. The only exception was specifically using the 0.25 friction coefficient and 0.0020 BTU/s/in^2/°F heat transfer coefficient instead of all three. Developing a mesh was also straight forward because DEFORM has a robust auto meshing and re-meshing program. Although the software limits user input in mesh development,

the simplification allows for better reproducibility between simulations.

When the baseline simulations were adequately replicated, additional parameters were updated to better reflect data from research and represent the desired tests in this thesis. Some simulation values were changed based on research conducted in Section 2.5.2. The primary differences between the updated simulations and baseline simulations are transfer and resting times as well as radiation emissivity, friction coefficient, and heat transfer coefficients. The transfer and resting times varied based on the average times measured at the AFRL forging press. The speed of the individuals performing forgings varied between tests. Timing is a critical value in simulations because of its effect on die chilling of the workpiece. Updating these values is essential to accurately account for cooling effects. Radiation emissivity was increased to 0.67 based on input provided by AFRL's Dr. S.L. Semiatin and research from Section 2.5.2. Friction coefficient was also increased to 0.3 based on DEFORM's recommended value for shear, lubricated, hot-forgings. Finally forging heat transfer was changed based on research discussed in Section 2.5.2.

The simulations and forging test were compared to validate this thesis's simulation. Three key methods for validating the simulations include dimensional analysis, material flow analysis, and load-stroke data comparisons. Dimensional comparisons require the workpiece forging profiles be compared to ensure they realistically predict final workpiece shape. These profiles are shown in Figure 3.3.

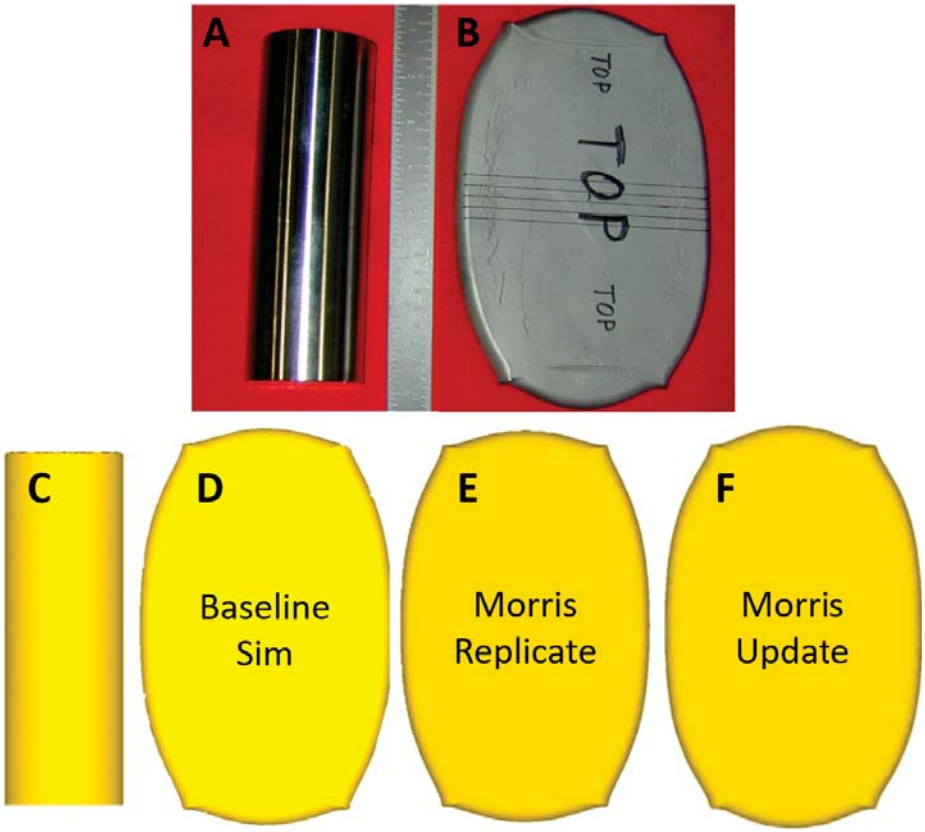

Figure 3.3. Profile comparisons between A) Representative sidepressing preform, B) Baseline forging test 8820, C) Original simulation sidepressing preform, D) Baseline simulation profile, E) Morris replication of baseline results, and F) Morris update to baseline simulation based on additional research.

A few characteristics are important to evaluate when comparing profiles. The forging developed crescent shaped folds on both ends of the cylinder. These folds would be attributed to the cylinder edges cooling at a faster rate than the rest of the workpiece. Cooler metal will inherently resist deformation and maintain shape better than hotter metal. For this reason the crescent/edge of the cylinder forms and maintains a mark after forging. When comparing to the simulation, this marking is nearly visible especially at the four pointed edges. Another important characteristic is the metal bulging in axial direction of the workpiece. When a cylinder is sidepressed, the material flows laterally and axially. Lateral flow is expected, but axial flow is due to lateral deformation resistance, which forces the material to flow axially

instead. Using Figure 3.3, the degree of axial deformation appears closest between the forging trial and image D that was updated with specific refined material values and processing times. Finally, the degree of lateral deformation appears to be consistent between all three images. The similarity of the profiles suggests the simulations are representative of the forging test.

Measurements between the four profiles were compared to determine similarity between simulations. The results of maximum measurements in the X and Y axis are shown in Table 3.2. The table highlights the differences between profiles. At a lower die stroke value of 1.07 inches, the baseline simulation has a closer deformation profile than the replication and update simulations. However, at higher deformations with a die stroke of 1.73 inches, the updated simulation has a closer dimensional profile shape to the forging trial than the other simulations. Based on these results the updated simulation appears better, or more representative, of the forging operations to be conducted in this research. Sidepressing forgings in this research were conducted between 1.62 and 2 inch strokes for which the updated simulation has the least amount of dimensional error.

Table 3.2. Maximum X and Y axis dimensional comparison between the forging trial, baseline simulation, and this thesis's simulations.

Measured (in.)			Baseline % Error		Replicate % Error		Update % Error	
Stroke	X_m	Y_m	$X_{Baseline}$	$Y_{Baseline}$	$X_{Replicate}$	$Y_{Replicate}$	X_{Update}	Y_{Update}
0.00	2.5	7.50	0	0	0	0	0	0
1.07	3.59	8.18	0.28	0.73	1.39	0.98	1.39	1.10
1.62	5.47	9.15	1.28	0.11	0.91	1.20	1.10	1.20
1.73	6.24	9.59	3.04	0.94	2.08	0.21	0.80	0.42

The load-stroke data of the forgings and simulations is another way to compare the simulation deformation loads to actual forging loads. All four sets of load-stroke data are in Figure 3.4.

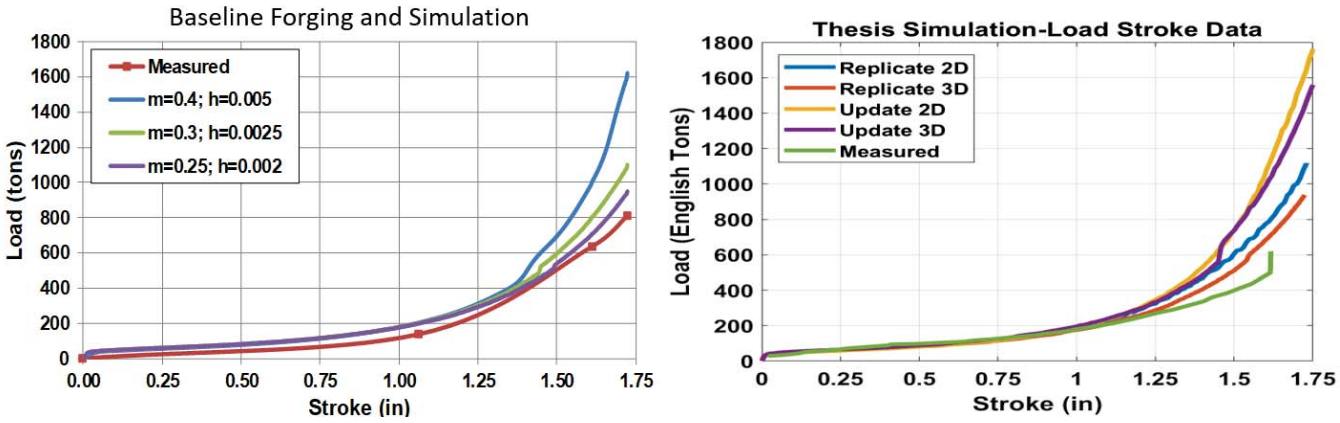

Figure 3.4. Both plots depict forging processes conducted at 955 °C initial furnace temperature and 1 $\frac{in}{s}$ ram speed. The left plot depicts the load stroke data from the forging test and baseline simulations. The right plot depicts the load-stroke data from 2D and 3D simulations in this thesis.

The plots provide an objective means to compare the forging data against the simulations. Unfortunately, data was not available to directly overlay and compare loading values, so a side-by-side comparison was conducted. In all cases the simulation data diverges from the measured data at large stroke values. One explanation of divergence might be because DEFORM uses flow stress data from a database which may not exactly represent the same Ti-6Al-4V used in this forging. Additionally, the simulation flow stress data was collected from hot isothermal compression tests, whereas the measured data is from a non-isothermal sidepressing forging. The difference in loading values between simulations and measured data likely results from a difference in the volume fraction of α and β grains at a given temperature. In an isothermal compression test, the material remains at a constant temperature while being compressed. In this state the material will have a larger volume fraction of β grains when forged close to the transus temperature. In contrast, during non-isothermal forgings, the material cools when removed from the furnace, and experiences accelerated cooling rates when in contact with the cooler forging dies. When the material is cooled, it will have a larger volume fraction of α grains in the regions experienc-

ing cooling effects, while the core of the material may remain representative of an isothermal forging. α grains are more difficult to deform than β grains because of the number of slip systems in each microstructure, as discussed in Section 2.2.2. The difference in microstructure composition between the isothermal simulation data and non-isothermal measured data may account for divergence in the load-stroke plots.

Aside from divergence, the differences between the baseline simulations and measured data decrease as friction and heat transfer values decrease. By visual comparison the replicated simulations in this thesis appear nearly identical to the baseline simulations. Both replicated and updated simulations show less error at low stroke values when compared to measured data than the baseline simulation and further justifies the validation of these simulations. The updated simulations, however, diverge more from the measured data. Greater divergence may be the result an increase in friction coefficient and longer transfer and dwell times on the dies. Increasing friction will increase the load required to deform the material at larger reductions in height because more material contacts the dies as deformation increases. Also, longer transfer and dwell time prior to forging results in increased cooling and die chill effects that may also increase forging loads. In a separate note, both sets of two dimensional simulations in this thesis have slightly larger loads than their three dimensional counterparts. This is likely the result of the simulations calculated in two dimensions and not allowing material to flow in the axial direction, which would relieve deformation resistance. The updated simulation also shows a large discontinuity as the result of re-meshing despite still following a similar curve pattern as its two dimensional simulation. Finally, measured data from an additional forging trial depicted in the right plot has measuring error at the peak values. They appear similar to the baseline forging trial, but the curve leading up to it is lower. This may indicate potential errors in the data retrieval system of the forging press.

Unfortunately the forging trials from the baseline test were not sectioned and processed in an as-forged condition to allow for material flow analysis. If an etched as-forged specimen existed, then the material flow lines from the specimen could be optically compared to the simulation predictions. The results would add an additional level of validity to the simulations.

Despite comparison limitations between physical forgings and simulations, there are several contour comparisons that can be evaluated between both sets of simulations. Cross-section contours comparing internal temperature, strain, and material flow provide insight to material behavior during forging. Figures 3.5 to 3.7 depict these contour comparisons at the midwidth of the workpiece. In Figure 3.5 the temperature contour between the baseline simulation and this thesis's simulations are similar.

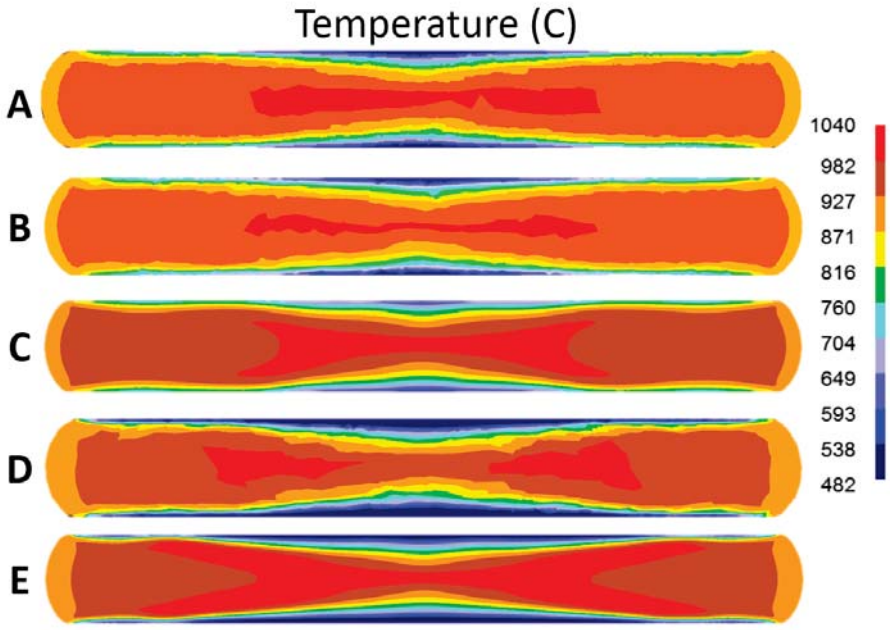

Figure 3.5. Three temperature contour at the midwidth of the workpiece representing 43.82 mm reduction in height. A) Baseline validated simulation temperature contour B) Replicated 3D simulation temperature contour C) Replicated 2D simulation temperature contour D) Updated 3D simulation temperature contour E) Updated 2D simulation temperature contour. *Note: slight color change due to DEFORM version updates.

All contours share a similar temperature distribution pattern. The primary difference between them is the maximum temperature distributions. However, this difference is small and indicates the updated simulations have a more conservative contour by potentially over predicting temperature. Each two dimensional contour has a different distribution than the three dimensional simulations. The distribution of the maximum temperature at the core of the workpiece is larger and has a distinct compressed "X" shape. This larger distribution is likely the result of two versus three dimensions. Metal flow in the two dimensional simulation is more restricted and leads to an increase in deformation resistance. This additional resistance in plasticity is expected to generate more internal heat, which is represented by the larger maximum temperature contour. The updated simulation also shows larger die chill regions, which can be attributed to longer transfer and dwell times.

Figure 3.6 compares effective strain contours for the baseline simulation against the two and three dimensional simulations.

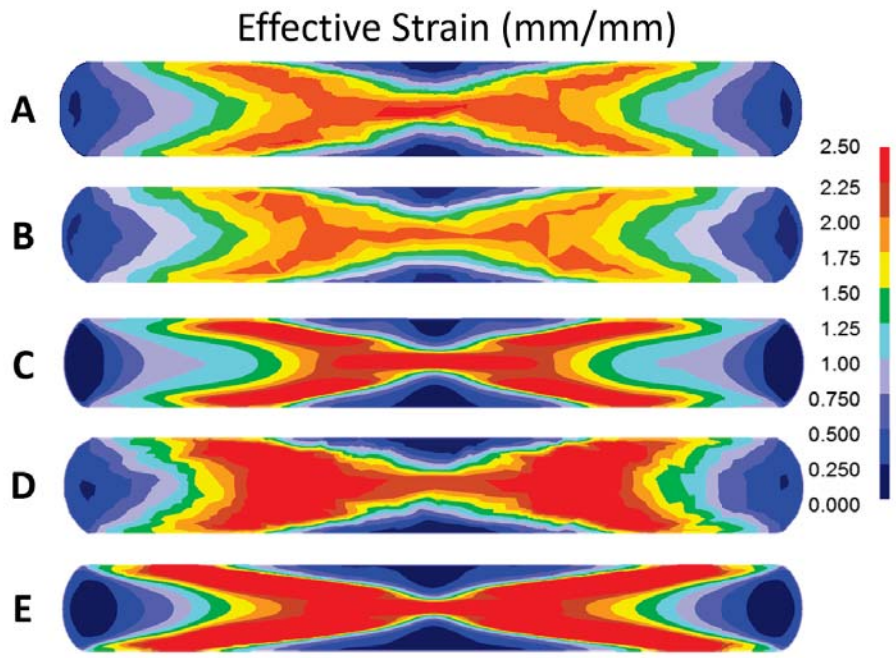

Figure 3.6. Effective strain contour comparisons at the midwidth of the workpiece for A) Baseline validated simulation, B) Replicated 3D simulation, and C) Replicated 2D simulation D) Updated 3D simulation, and E) Updated 2D simulation.

Similar to the temperature contour, the three dimensional effective strain (also referred to as von-mises strain) contours share similar contour patterns. Effective strain is derived from the three principle strain values in the material and is defined by equation 3.1.

$$\bar{\epsilon} = \frac{\sqrt{2}}{3}\sqrt{(\epsilon_1 - \epsilon_2)^2 + (\epsilon_2 - \epsilon_3)^2 + (\epsilon_3 - \epsilon_1)^2} \tag{3.1}$$

where $\epsilon_1, \epsilon_2, \epsilon_3$ are principle strains and $\bar{\epsilon}$ is the effective/von-Mises strain [28]. The distribution of effective strain contours share identical shear patterns. The primary difference is the updated simulations achieve higher effective strain at the center of the workpiece. This difference suggests greater resistance to deformation and may be the result of larger chilled regions and increased friction coefficient. Despite variations in magnitude, the effective strain patterns are similar between simulations as shown in Figure 3.6. The two dimensional simulations have a much greater effective strain

than three dimensional simulations. This is the result of metal flow restricted to two dimensions in the simulation. In three dimensions metal would also flow axially and relieve deformation resistance and effective strain.

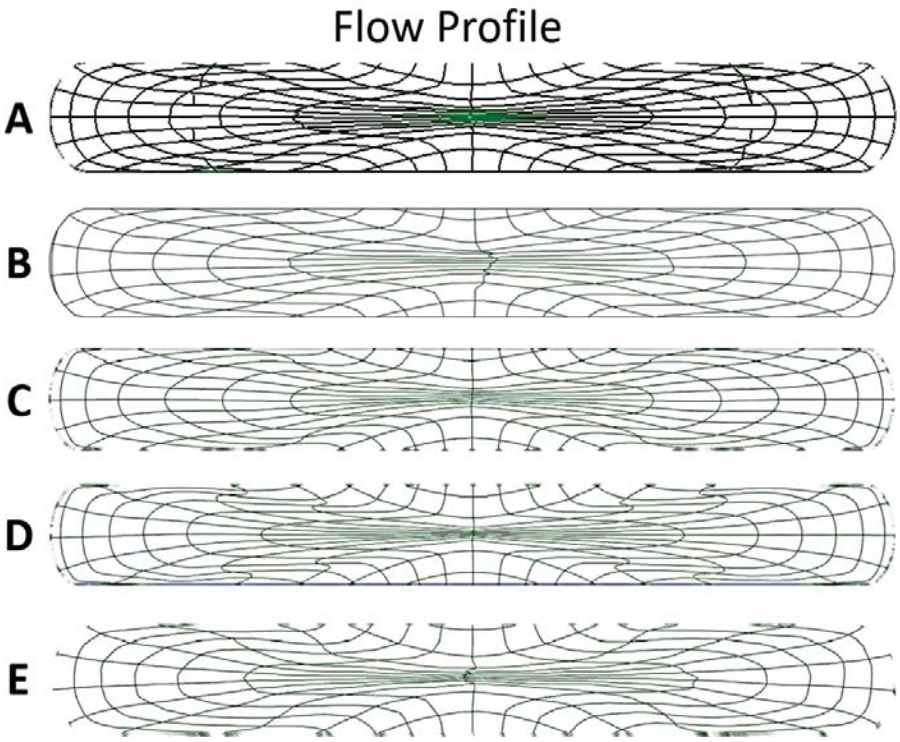

Figure 3.7. Metal flow profile comparisons at the midwidth of the workpiece for A) Baseline validated simulation (black lines represent edges of workpiece), B) Replicated 3D simulation, and C) Replicated 2D simulation D) Updated 3D simulations, and E) Updated 2D simulation..

Figure 3.7 compares the metal flow profile between all three simulations. The flow profiles are set up by overlaying a square grid over the cross-section of the forging of interest. As the material is deformed, the gird becomes distorted and depicts material flow by the angles created between grid lines. Therefore, the grid lines represent a comparison between normal and shear strain in the material. Lines remaining closer to the original 90° angle represent normal strain, while lines with large or small angles from 90° represent shearing strains. Despite noticeable differences between temperature and strain contours, the flow profiles appear similar. The primary differences

appear in the updated simulations where material at a 45° to the center show signs of greater shearing strain, which agrees with the strain contour images in Figure 3.6. Additionally, the regions of normal strain appear to agree with the locations of low strain and temperature caused by die chill and cooling effects.

3.5 Simulation Tests

With a validated two and three dimensional simulation, the next step in this research was to develop test matrices and conduct simulations with varying forging process parameters to identify temperature and strain conditions that may result in the formation of AGG. The test matrices and simulations were designed around sidepressing and forging tests that were discussed previously in Section 2.3.5. The parameters chosen were also discussed in the previous section and include material reduction in height, ram speed, and initial workpiece temperature A single test matrix was designed for both forging operations. The matrix for each operation is shown in Table 3.3.

Table 3.3. Sidepressing and upsetting simulation test matrix

Reduction in Height	Ram Speed ($\frac{mm}{s}$)	Initial Workpiece Temperature (°C)
65%	8.5	912.78
65%	8.5	954.44
65%	25.4	912.78
65%	25.4	954.44
65%	38.1	912.78
65%	38.1	954.44
80%	8.5	912.78
80%	8.5	954.44
80%	25.4	912.78
80%	25.4	954.44
80%	38.1	912.78
80%	38.1	954.44

The test matrix does not specifically label each test conducted, but rather shows

the three process parameter variables analyzed and the values evaluated. A full factorial test of this matrix for a single process results in twelve total forging tests. As a result, two forging tests will result in 24 total tests for this research. The number of tests alone for these operations justifies the use of simulations to save time and resources. Even still, conducting 24 three dimensional simulations is time intensive. Therefore, two dimensional simulations were heavily relied on because they require a fraction of the computational time. By conducting simulations based on these test matrices it is possible to identify forging parameters likely to result in conditions of temperature and strain that possibly result in AGG.

Sidepressing and upsetting processes were chosen because they represent idealized forging operations conducted in industry. The parameters for each test were selected because of their affect on workpiece strain, strain rate, and internal temperature. Additionally, these parameters have a large influence on the development of forging defects. The values for each parameter were selected based on research from Chapter II. Reduction in height of 65% and 80% were selected as the upper end of typical forging reductions. Large reductions in height were desired in an attempt to produce large strains and potentially induce large grains. Ram speeds were selected to cover the range of slow, moderate, and fast deformation rates to induce differing degrees of strain rates on the material. Finally, two initial workpiece temperatures, 912.79 °C and 954.44 °C, in the range of ideal forging temperature were selected to evaluate their effects on deformation and potential grain growth.

The simulation parameters used to develop the sidepressing and upsetting simulations were based on the updated simulation developed in Section 3.4. Tables 3.4 and 3.5 outline the inputs used for the sidepressing and upsetting simulations.

Table 3.4. 2D and 3D Sidepressing Test Simulation Inputs

Parameter	**Input**
Transfer Time	5s
Resting Time	8s
Environmental Temperature	21.1 °C (70°F) during Transfer Time
Environmental Temperature	37.78 °C (100°F) during Resting and Forging
Die Temperature	37.78 °C (100°F)
Radiation Emissivity	0.67
Flow Stress and Thermal Data	DEFORM Ti-6Al-4V Data
Billet Diameter	63.50 mm (2.5 in)
Billet Length	190.50 mm (7.5 in)
Die Diameter	355.60 mm (14 in)
Number of Elements (3D)	100,000
Number of Elements (2D)	8,000
Step Ratio	0.01 $\frac{s}{step}$
Friction Coefficients(m)	0.30
Forging Heat Transfer Coefficient(h)	20 $kW/m^2 \times K$
Resting Heat Transfer Coefficient(h)	2 $kW/m^2 \times K$

Table 3.5. 2D and 3D Upsetting Test Simulation Inputs

Parameter	**Input**
Transfer Time	5s
Resting Time	12s
Environmental Temperature	21.1 °C (70°F) during Transfer Time
Environmental Temperature	37.78 °C (100°F) during Resting and Forging
Die Temperature	37.78 °C (100°F)
Radiation Emissivity	0.67
Flow Stress and Thermal Data	DEFORM Ti-6Al-4V Data
Billet Diameter	76.2 mm (3 in)
Billet Length	114.3 mm (4.5 in)
Die Diameter	355.60 mm (14 in)
Number of Elements (3D)	100,000
Number of Elements (2D)	4,000
Step Ratio	0.01 $\frac{s}{step}$
Friction Coefficients(m)	0.30
Forging Heat Transfer Coefficient(h)	20 $kW/m^2 \times K$
Resting Heat Transfer Coefficient(h)	2 $kW/m^2 \times K$

Sidepressing simulations were divided into two and three dimension tests. The forging layout for the three dimension simulation and workpiece are shown in Figure 3.8. The simulation used a 132,479 tetrahedral element mesh with finer mesh near the core. Equal weight was applied to boundary curvature, temperature distribution, strain distribution, and strain rate distribution when generated with DEFORM.

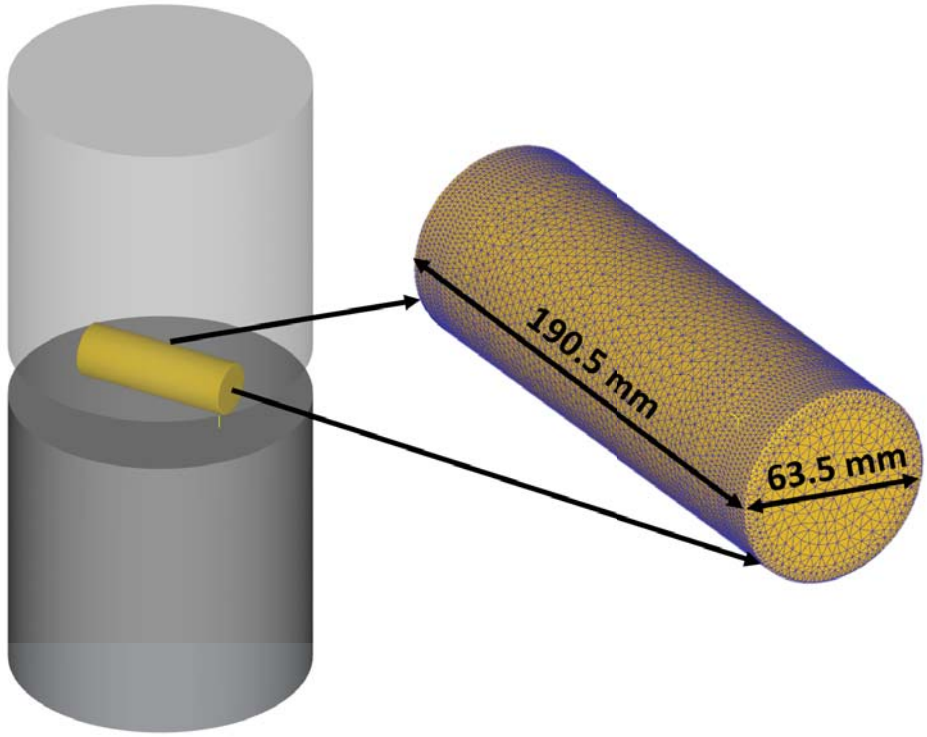

Figure 3.8. 3D sidepress simulation workpiece with dimensions as it relates to the sidepressing forging simulation.

The two dimensional sidepress test is shown in Figure 3.9. This simulation is a plane strain problem, and therefore the material is represented as a circle in two dimensions. The mesh was determined to converge by 8,000 elements at about 0.000625 inch^2 per quadrilateral element, which still allowed for a fast computational time at an average of 1.3 hours. It was also equally weighted for boundary curvature, temperature distribution, strain distribution, and strain rate distribution Plots showing convergence of the two dimensional sidepress simulation are available in Appendix A.

Figure 3.9. 2D sidepress simulation with 8,000 element mesh and dimensions.

Upsetting operations are axial compressions of a cylindrical workpiece. In this type of forging process, it is reasonable to expect that the material will deform identically along the radius about the centerline of the cylinder. For this reason, simulations were simplified to two dimensional axisymmetric representations of the three dimensional layout shown in Figure 3.10. This simplified the simulation resulting in smaller computational requirements to reach a converged solution.

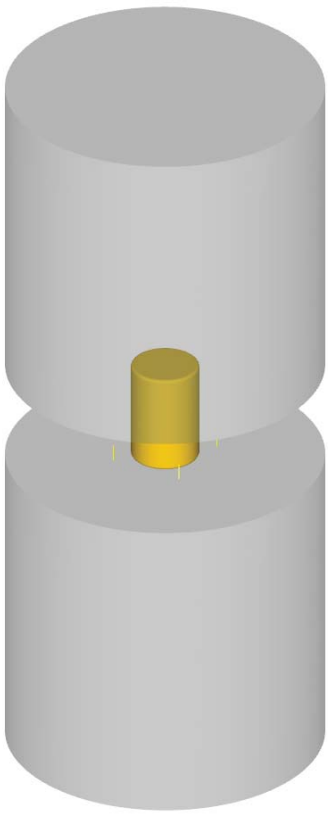

Figure 3.10. Typical 3D upsetting forging layout

The simplified two dimensional axisymmetric workpieces used for the upsetting simulation is shown in Figure 3.11. This figure has a 4,000 quadrilateral element mesh with the average element size of about 0.0016 inch^2. The mesh was generated with equal weighting of boundary curvature, temperature distribution, strain distribution, and strain rate distribution. The mesh has fewer elements than the two dimensional sidepress workpiece because it is an axisymmetric simulation instead of full representation. The axis of symmetry is therefore pinned and does not allow element interaction or material flow beyond the axis. Simplification of the workpiece brought average computational time down to 12.5 minutes.

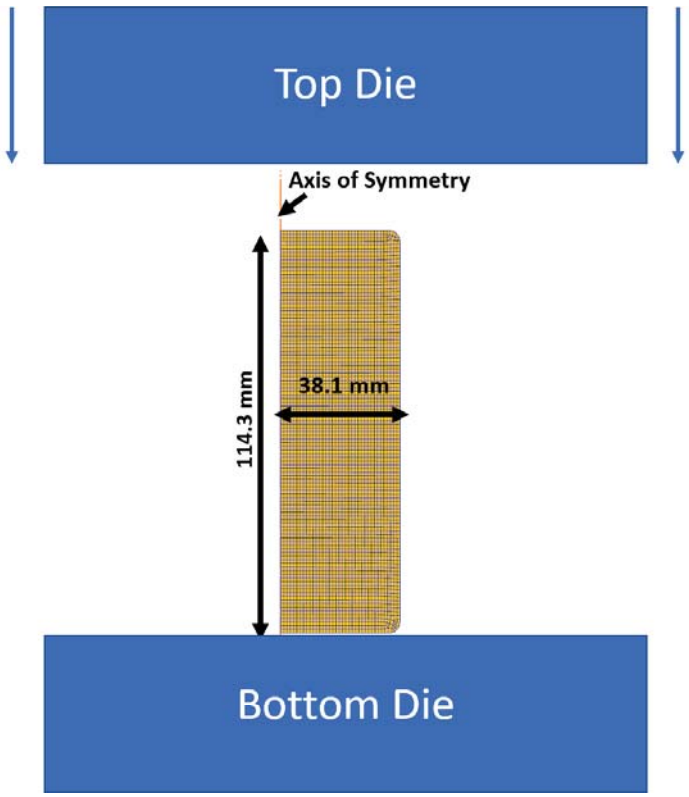

Figure 3.11. 2D axisymmetric upsetting simulation workpiece with 4,000 element mesh.

Full factorial two dimensional simulations were conducted based on the test parameters in Table 3.3. Additional three dimensional simulations were conducted where necessary to gain more insight into specific tests. The simulations were used to guide the selection of parameters for forging tests of the available Ti-6Al-4V workpieces. The selection of forging tests from simulations was based on flow localizations and temperature or strain anomalies. Regions of high local strain or temperature required further analysis and comparison for similar simulations from the test matrix. Forging tests were selected for further analysis based on simulation trends and patterns.

3.6 Forging Tests

Forging tests were conducted based on parameters from selected simulations. A forging test is primarily made up of the workpiece, forging press, and furnace. Mate-

rial for the tests was provided by AFRL and included Ti-6Al-4V cylinders machined to workpiece dimensions for upsetting and sidepressing tests. The titanium was acquired from B&S Aircraft Alloys, Inc in May of 1997. The workpieces were machined from 3 inch diameter and 144 inch length bar stock. The material met Mil-T-9047-G specification for aircraft quality commercially pure Ti-6Al-4V rolled or forged bar and reforging stock products [33]. A comparison of the material specification and the provided chemical composition of the Ti-6Al-4V is shown in Table 3.6 [33]. The provided material meets the maximum chemical composition percent by weight for Ti-6Al-4V [33].

Table 3.6. Ti-6Al-4V chemical composition percent by weight comparison between Mil T-9047-G Specification and provided material

Composition	Al	V	Fe (Max)	C (Max)	N (Max)	H (Max)	O (Max)	Yttrium (Max)
MIL T-9047-G Ti-6Al-4V [33]	5.50-6.75	3.50-4.50	0.3	0.08	0.05	0.015	0.2	0.005
B&S Ti-6Al-4V	6.29	3.80	0.22	0.01	0.01	0.0037	0.17	0.001

The workpieces were previously machined into two sets of samples. Six sidepressing samples were machined to 2.5 inches diameter by 7.5 inches length. A picture of a representative workpiece is shown in Figure 3.12. Additionally, six upsetting samples were machined to 3 inch diameter by 4.5 inches length with $\frac{1}{8}$ inch chamfer on the edges. Chamfers exist on the upsetting workpiece edges due to die chilling effects during forging. Sidepressings do not have the same surface area contact as upsettings because of its orientation on the dies. Upsetting workpieces have complete contact on both ends, which leads to greater heat transfer. As a result, cooling rate is faster at the 90 degree edge because there is less material and may lead to un-deformed or folded material defects. Defects are less likely to occur when a chamfer is used because less material is available for heat transfer. A representative upsetting workpiece

is shown in Figure 3.13.

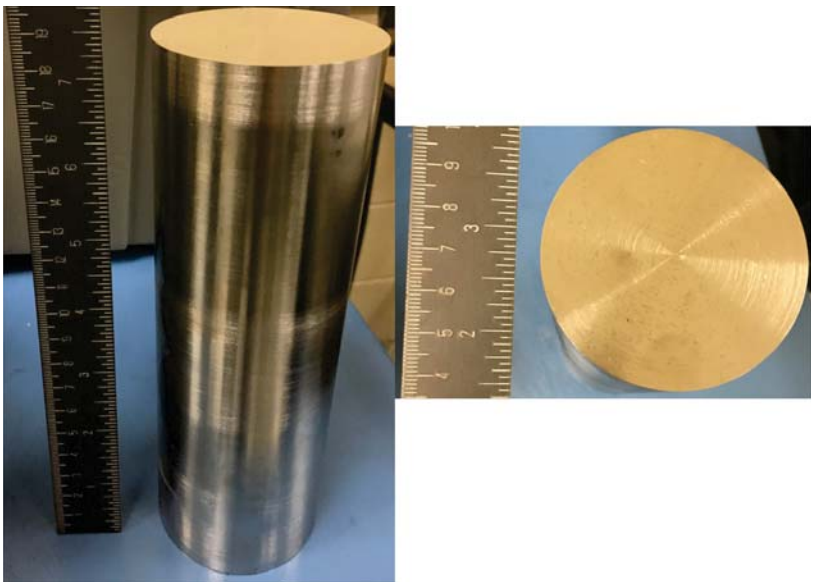

Figure 3.12. A sidepressing workpiece preform machined to 2.5in diameter x 7.5in length

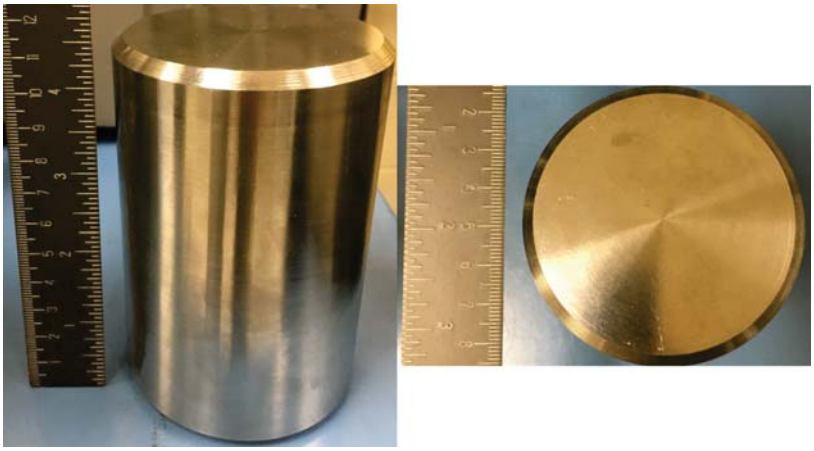

Figure 3.13. An upsetting workpiece preform machined to 3in diameter x 4.5in length

A successful forging is the result of a series of properly timed events. The AFRL Materials and Manufacturing Directorate's 1,000 ton hydraulic forging press custom manufactured by Erie Press Systems was used to conduct forging tests. The side-pressing and upsetting operations use two parallel flat (open) 14 inch diameter dies made from H-13 tooling steel. Additionally, an electric furnace, model NMR-18-4430,

from Harrop Furnace Company was used to heat each workpiece to the desired initial temperature. The entire forging process is conducted by UES, Inc. on-site contractors at AFRL. Prior to forging, each workpiece is coated with Deltaglaze glass billet lubricant and the electric furnace is brought to temperature with the workpiece heated for 90 minutes total time in furnace. Immediately prior to forging, both dies are coated with Fel-Pro C-300 die lubricant and the press operator runs three warm up pressing operations without a workpiece. The billet and die lubricants are important to the reduction of friction during forging. Reduced friction leads to more uniform metal flow and less risk of developing forging defects and is necessary for matching the simulation forging friction coefficient of 0.30 for lubricated hot forgings. Additionally, warming up the forging press is necessary to ensure uniform ram speed through the desired reduction in height of the workpiece.

At the time of forging, each step is conducted as quickly as possible to reduce workpiece cooling when removed from the furnace. A spotter is stationed at the furnace for safety and to measure transfer time of the workpiece from furnace to forging press. Radiation and environmental cooling effects begin immediately when the workpiece is removed from the furnace. Heat transfer and die chilling begin instantly when the workpiece is placed on the bottom die of the press. Transfer time changes to dwelling time when the workpiece is placed on the bottom die and continues until the top die makes contact to signal the start of deformation. Measuring transfer and dwelling time with a stopwatch and recording these values, provides insight to cooling effects and allows for refinement of forging simulations to better predict workpiece temperature, strain, and strain gradient throughout the forging operation. At the conclusion of deformation, the workpiece is removed from the bottom die and placed on metal edges to begin air cooling until cool to the touch.

Figure 3.14. The standard forging process consists of A)removing the workpiece from the furnace and transferring to B) the press where where it dwells until C) the top die contacts the workpiece D) shows the conclusion of deformation. E) The workpiece is removed from the press and F) places on metal edges to air cool.

During deformation the forging press records loading data per die stroke distance. This data is retrieved to identify maximum load and compare against simulation results. Additionally, final workpiece dimensions are measured for comparison before workpiece is prepared for analysis.

3.7 Specimen Preparation

After forging tests are complete, the workpiece is prepared so the internal material can be evaluated and compared against forgings and simulations. Key material features to be evaluated include microstructure size and distribution as well as ma-

terial flow. Obtaining this data requires additional workpiece preparation. First, the workpiece must be sectioned to reveal a surface of the internal material. Next, specimen must be β annealed to achieve the desired microstructure and to emulate thermal processes used in industry. Finally, each specimen surface must be polished and etched to optically reveal the microstructure or metal flow of the material.

3.7.1 Workpiece Sectioning

The first step is to section each forging into specimen to be evaluated. Sectioning exposes the internal material of the forging and offers a glimpse of the overall microstructure of the material. To start, sidepressing workpieces are sectioned into four $\frac{1}{4}$ inch slices from the mid-width. These specimen are oriented so plane strain effects can be evaluated. Assistance from the AFIT model shop was requested to section the material by wire EDM without artificially annealing the specimen with excessive heat. Figure 3.15 shows a representation of the cutting paths used to section each workpiece. Also, their location at the mid-width eliminates cooling effects that may propagate from the ends of the cylinder prior to and during forging. As a result, each specimen from the same workpiece will have only minor differences primarily attributed to prior material inhomogeneity.

Figure 3.15. Sidepressing workpieces have four $\frac{1}{4}$inch slices sectioned for internal microstructural analysis and labeled alphabetically for specimen tracking.

Upsetting workpieces are sectioned into six wedge shaped specimen due to symmetry of the workpiece during forging. Each wedge is wire EDM'ed at a 60 degree angle about the center of the workpiece. Figure 3.16 shows a representation of the cutting paths for sectioning the workpiece. Minimal material variations should exist between specimen. The largest variation will likely result from centering and cutting precision. If the center of the workpiece is not sectioned properly, then forging characteristics of between specimen will be off-center or shifted.

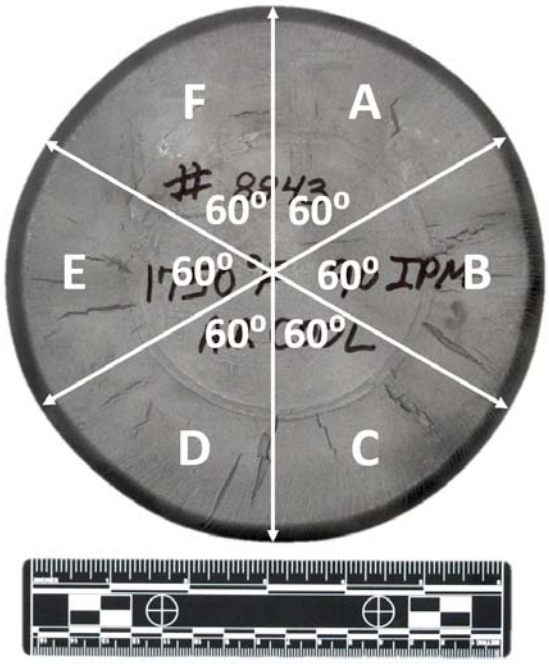

Figure 3.16. Upsetting workpieces have six 60 degree wedges sectioned for internal microstructural analysis and labeled alphabetically for specimen tracking.

3.7.2 Specimen Annealing

As mentioned previously in Section 2.3.6 thermal processing of titanium is used to achieve desired mechanical properties by changing the microstructure of the material. According to the AFRL, the typical annealing process used by manufacturers experiencing AGG is 1037.78 °C for one hour in air with subsequent air or furnace cooling. Therefore the thermal process raises the specimen approximately 100 °C above β transus for one hour. Ti-6Al-4V will transform to an all β microstructure where β grains continue to grow until the material drops below transus.

Traditionally, thermal processing titanium requires an inert atmosphere to limit or prevent exposure to Oxygen. The material develops a brittle α case or oxide layer when heated in regular atmospheric conditions and must be removed before being placed into service. Additionally, cooling rates have large effects on microstructure from developing martensitic structure to coarse lamellar secondary α.

Both in air and vacuum nitrogen annealing thermal processes were emulated in this thesis. The process currently used by industry was conducted at the AFIT model shop with an electric furnace. The furnace was brought to 1037.78 °C and a specimen placed inside for 70 minutes. The first 10 minutes of the annealing process are dedicated to raising the specimen temperature and the remaining 60 minutes represents the hour annealing process. At the end of the process, the specimen was removed from the furnace and placed on the edges of two alumina blocks to air cool. Figure 3.17 shows an example of the furnace in use at the end of an annealing process.

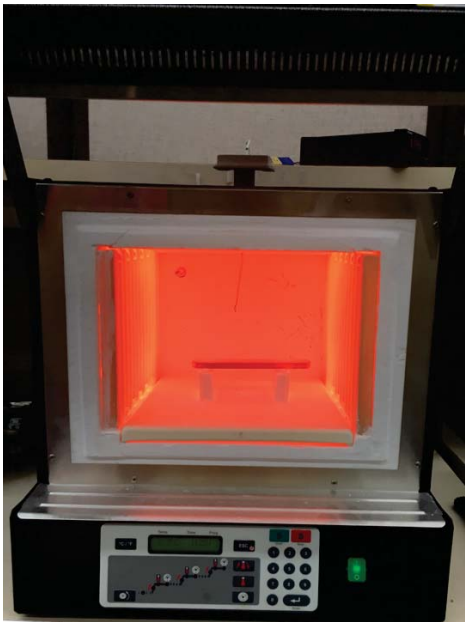

Figure 3.17. An electric furnace was used to anneal Ti-6Al-4V specimen for 70 minutes and then removed to air cool.

Thermal processing of specimen in an oxygen free atmosphere was conducted by Winston Heat Treating Inc. The specimen were placed in a vacuum and annealed at 1037.78 °C for one hour. Next, the specimens were Nitrogen quenched to induce a rapid cooling rate. Winston's annealing process was conducted in a highly controlled environment and the external results convey the difference. Figure 3.18 shows a comparison between the two annealing process. Winston's vacuumed and quenched

sidepressing specimen, appear heat affected by the change in coloration of the titanium. AFIT's open air furnace sidepressing specimen has a large amount of scale flaking from the substrate, revealing the brittle oxide layer. Following the annealing processes, each specimen require surface preparation to optically reveal microstructure.

Figure 3.18. The three sidepressing specimen on the left were β annealed at Winston Heat Treating Inc. in a vacuum, while the one specimen to the right was β annealed at AFIT in oxygen. It is evident that the AFIT annealed specimen was conducted in air due to the large amount of scale on the surface of the material.

3.7.3 Specimen Surface Preparation

3.7.3.1 Oxide Layer Removal

Specimen surface preparation is one of the most critical and delicate steps to preparing the material for optical analysis. Developing a surface preparation process with the resources available between AFIT and AFRL was one of the most challenging aspects to this thesis. The process is based on research described in Section 2.4 and

includes machining, polishing, and etching.

Machining is only necessary for a heat treated specimen to remove the oxide layer. The exact depth of the oxide layer varies between specimen and heat treatments. To ensure removal, 0.03 inches was machined from the surface of interest. Approximately 0.028 inches was milled and the remaining depth was surface ground. The AFIT model shop was essential in removing oxide layers from specimen as the process was not initially intuitive. The first attempts at removal involved a combination of hand polishing with 100 grit silicon carbide paper on a semi-automatic polishing wheel, a pneumatic scotch brite abrasive disk, and etching with HF. These methods did not successfully remove the layer, but instead resulted in a wavy material surface. Additionally, hand polishing with a low grit silicon carbide paper is dangerous and resulted in minor cuts to the hands. Ultimately, the initial specimen were sectioned into smaller pieces using a diamond blade saw and mounted in a compression mounting compound. A semi-automatic polishing wheel was able to secure each mount and use 100 grit silicon carbide paper to effectively remove the oxide layer. Despite successfully removing the layer, the goal of optically evaluating large sections of forgings was not met.

The AFIT model shop was enlisted to improve the oxide removal process. They developed a two step process to include milling and surface grinding. Both steps required high precision machining to reduce variation in surface flatness. The initial milling step accomplished most of the work by removing approximately 0.028 inches of the estimated oxide layer. Surface grinding was then utilized to remove the final 0.003 inches of material. Challenges existed in surface griding each specimen due to the non-magnetic nature of titanium. Typically the model shop uses magnets to secure parts while surface grinding, but was unable to with titanium. In response, they use a Blue Photon Epoxy kit to secure the titanium to a block of steel to allow

controlled grinding. The success of the process enabled evaluation of full size specimen and revealed clear microstructural trends.

3.7.3.2 Surface Polishing

After necessary oxide layers were removed, each specimen required surface polishing. The goal of polishing is to produce a mirror-like, scratch free surface for analysis. Under a microscope, scratches smaller than the grain size are desired so they will not detract or interfere with optical analysis. The forging specimen of this thesis are significantly larger than typical specimen and require non-traditional methods to polish a mirror-like finish. Hand polishing was the most effective method used, but required a lot of experience and time to produce quality finishes. In this method a simple polishing wheel is used with an adhesive silicon carbide paper and water. A lot of variability is created on a material surface if uneven pressure is applied while polishing. Rounding edges and creating wavy surfaces are common errors.

Machining the oxide layer from the material prior to hand polishing allowed finer grit silicon carbide paper to be used initially. The possibility of injuring oneself by hand polishing greatly diminishes with finer grit paper. Sidepressing specimen were particularly challenging because they are $\frac{1}{4}$ inch thick and difficult to hold on a fast spinning surface. The most effective method used for both sets of specimen starts with 240 grit silicon carbide paper and requires polishing until the surface appears uniformly flat. This step typically requires the most time and lasts about 10-15 minutes per specimen depending on initial flatness. Next, each specimen is polished using a sequence of 320, 400, 600, and 800 grit silicon carbide papers ensuring all large scratches are removed from the previous grit paper before using the next finer grit. A mirror like surface is developed after 800 grit, but typically scratches are still noticeable under optical microscope. A Buehler one micrometer TexMet C specialty

polishing pad, with one micrometer water based diamond suspension liquid was used to achieve the final polish. Immediately following, each specimen was rinsed and a blast of compressed air used to dry the surface to prevent staining.

An etchant solution was used to reveal the microstructure of each specimen after polishing. Based on Section 2.4.1 a 2% HF solution with water was used as the etchant. Different methods were used to etch specimen due to their varying sizes. Individual specimens were etched using a pipette to add drops of solution to the surface of interest. The etchant was allowed to sit for approximately one minute to effectively attack the grain boundaries and reveal distinct grains. When multiple specimens were etched, a plastic tub was filled with 200 mL of etchant for bulk etching and the specimen were allowed to sit for approximately 10 minutes to allow distinct grains to be revealed. When each specimen was finished being etched, it was thoroughly rinsed in water and dried with a burst of compressed air to prevent surface staining. The AFRL Materials Integrity Branch head laboratory technician provided assistance in conducting this highly dangerous process. Exposure to HF can be lethal if proper safety equipment, training, and precautions are not taken. Each specimen has been adequately prepared for analysis after etching.

3.8 Specimen Analysis

When each specimen had been prepared they were then be evaluated under microscope to identify grain size, distribution, and metal flow. These results were compared against simulation temperature, strain, strain gradient, and material flow to draw conclusions about the validity of simulations and their capacity to predict large grains.

3.8.1 Specimen Imaging

The initial step in evaluating a specimen is to take macro scale images of the entire surface of interest. This process was completed at AFRL's Materials and Manufacturing Directorate, Materials Integrity Branch using their professional photography stand with Zeiss camera and AxioVision software. Macro images are used as a reference to the location of higher magnification images and can also be used to evaluate patterns or trends in a material. The macro scale images were used for both purposes in this thesis. Specimens were laid out in the same way they were sectioned as shown in Figures 3.15 and 3.16 and were labeled alphabetically for reference. In the interest of organization and process tracking, specimen labeled "A" were β annealed at the AFIT model shop "B"s are as-forged, and "C"s were β annealed at Winston Heat Treating, inc. The remaining specimen were not evaluated, but remain as extra for further research at a different time. Patterns in forging metal flow were evaluated by comparing macro images of as-forged specimen with flow predictions from simulations. Mating surfaces between as-forged and heat treated specimen were also compared for possible forging trends and relationships. After macro imaging was complete, a microscope was used to evaluate grain size and distribution.

Grain analysis was accomplished using a Zeiss inverted microscope to clearly distinguish grain boundaries at AFIT. American Society for Testing and Materials (ASTM) standard E112-13, "Standard Test Methods for Determining Average Grain Size", and ASTM standard E1382-15, "Standard Test Methods for Determining Average Grain Size Using Semiautomatic and Automatic Image Analysis", were used to analyze average grain size of each specimen. [22] [34]. The standards provides a basis for determining average grain size of each specimen by use of the lineal intercept procedure with automatic image analysis. The procedure is used to estimate the average grain size by counting the number of grains intercepted by hundreds of thousands of

lines in 0°, 45°, 90°, and 135° angles from the origin of the image [22] [34]. One test is typically sufficient to estimate grain size, but additional fields of view will improve accuracy of the procedure [22] [34]. For reasonable precision, the standard suggests using the procedure on three to five widely separated fields of view [22] [34]. As a result, each specimen was measured and marked to identify regions of interest to be photographed under microscope.

Regions of interest were selected based on grain patterns observable without magnification and based on overall specimen size. Five regions approximately 12 mm wide spanning the entire height of the specimen and spaced in 10 mm increments were identified on sidepressing specimen. The size and spacing of these regions effectively covered all major patterns and changes in grain size across each specimen. Figure 3.19 shows the layout of the regions on a representative sidepressing specimen.

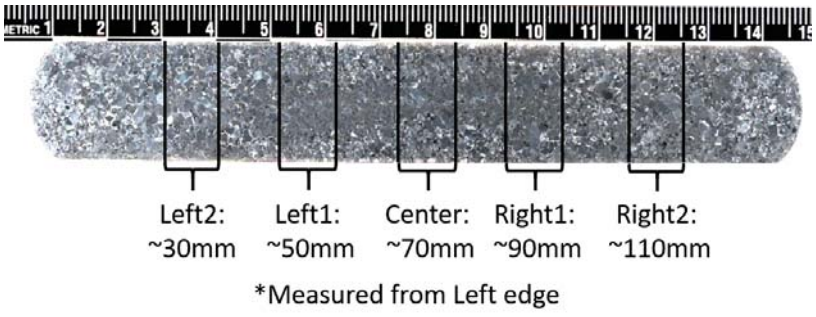

Figure 3.19. Representative sidepressing regions of interest measured from the left edge of the specimen starting at 30 mm from the edge and measured in 20 mm increments. The locations were selected by specimen comparison to cover all major observable grain patterns.

Six regions of interest approximately 12 mm wide spanning the entire height of the specimen and spaced in 10 mm increments were identified on upsetting specimen. Each specimen has two polished surfaces and therefore three regions of interest were identified on each side and measured from the center edge. Figure 3.19 shows the layout of the regions on a representative upsetting specimen. Using the lineal intercept method on multiple planes of the same specimen will improve the accuracy and

precision of the average grain size analysis [22] [34].

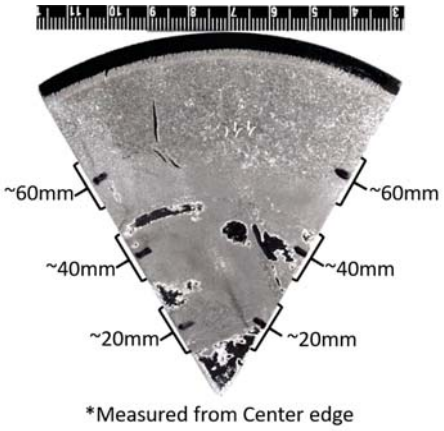

Figure 3.20. Representative upsetting regions of interest measured from the center edge of the specimen starting at 20 mm **from the edge and measured in** 20 mm **increments. The locations were selected by specimen comparison to cover all major observable grain patterns.**

Each region of interest was photographed at 2.5x magnification using a Zeiss inverted microscope. The microscope was initially configured with an automatic slide table and AxioVision software. Producing images spanning an entire region of interest proved challenging because a single image at 2.5x magnification can only capture a portion of the region. To establish an average grain size and distribution, it is essential to have one continuous image of a region for analysis. To resolve the issue, it was discovered that Zeiss has an AxioVision software package, called Mosaix, that allows the user to program the microscope and automatic stage to take a series of images in a predefined region. The tiled images are later stitched and compiled to produce a single continuous image. The acquisition of Mosaix to the existing AxioVision software allowed for a greater range of imaging analysis.

Mosaix was applied to this research by defining the region of interest labeled on each specimen into the imaging software. An overall rectangle consisting of eight columns by eleven rows of image tiles was used. A 20% image overlap was assigned to ensure accurate stitching after image tiles were acquired. Due to slight rotation

in image acquisition by slide motion, the compiled image was cropped as necessary to produce an image of the overall region of interest. An example of a resulting tiled image is shown in Figure 3.21

Figure 3.21. Example of a 11x8 tiled image from Mosaix.

3.8.2 Determination of Average Grain Size

In continuation of the lineal intercept procedure, a matlab program produced by Funk and Meister designed to assist in the procedure was used to analyze grain size [35]. The code produces a Graphical User Interface (GUI) that allows a user to upload an image, assign scaling via scale bar and pixel ratio, overlay lines, and manually select grain intersections [35]. The value of this code comes from automatically counting and measuring all user intersection selections and compiles the information into a data text file. The file can be used to produce a cumulative distribution function of linear intercept lengths and provides average length [35]. The average intercept length is used in the ASTM standard E112-13 to determine the average grain size number, which relates the length to average grain diameter and area [22].

Each image evaluated was at 2.5x magnification and therefore does not directly relate to the grain size numbers provided in the standard. Therefore, the linear intercept lengths must be converted to 1x magnification [22]. Equation 3.2 is used to convert between the mean intercept length measured from the image to the length used in the ASTM standard [22].

$$\bar{l}_o = \bar{l}\frac{M}{M_b} \tag{3.2}$$

Where $\bar{l}$ represents the mean lineal intercept length of the image, $\bar{l}_o$ represents the mean lineal intercept length at the magnification of the ASTM standard, M is the magnification of the image, and M_o is the magnification used in the ASTM standard [22]. The ASTM grain size number can be determined from the converted mean lineal intercept length through equation 3.3 [22].

$$G_o = 2 \cdot \log_2 \frac{32\,\text{mm}}{\bar{l}_o} \tag{3.3}$$

In this equation, G_o represents the apparent ASTM grain size number [22]. Still, a magnification correction factor must be applied when using the grain size number with the ASTM macroscopic grain size relationship chart from the standard [22]. The expression for the correction factor is shown in equation 3.4 [22].

$$G = G_o + Q \tag{3.4}$$

where

$$Q = 2 \cdot \log_2 \frac{M}{M_b}$$

In the above equation, G represents the actual ASTM grain size number and Q represents the correction factor for comparison of ASTM chart ratings using a

non-standard magnification for macroscopically determined grain sizes [22]. Upon determination of G, the macroscopic grain size relationship table from ASTM standard E112-13 can be used to determine grains per unit area, average grain area, and average grain diameter [22]. The value determined for each specimen can be compared to determine the effect of forging parameters on average grain size.

3.8.3 Determination of Grain Distribution

The last step to image analysis is to determine the grain size distribution across the height of each region of interest. This analysis was the most time intensive of the three because Ti-6Al-4V is a two phase material and does not produce simple clean grain boundaries. Additionally, the texture and grain orientation of an optical image creates bright and dark reflections of light that further complicate image processing and analysis. Currently, AFIT does not have software available to automatically process optical two phase grain boundary images. As a result, each image was altered by manually tracing prior β grain boundaries through image editing software. The selection of each boundary allowed the removal of all other microstructural features so image analysis could be conducted without additional complications.

A Matlab code was adopted from Lehto's "Point-Sampled Intercept Length Measurement Code" to evaluate the processed images for grain size distribution and volume-weighted average grain size [36][37]. This code specifically, characterizes the local variation of grain size in each region of interest captured earlier [37]. The code uses a point-sampled intercept method to measure grain size [37]. Given a material with clearly defined grains, the code produces a large number of random points throughout the image [37]. When a point hits a grain interior(does not touch a boundary line) a line is generated in the direction of current analysis and terminates when it contacts a grain boundary [37]. Similar to the lineal intercept method, 0°, 45°, 90°,

and 135° line orientations are iterated through the code [37]. The results from each direction are combined to produce a densely measured grain size [37].

The code presents grain size distribution across the X and Y axes of the image and a contour plot using the Hall-Petch grain size parameter $d^{-0.5}$ [37]. Traditionally, the parameter is used to show the effect of change in grain size on mechanical properties, but in this thesis is only used to improve the resolution of change in grain size [37]. It is important to note, large grains correspond to lower Hall-Petch values and vice-versa. This is based on large grains being associated with low strength due to the length of slip bands, causing them to yield before smaller grains [38].

Additionally, the code calculates a volume-weighted average grain size from the point-sampled intercept method [38]. Equation 3.5 defines volume weighted grain size [38].

$$d_v = \frac{1}{V_T} \sum V_i d_i \tag{3.5}$$

Where d_v is the volume weighted grain size, V_T is the total volume of the material, V_i is the volume of grains corresponding to the grain size d_i. Determining three dimensional grain information is highly labor intensive and therefore, this method uses three dimensional estimations from the images selected. By use of the point-sampled intercept method, the different grains sizes are measured proportionally to their surface area fractions. As a result, Lehto et al. are able to use relationships of stereology and the surface area fraction to estimate the volume fraction. This means the average value of the distribution can be considered the volume-weighted average grain size, d_v [38].

Grain size distribution of Ti-6Al-4V is of particular interest because effects of AGG on mechanical properties is not yet well understood. This technique, if paired with mechanical testing, may offer unique insight into the effects of non-uniform dispersion

of large grains on titanium's mechanical properties.

3.9 Summary

This chapter summarized the methods used to test the effect of temperature, reduction in height, and forging speed on the development of AGG in titanium forgings. The investigation was conducted using computational simulations, forgings, and optical analysis. The FEM was used as a foundation to predict the potential results of various forging parameters on sidepressing and upsetting tests. Based on these results, select forging tests were conducted and processed for optical analysis to determine grain size and distribution. The forging tests were then compared to determine the effects of forging parameters on development of AGG. The next chapter of this thesis analyzes these results and discusses notable findings.

IV. Results

4.1 Chapter Overview

The goal of this thesis is to demonstrate that Finite Element Method (FEM) simulations can be used to correlate experimental conditions to forging Abnormal Grain Growth (AGG). As mentioned in Chapters II and III, the forging parameters of focus in this research are initial furnace temperature, ram speed, and reduction in height. Varying these parameters in Design Environment for Forming (DEFORM) simulations allowed for the analysis of workpiece strain, temperature, and material flow. Variables that resulted in areas of localized strain and temperature led to the forging tests at this condition that were conducted by the Air Force Research Laboratory (AFRL). Each forging workpiece was prepared for metallography and extensively photographed. These images were processed and evaluated with the lineal intercept and point-sampled intercept methods to determine grain size and distribution across specimen to determine conditions, if any, that led to the development of AGG.

4.2 Sidepressing Results

Sidepressing was the first forging test of focus for this thesis. Sidepress forging simulations are more challenging than upsetting because it represents a plane strain forging and cannot be simulated axisymmetrically. In the time available to complete this work, all two and three dimensional design of experiments sidepressing simulations and four forging tests were conducted.

As described in Sections 3.4 and 3.5, the DEFORM simulations were based on, and validated from previous work conducted by AFRL. Updates to the baseline model simulations used in this thesis were made based on advisor input and research described in Section 3.5. Using the validated simulation as a foundation, sidepressing

simulation tests were developed based on the test matrix from Table 3.3. Internal strain, temperature, and metal flow predictions were then evaluated and compared against simulations with similar parameters. Analysis of these results guided the decision of forging parameters to be used in forging trials.

Simulations for sidepressing tests can be represented both two and three dimensionally. However, as a plane strain test, some information is lost when only simulated in two dimensions. Two-dimensionally, the workpiece can be represented by a circle, but must also be simulated in three dimension to account for axial deformation that is otherwise simplified. The difference between the two sets of simulations is noticeable as tests result with greater strain when the material cannot flow in the third, axial, dimension.

As sidepressing simulations were conducted it was clear that 80% reduction in height was too far for further analysis. The sidepressing workpieces used were 2.5inches in diameter leaving 0.5 inch of material height after forging for 80%. The small remaining height of the specimen was challenging to analyze in simulations due to highly concentrated strain, temperature, and flow results. In contrast, the 65% reduction offered clearer images for analysis while still achieving high temperature and strain localizations. Additionally, it would have also been very difficult to process and evaluate in a forging test. As discovered in specimen preparation, the smaller the object, the harder to polish by hand. The specimen would have been very wide, but only 0.25 inches thick and 0.5 inches tall. Even adhering epoxy to a surface to mount a grip would have been challenging because of the limited surface width. As a result, this sidepressing research is focused only on 65% reduction in height processes because it was predicted that more meaningful results would exist.

4.2.0.1 Sidepressing Simulation Temperature Results

Two dimensional temperature contours from the simulations are shown in Figure 4.1. These results are cropped at the midwidth line of symmetry (z-axis) to allow for easier analysis. They are divided into two columns that represent the two initial furnace temperatures analyzed, 913 °C and 955 °C. Additionally, the figure is divided into three rows representing the three different ram speeds analyzed: 8.5 $\frac{\text{mm}}{\text{s}}$, 25.4 $\frac{\text{mm}}{\text{s}}$, 38.1 $\frac{\text{mm}}{\text{s}}$. Each test condition is labeled directly above the simulation contour image. This is the standard layout for all simulation images depicted in this thesis.

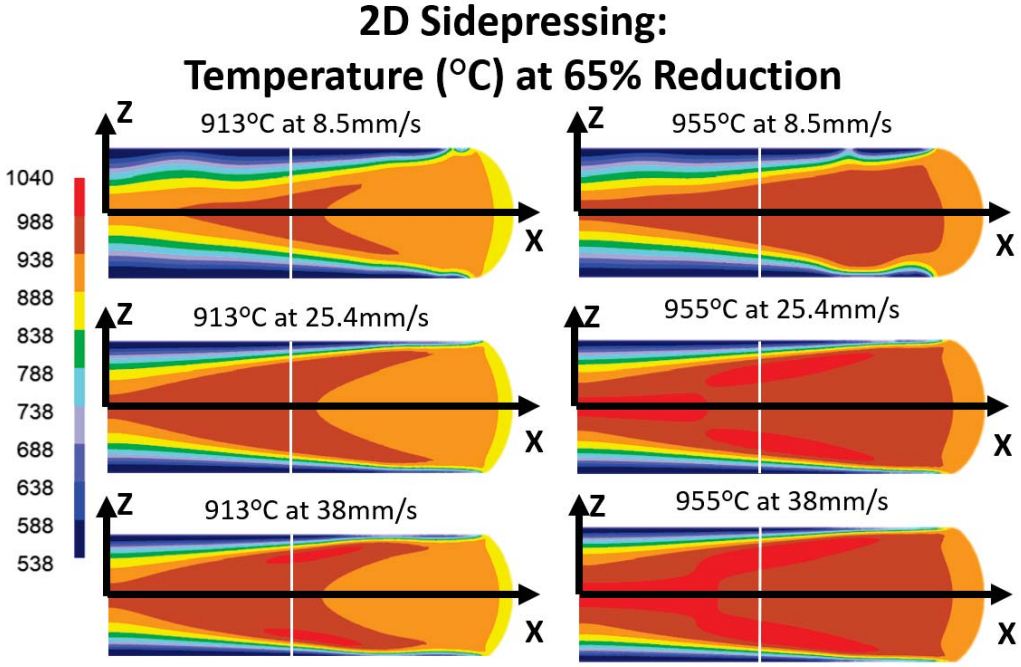

Figure 4.1. The two-dimensional sidepressing results conducted at 65% reduction are shown at the midwidth of the workpiece, cut in half at the midwidth of the specimen due to symmetry and for better clarity. The images are organized into two columns for each temperature and three rows for each ram speed. Faster ram speed resulted in greater internal heat generation in the specimen causing some regions to exceed the β transus(993 °C).

Figure 4.2 shows four plots related to the contour images in Figure 4.1 before it. These plots are also organized in two columns representative of the two initial furnace temperatures. The first row of plots represents temperature data collected

along the vertical line of symmetry of the simulation image where the x-axis is zero. The second row represents a similar line of data collected at an offset location from the line of symmetry. In the case of sidepressing simulations, this line of data is located 31.75 mm from the line of symmetry and is represented by a white vertical line in the contour image. This format for data distribution plots is also the same throughout this thesis.

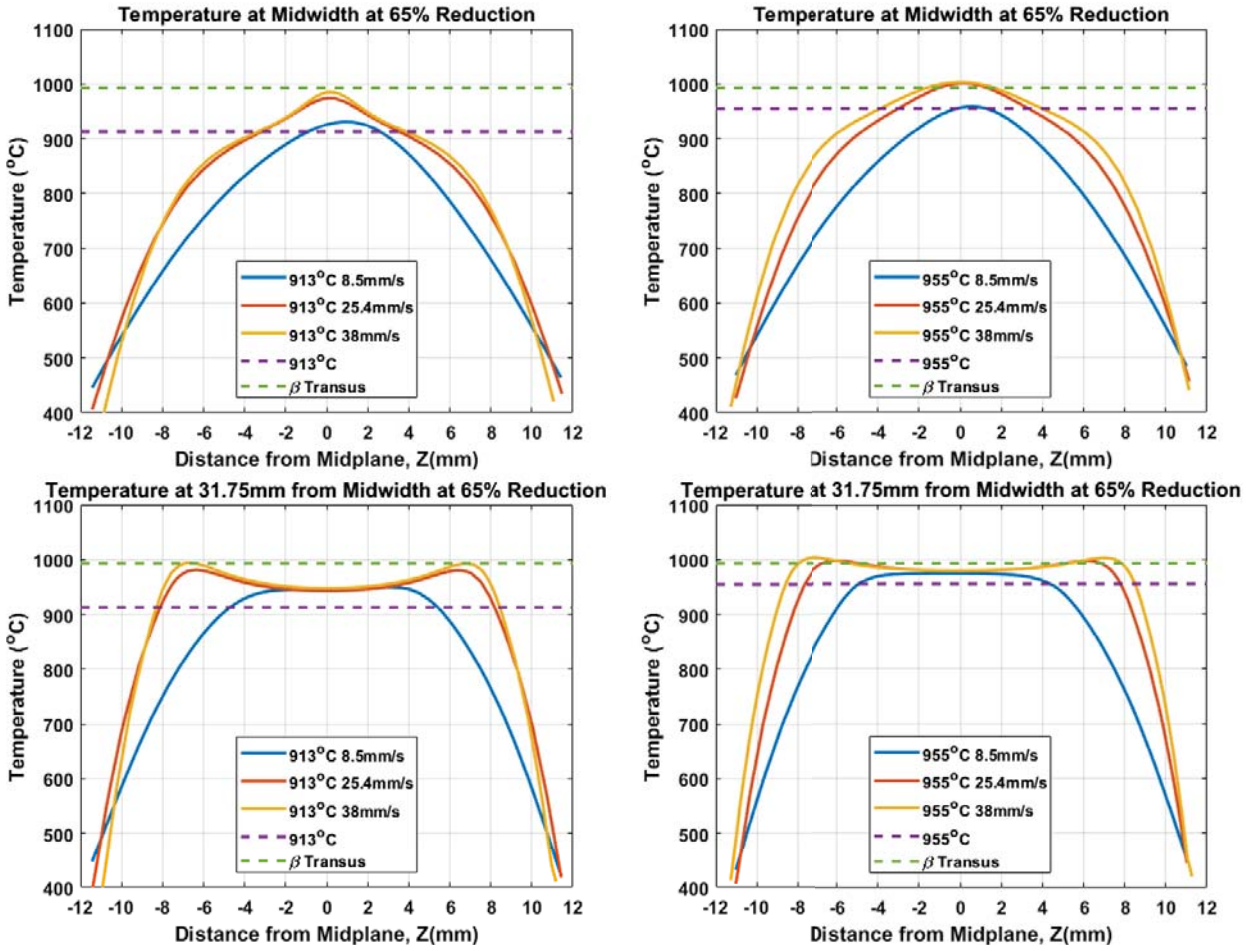

Figure 4.2. The plots depict temperature distribution of each simulation from Figure 4.1. The left column shows results from 913 °C simulations and the right from 955 °C simulations. The top row depicts temperature data from the vertical midwidth line/ line of symmetry of the specimen along the z-axis, while the bottom row depicts temperature data from a vertical line 31.75 mm from the line of symmetry along the z-axis. The location of this data is represented in Figure 4.1 by a vertical white line. Initial furnace temperature and β transus are plotted for reference.

Clear trends exist when evaluating Figures 4.1 and 4.2. One notable trend is when

ram speed increases, internal temperature increases. The first reason this is an intuitive trend is because forgings have less time for heat transfer when the workpiece is forged faster. With less heat loss from die chill, the workpiece should be hotter overall. Second, material naturally resists deformation and generates internal heat when deformed. Faster ram speeds deform a workpiece at a higher rate and is more likely to generate heat as a result. This trend is also supported by the plots in Figure 4.2. In each plot the initial forging temperature and β transus are shown as reference. A portion of every forging simulated exceeds the initial forging temperature, confirming deformation heat generation. In some cases the heat generated causes a temperature localization to exceed the β transus. This occurred in both fast ram speed simulations and the higher temperature moderate ram speed simulations. Closer evaluation of each of these simulations showed a prediction that the material would exceed β transus temperature for no more than two seconds, essentially pre-exposing the material to β phase before being β annealed. This observation led to the moderate and fast ram speeds at 955 °C being selected for forging trial because they predict exceeding the β transus.

Additionally, the effects of die chill are noticeable in these simulations. Every temperature contour image shows notably lower temperatures at the bottom and top of the simulation where dies make contact with the specimen. The faster the ram speed the smaller and less intrusive this dead zone is to the core of the material. This observation further supports the conjecture that faster ram speeds result in higher temperature workpieces. Furthermore, the effects of die chill are observable in each plot in Figure 4.2 because the moderate and fast ram speeds have a higher temperature across a larger distance from the midplane of the workpiece. This produces a broader appearing arch in each plot, whereas the slow ram speed has a lower temperature slope leading up to the midplane.

Three-dimensional temperature contours showed similar trends as described with the previous figures but to a lesser degree. This may be the result of two factors, a coarse mesh or computation in a third dimension. The contour images are shown in Figure 4.3. It is clear that the simulations have a coarse mesh from the lack of smooth contour lines. The three dimensional simulations were only conducted with a 100,000 element mesh due to computational limitations at the time. Further analysis was not prioritized due to a tight research schedule. The coarse mesh may be one factor contributing lower temperatures. Another reason lower temperatures are likely is because there was less heat generated in three-dimensions from the material being able to deform axially. In these contours only the high temperature, high ram speed simulation show signs of approaching the β transus.

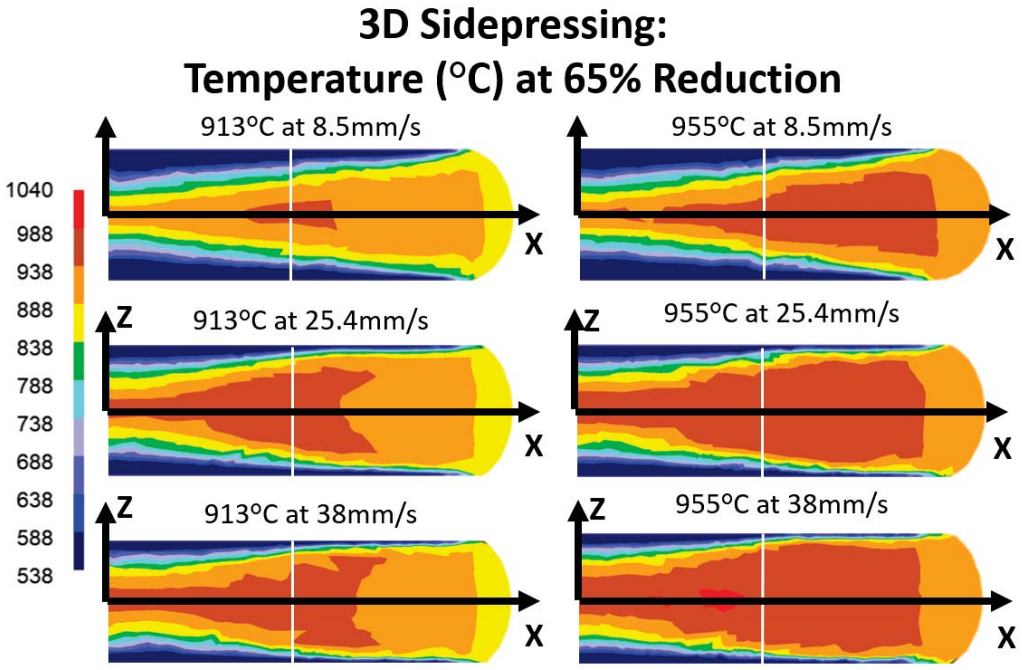

Figure 4.3. The three-dimensional sidepressing results conducted at 65% reduction are shown at the midwidth of the workpiece, cut in half at the midwidth of the specimen due to symmetry and for better clarity. The images are organized into two columns for each temperature and three rows for each ram speed. Faster ram speed resulted in greater internal heat generation between both sets of temperature. Only 955 °C at 38 $\frac{\text{mm}}{\text{s}}$ showed signs of exceeding β transus(993 °C).

Figure 4.4 shows both two dimensional and three dimensional temperature data plotted against each other. Overall, the three dimensional data has a steeper slope than the two dimension data, indicating a larger effect from die chill on the top and bottom surfaces. When evaluated from the line of symmetry, a temperature bias is also noticeable. The bottom surface of the workpiece is in contact with the bottom die longer than the top die with the top surface. As a result, the bottom material will be cooler than the top and have a larger dead zone. Therefore, in the plots, the temperature curve is slightly skewed so the peak temperature is slightly closer to the top surface.

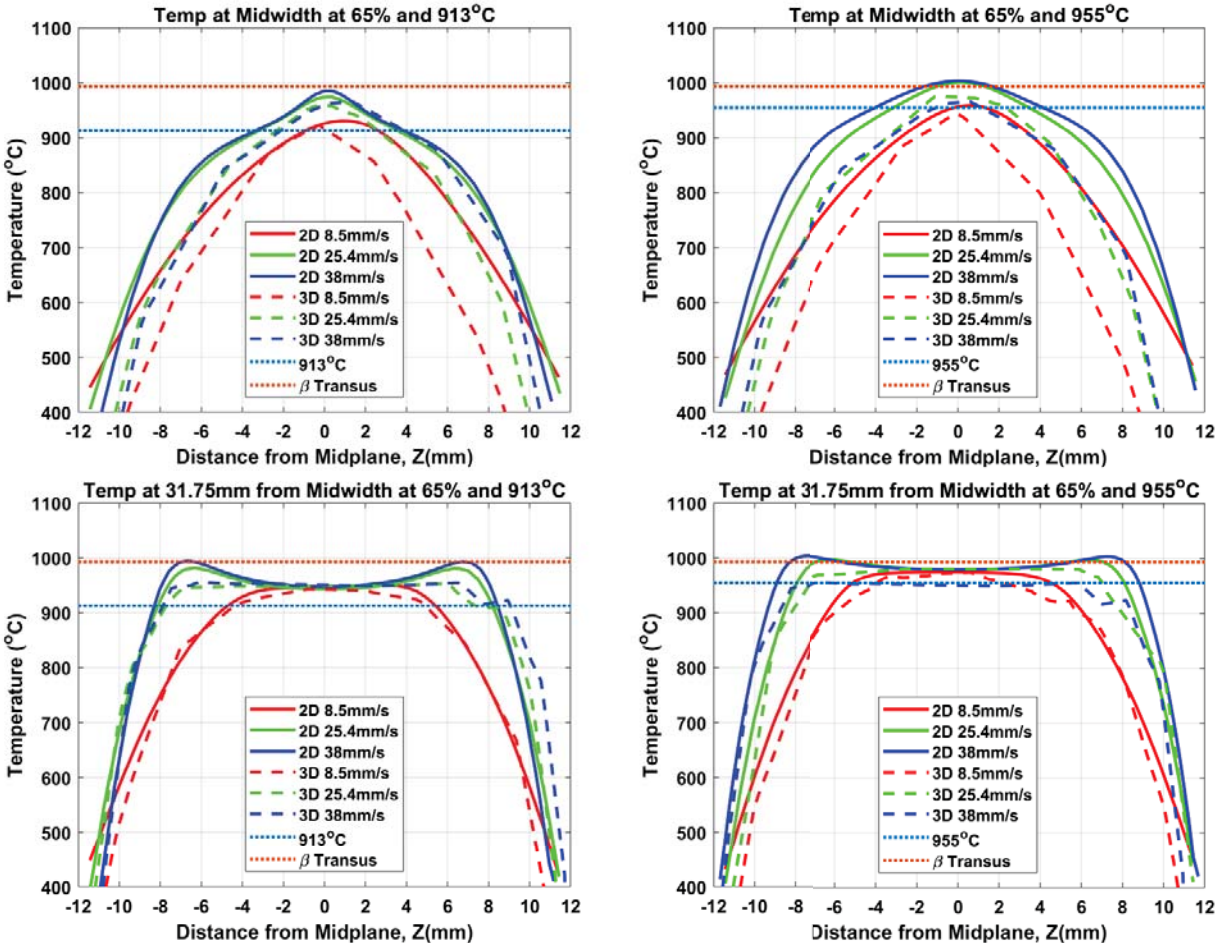

Figure 4.4. The plots depict temperature distribution comparisons of each simulation from Figures 4.1 and 4.3. The left column shows results from 913 °C simulations and the right from 955 °C simulations. The top row depicts temperature data from the vertical midwidth line/ line of symmetry of the specimen along the z-axis. The bottom row depicts temperature data from a vertical line 31.75 mm from the line of symmetry along the z-axis. The location of this data is represented in Figures 4.1 and 4.3 by a vertical white line. Initial furnace temperature and β transus are plotted for reference.

4.2.0.2 Sidepressing Simulation Strain Results

Two and three dimensional strain contours and plots are represented similar to temperature, but depict different trends. Figures 4.5 and 4.6 shows the contour images and plots for two dimensional simulations. It is difficult to observe a clear trend in the effective strain contour images of Figure 4.5. Clearly shearing is occurring in the images by the "X" shape contour, but the severity of the strain in each region and the degree of localization is not easily determined. The distribution plots in Figure 4.6 provides clearer insight. In each workpiece, low strain exists in the dead zones near the top and bottom surfaces where the dies contact the material. This is represented by the low temperature to the left and right of each plot. These regions exists from heat transfer between the workpiece and dies resulting in two distinct cool zones that are less likely to deform than hotter material regions. Material flow is limited in dead zones and instead causes hotter areas to deform resulting in shearing and large strain localizations. At the midwidth of the workpiece, where X equals zero, a peak strain occurs between both dead zones. This is caused by cooler material resisting deformation more than the hotter core material resulting in greater strain between the dead zones. Each 913 °C workpiece has very similar peak strains along the line of symmetry. The larges difference results from the slow ram speed with a peak strain biased towards the top surface due to longer forging time, greater heat transfer through the bottom surface, and a larger bottom dead zone. The simulations at 955 °C generally have smaller dead zones and lower peak strains with the exception of the low ram speed condition. Faster forging speeds at this temperature resulted in less heat transfer and lowered the peak strain.

Shear strains appear to be largest near the offset locations in Figures 4.5 and 4.6. At 913 °C, shear strain is larger at faster ram speed, while at 955 °C slower ram speeds results in larger shear strain. Both sets of temperatures share similar curve

profiles between ram speeds with the most notable difference being peak strain values between the slowest ram speeds. Ram speed will have a large effect on the location of strain peaks at this location due to dead zones caused by die chill. Slower speeds will have larger chilled zones due to more time for heat transfer. Interestingly, at 955 °C the slower ram speed shows much larger strain values than the same simulation at 913 °C. The likeliest explanation for this phenomenon, aside from slow speed, is the temperature gradient during deformation. The higher temperature forging requires more heat transfer to achieve an equilibrium state than the lower temperature forging. The the amount of temperature change during deformation may be such that strain is significantly greater. The abnormal difference between strain values is significant enough to warrant further evaluation by selecting these parameters for forging trial.

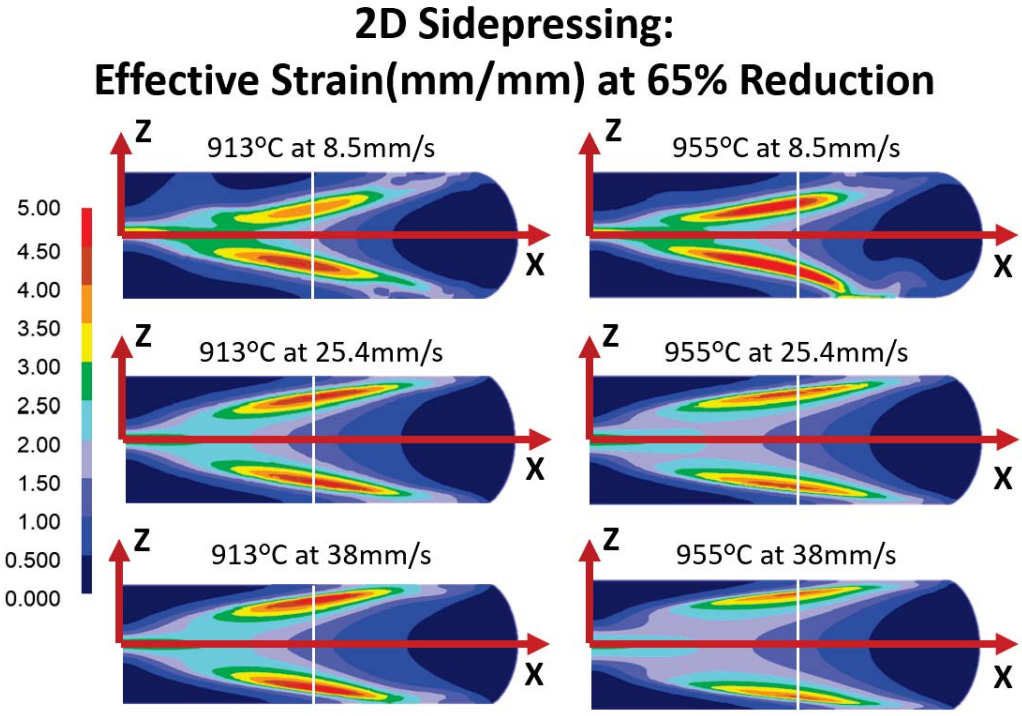

Figure 4.5. The two-dimensional sidepressing results conducted at 65% reduction are shown at the midwidth of the workpiece, cut in half at the midwidth of the specimen due to symmetry and for better clarity. The images are organized into two columns for each initial furnace temperature and three rows for each ram speed. Faster ram speed generally resulted in less severe strain localization due to less time for heat transfer and die chilling effects.

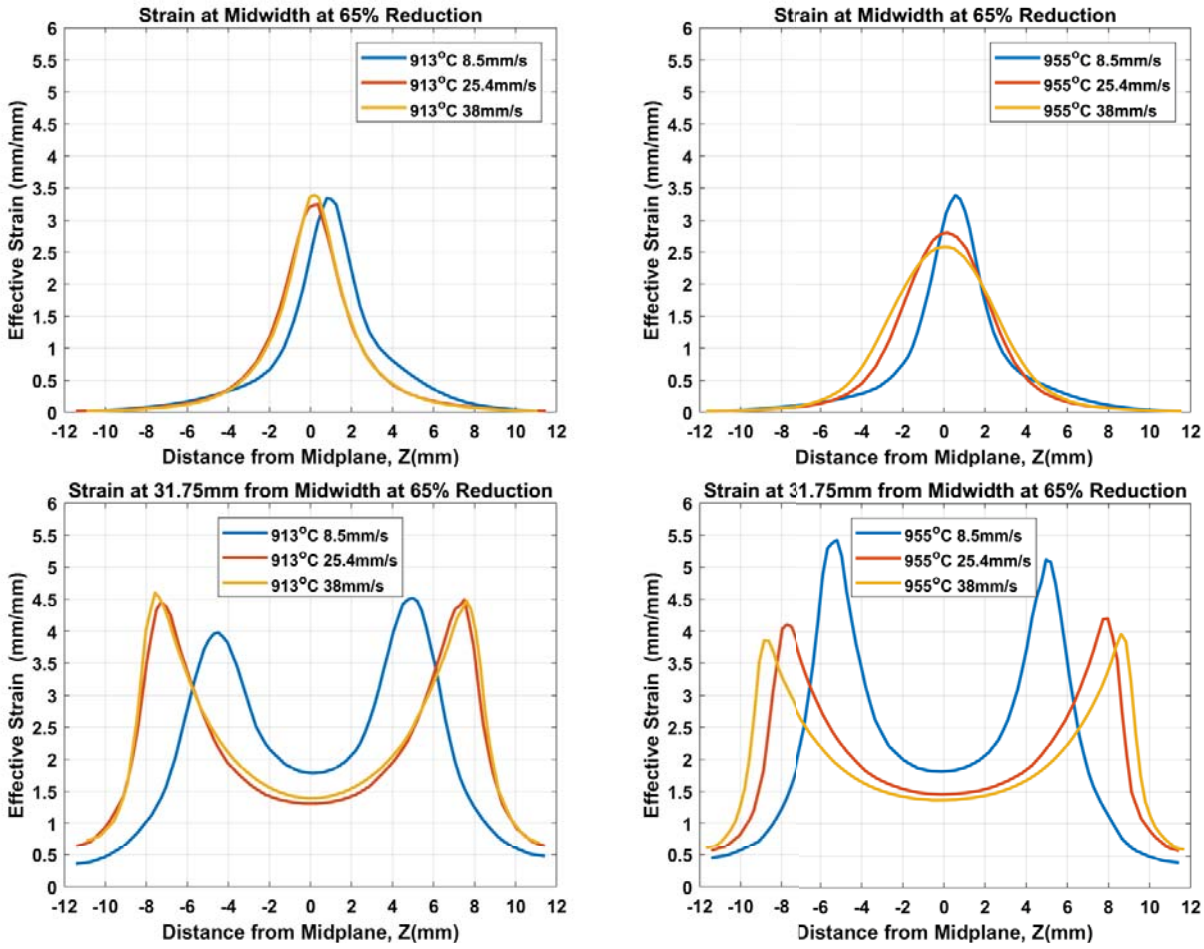

Figure 4.6. The plots depict strain distribution of each simulation from Figure 4.5. The left column shows results from 913 °C simulations and the right from 955 °C simulations. The top row depicts strain data from the vertical midwidth line/ line of symmetry of the specimen along the z-axis, while the bottom row depicts strain data from a vertical line 31.75 mm from the line of symmetry along the z-axis. The location of this data is represented in Figure 4.5 by a vertical white line.

The three dimensional strain results are noticeably more coarse in Figures 4.7 and 4.8 when compared to the two dimensional results. A mesh with approximately 100,000 elements was used due to computational limitations at the time of these simulations. The mesh is coarse and needs a much larger number of elements to achieve finer results. Before receiving additional licensed cores, it would take the majority of a day to complete a single simulation. In the interest of time, a convergence study could not be accomplished and two and three dimensional results had to be analyzed

together to form a more reasonable prediction. Simulation trends seen in the two dimensional strain results were similar to the respective three dimensional simulations. Of notable similarity, though to a lesser degree, is the abnormal larger strain curve produced along the offset location of the 955 °C, slow ram speed simulation. These results further justify the selection of this condition for testing.

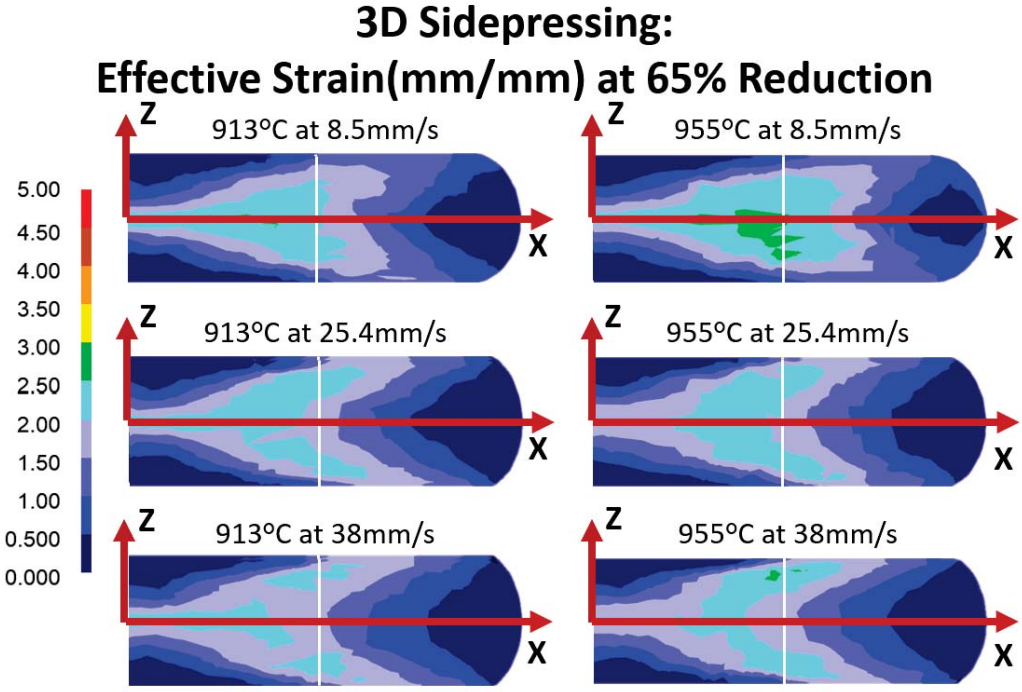

Figure 4.7. The Three-dimensional sidepressing results conducted at 65% reduction are shown at the midwidth of the workpiece, cut in half at the midwidth of the specimen due to symmetry and for better clarity. The images are organized into two columns for each temperature and three rows for each ram speed. Faster ram speed resulted in less strain localization and overall less strain in the material. This is likely the result of faster forging, less heat transfer, and therefore less die chill effect.

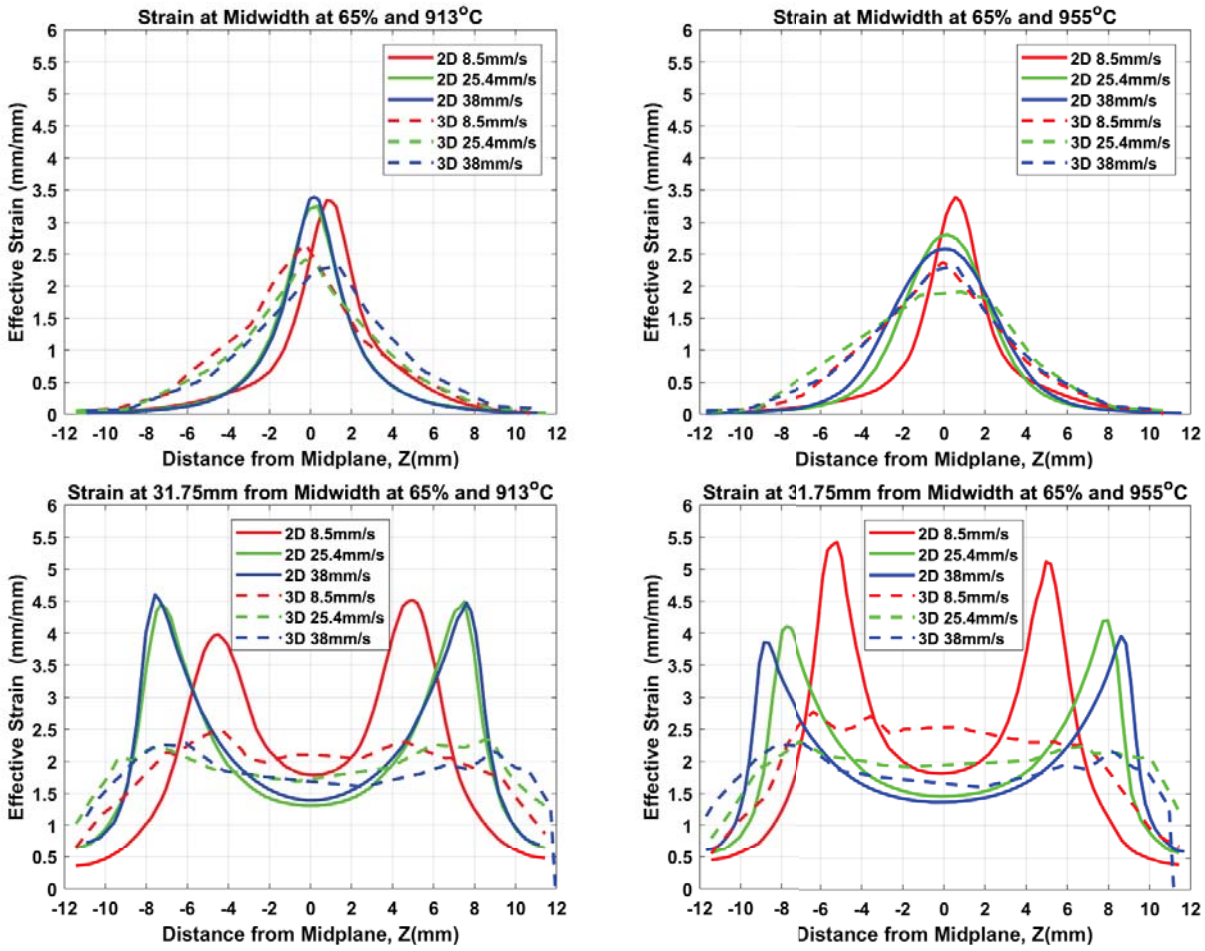

Figure 4.8. The plots depict strain distribution of each simulation from Figures 4.5 and 4.7. The left column shows results from 913 °C simulations and the right from 955 °C simulations. The top row depicts strain data from the vertical midwidth line (line of symmetry) of the specimen along the z-axis, while the bottom row depicts strain data from a vertical line 31.75 mm from the line of symmetry along the z-axis. The location of this data is represented in Figures 4.5 and 4.7 by a vertical white line.

4.2.0.3 Sidepressing Simulation Flow Results

The final results used to guide selection of forging trial conditions were material flow predictions using DEFORM floewnet tool. The flownet results are shown in Figure 4.9. The impact of ram speed on material flow is evident by the change of dead zones sizes between simulations. The dead zones are visible at the top and bottom surfaces with regions of normal strain indicated by grid lines closer to perpendicular angles. At 913 °C material flow appears to be concentrated at the core of

the simulation from a more densely gathered set of lines indicating large shear strain emanating from this position. In contrast, simulations at 955 °C appear slightly more uniformly spaced near the core. There are many similarities between each simulation and therefore, challenging to draw any strong conclusions from these results. The most notable observation from the flownet are indications of larger shear strain present predominately in the higher temperature simulations.

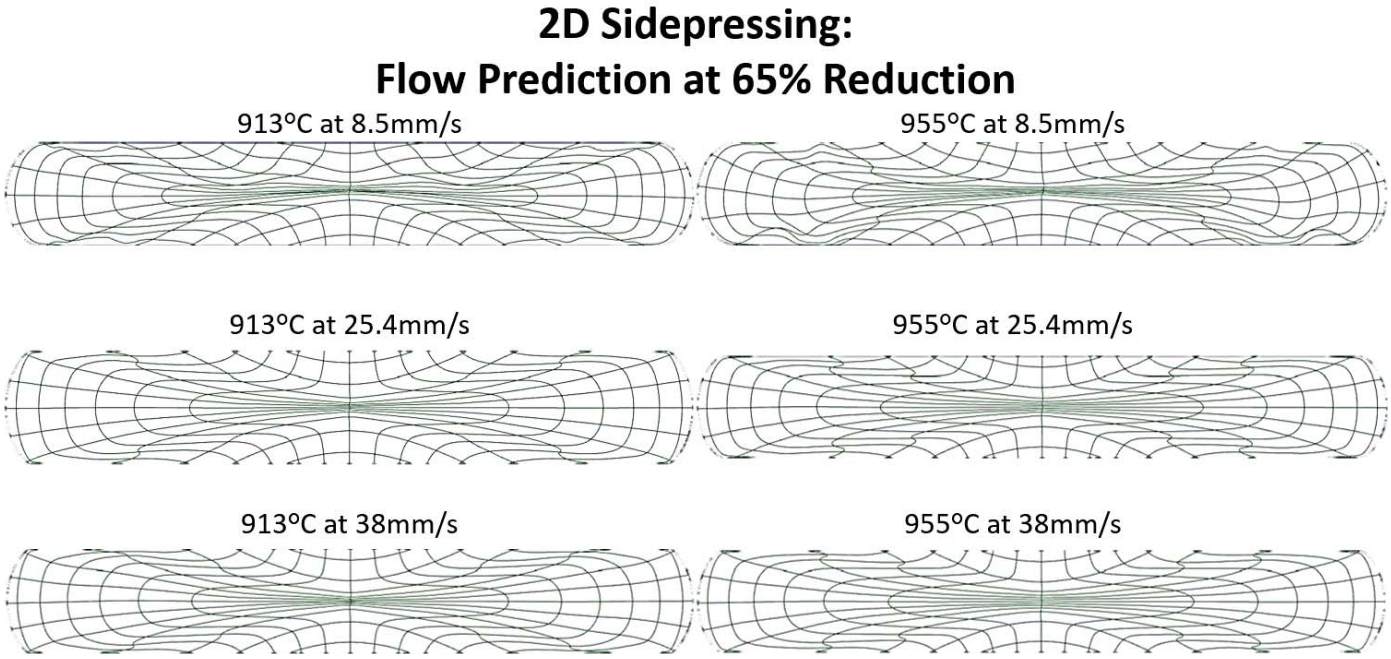

Figure 4.9. The two-dimensional sidepressing results conducted at 65% reduction are shown at the midwidth of the workpiece. The images are organized into two columns for each temperature and three rows for each ram speed.

4.2.0.4 Sidepressing Forging Test Conditions

Four simulation conditions were selected for forging trials based on the observations gathered from the simulation results. The Initial hypothesis developed for AGG was that large strain localizations from shearing may have a significant effect on development. As a result, simulations at 913 °C with 25.4 $\frac{\text{mm}}{\text{s}}$ and 955 °C with 8.5 $\frac{\text{mm}}{\text{s}}$ and 25.4 $\frac{\text{mm}}{\text{s}}$ were hypothesized to most likely result in AGG or coarse β grains. Sim-

ulation 913 °C with 8.5 $\frac{mm}{s}$ was not selected due to concerns that deformation load might exceed the capacity of the hydraulic press. After processing the material, the only sign of AGG were found in 955 °C with 25.4 $\frac{mm}{s}$.

A new hypothesis was developed based on large deformation heat generated in the simulations conducted at 955 °C with 25.4 $\frac{mm}{s}$ and 38 $\frac{mm}{s}$. Both simulations exceeded β transus, potentially exposing the material to β phase prior to annealing. The impact of this effect was unclear and was hypothesized to result in early development of β grains. If this occurred, then the β grains in this region would likely grow larger or coarser than the surrounding grains that were not pre-exposed to the β phase. Result of the forging trial at 955 °C with 38 $\frac{mm}{s}$ were more promising, linking simulation results to forging results. A summary of the conditions selected for sidepressing forging tests is shown in Table 4.1.

Table 4.1. Selected sidepressing forging test conditions base on simulation predictions

Forging No.	Temperature (°C)	Ram Speed ($\frac{mm}{s}$)	% Reduction	Signs of AGG
8835	955	25.4	65	Yes
8836	955	8.5	65	No
8837	913	25.4	65	No
8842	955	38	65	Yes

4.2.1 Forging Results

Forging results were tedious to analyze and required a lot of material preparation. Only three specimen from each of the four forgings were prepared and analyzed for microstructural characteristics. Initial efforts resulted in poor quality material preparation, however, after many processing attempts, results became more clear and easy to analyze. Key characteristics are evident in the open air β annealed specimen and the microstructure is optically clearer than the Winston heat treatments. This is likely the result of being β annealed in a vacuum and nitrogen quenched. The grain

boundaries are less prominent because less precipitate was able to form under more controlled conditions. Additionally, grain size appears optically smaller than the open air β annealed specimen and is also likely due to the more controlled conditions. the rapid quenching performed at Winston likely limits the development of AGG by limiting the time a specimen remains above β transus when annealing is complete. When a material is furnace or air cooled from above β transus, the material remains above transus even after the furnace is shutdown because of slower cooling rates. For these reasons, the results of this thesis focus on specimens air β annealed and air-cooled. These results are more realistic to Air Force forgings because large structural component are typically β annealed in air in massive furnaces and then either air or furnace cooled. Optical results of the Winston annealed specimen are located in Chapter B for comparison.

Before analyzing forging results, it is possible to get a sense of simulation accuracy by comparing load-stroke data from the forging press with computational predictions. Figure 4.10 shows a load stroke plot comparison for each forging trial. The comparison shows how well the simulations predict each forging trial.

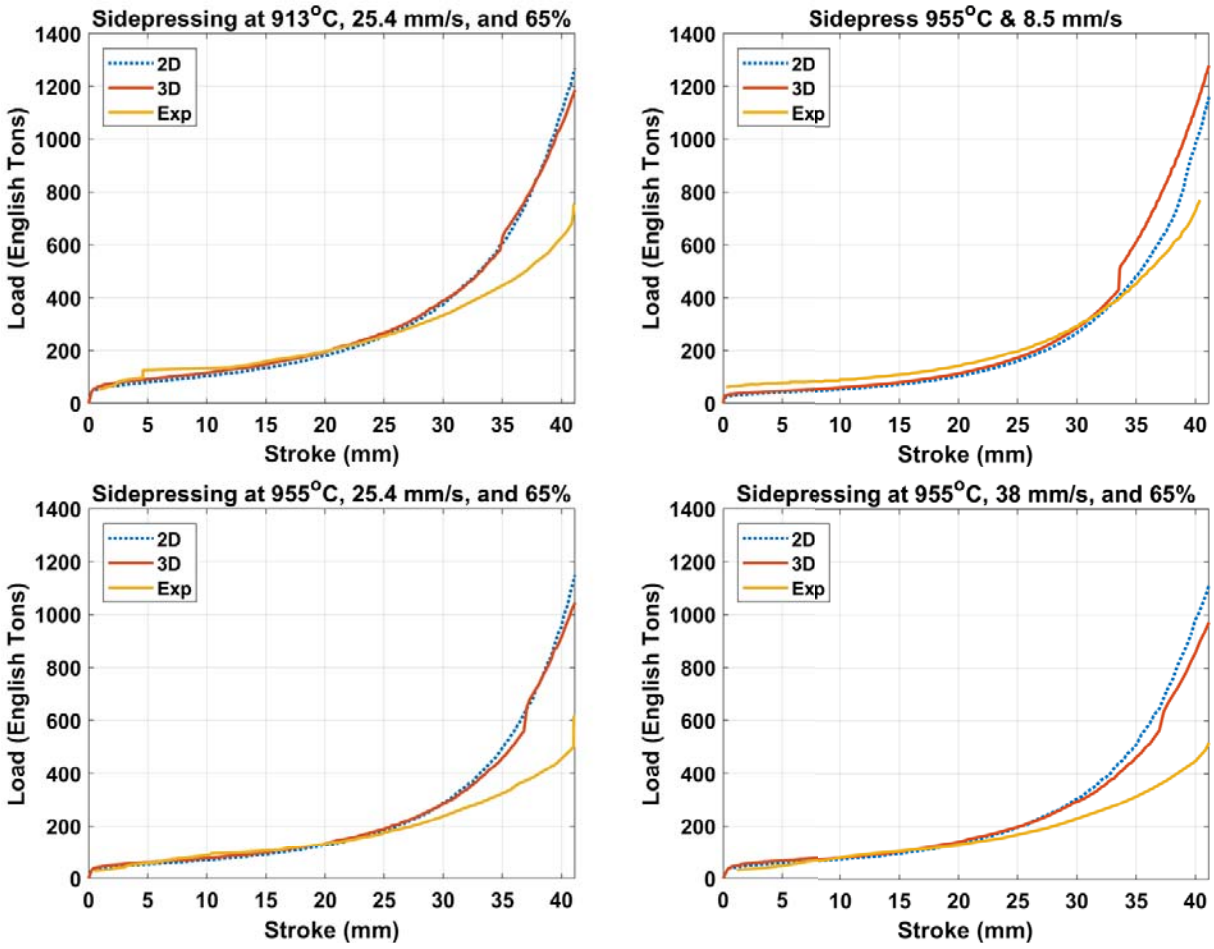

Figure 4.10. Load-Stroke plots for each forging trial are shown comparing two and three dimensional simulation results against experimental forging results. Curves generally diverge near 25 mm reductions, except for the 955 °C and 8.5 $\frac{\text{mm}}{\text{s}}$ condition. This condition is represented well by the two dimensional simulation.

At low stroke values (under 25 mm) the simulation appears to predict deformation loads well. However, above 25 mm the simulations diverge. As discussed in Section 3.4 this may be caused by differences in the predicted volume-fraction of α and β grains resulting in the simulation predicting larger loads than are measured in the forging trial. While over predicting loads is good when designing forging tests to prevent overloading, it also means the other simulation predictions are more extreme. Large deformation loads indicate the simulations may show higher strains and consequently higher temperatures from deformation heating. As a result, simulations should be

viewed as a guide to the results and less as an exact match. Also, two and three dimensional results generally agree well and further justify the use of two dimensional simulations.

4.2.1.1 Sidepressing Forging 8835 - 955 °C Initial Furnace Temperature - 25.4 $\frac{mm}{s}$ Ram Speed - 65% Reduction

Results for forging 8835 are divided into specimen A through C and shown in Figure 4.11. Specimen A and C were β annealed, while specimen B is as-forged material. Two different annealing processes were used as described in Section 3.7.2. Specimen A was β annealed at Air Force Institute of Technology (AFIT), while specimen C was β annealed at Winston Heat Treating. The specimen labels represent the same annealing process for each forging in this thesis. Additionally, the figure shows the material flow prediction for comparison. Despite differences between load-stroke data, flow prediction appears very similar to specimen B.

Further analysis of the optical results of specimen A are shown in Figure 4.12. The figure compares simulation temperature and strain results with the macroscopic optical image of the specimen. Additionally, each region of interest location is identified on the macroscopic image and labeled with the resulting 2.5x magnification image. Every sidepressing forging has a similar figure for easier optical comparison.

Forging 8835 was conducted at 955 °C initial furnace temperature, 25.4 $\frac{mm}{s}$ ram speed, 65% reduction in height, and β annealed at AFIT. When compared to other forging trials, these conditions represent high temperature with moderate ram speed. Using the line intercept method, the average grain diameter and area are approximately 0.976 mm and 0.868 mm^2, respectively. Optically the specimen has coarse grains near the edges, particularly in the right (E) and left (A) regions of interest. Grains appear to grow smaller as one moves visually closer toward the core of the

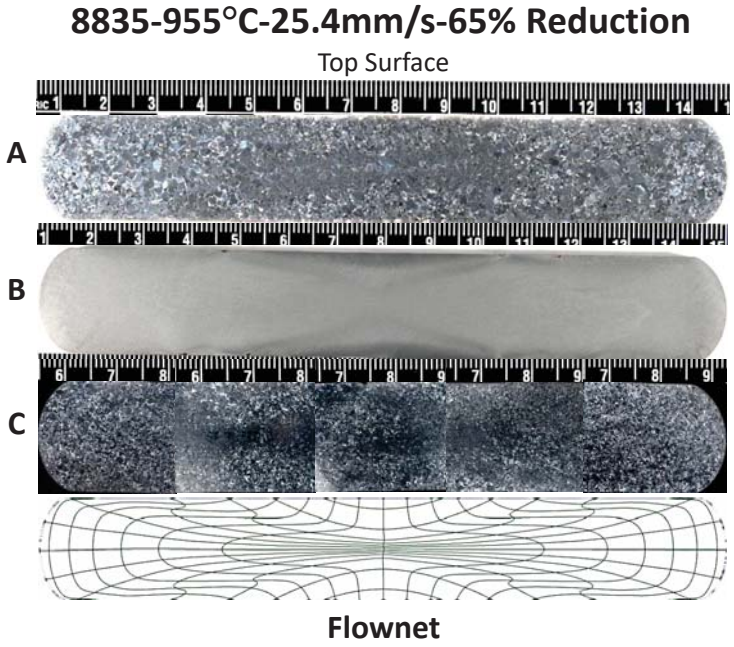

Figure 4.11. Side-by-side comparison on forging 8835 specimen A, B, and C. Material flow prediction is included for comparison with specimen B. Scale bar: cm

specimen, but grow large again at the center in region C. Two lobes of smaller grains appear primarily around region B and D. When compared to simulation results the specimen does not show an obvious relationship with either contour image.

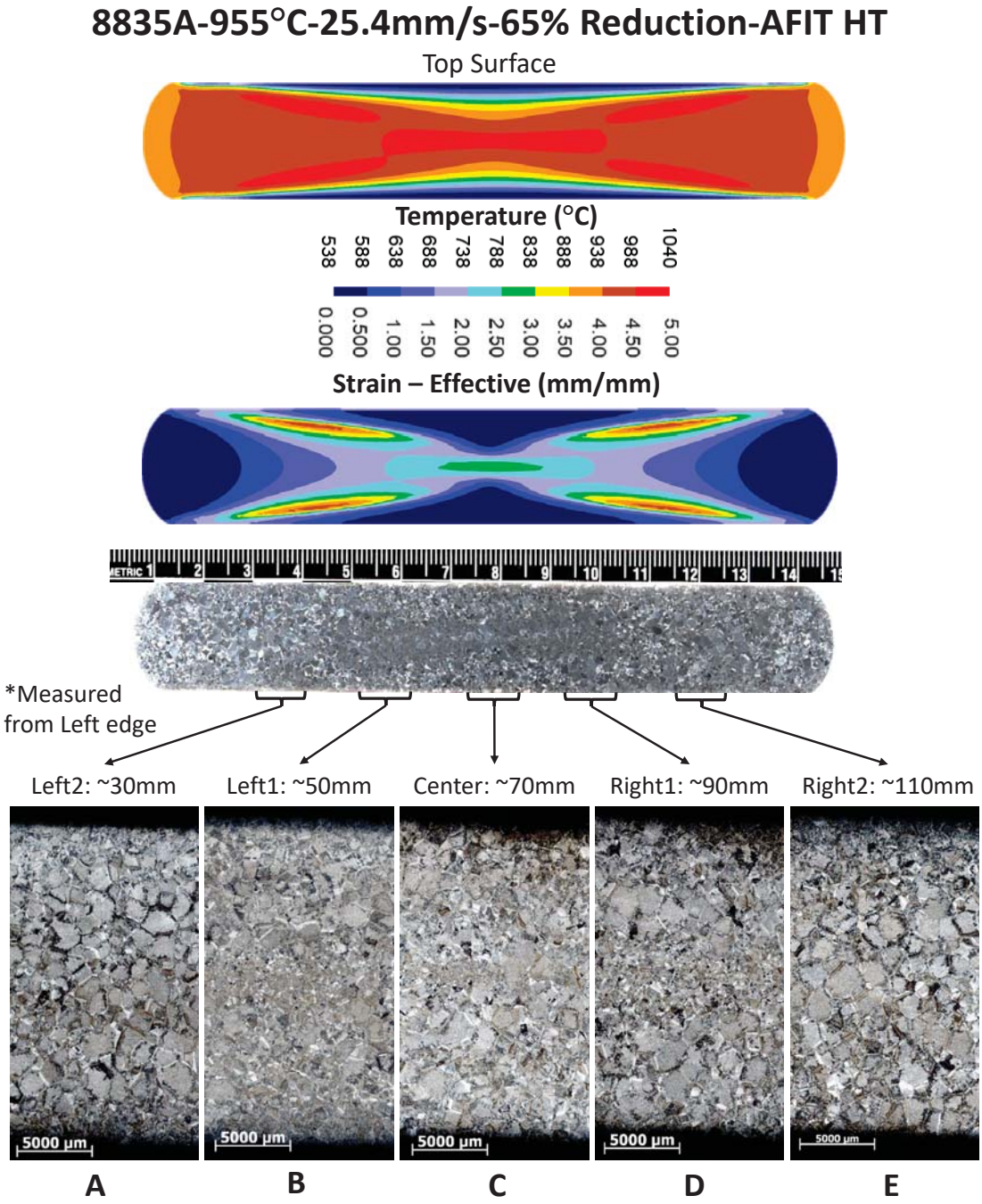

Figure 4.12. Sidepressing forging result at 955 °C initial furnace temperature, 25.4 $\frac{\text{mm}}{\text{s}}$ ram speed, 65% reduction in height,and AFIT heat treatment. The macro scale image provides comparison between the predicted strain and temperature contour images. Each region of interest is labeled for closer grain size evaluation. This specimen appears to be developing coarse grains in the center and on the left and right edges with lobes of smaller grains in between. Scale bar: cm

The hypothesis developed in Section 4.2.0.1 states fast ram speed and high initial furnace temperature may cause a small region of material to exceed β transus temperature during deformation. Material would exceed β transus temperature from the addition of deformation heat due to high strain during forging. The region would be pre-exposed to β phase and potentially result in large growth when annealed above β transus. Based on the simulation results, the region most likely to exceed the β transus temperature is the core of the specimen. When the forging specimen is optically evaluated and compared to the simulation temperature contour in Figure 4.12, it is clear that large grains exist in the same predicted location.

Grain size of the specimen changes drastically from edges to core creating a non-uniform grain size distribution. A key element to AGG is the abnormal development of larger or coarse grains in contrast to the average grain size. In the case of forging 8835, two regions of smaller grains developed, but are divided by notably larger grains at the center. These grains are in a region the simulation predicted to exceed the β transus and warrant a closer analysis.

A 5 mm vertical strip of specimen C was optically processed to evaluate vertical grain size distribution. The image was evaluated using the "Point-Sampled Intercept Length Measurement" produced by Lehto et al. [36]. The result is shown in Figure 4.13 using the Hall-Petch grain size parameter. The parameter is inversely related to grain size as it is traditionally used as a measure of material strength based on grain size. Therefore, large grains have smaller values and vice-versa.

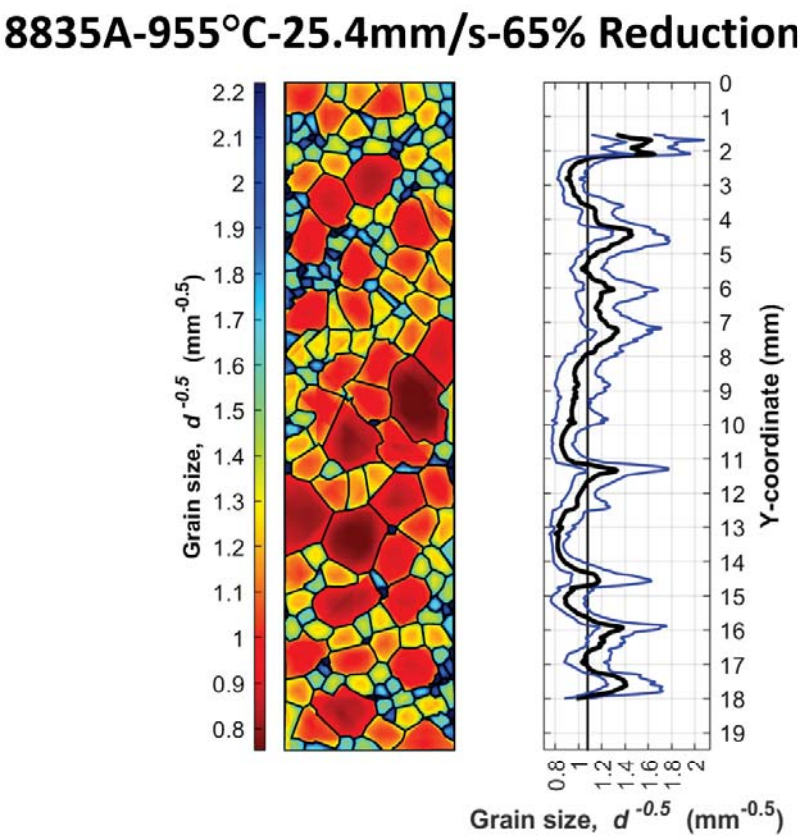

Figure 4.13. Sidepressing grain size heat map and distribution of forging 8835, specimen A, region of interest C. A 5 mm **vertical section was optically processed to determine variation in grain size. Values are represented using the Hall-Petch grain size value mentioned in Section 3.8.3.**

The heat map and distribution plots show regions of large and small grain size. A cluster of larger grains exists near the center of the region of interest. Further analysis of these grains shows a maximum dimension of 2.646 mm length as shown in Figure 4.14. The difference between average grain size diameter and the largest grain length at the center of the specimen is 1.670 mm. The difference between the average lineal intercept length and the maximum grain length is larger at 1.819 mm. Additionally, the 95% confidence interval of lineal lengths in the specimen is 0.710mm to 0.944mm of which the maximum grain length exceeds by 1.696 mm. The fact that the max grain length at the core of the specimen far exceeds the 95% confidence interval for lineal grain length in the specimen indicates the development of AGG in

this specimen.

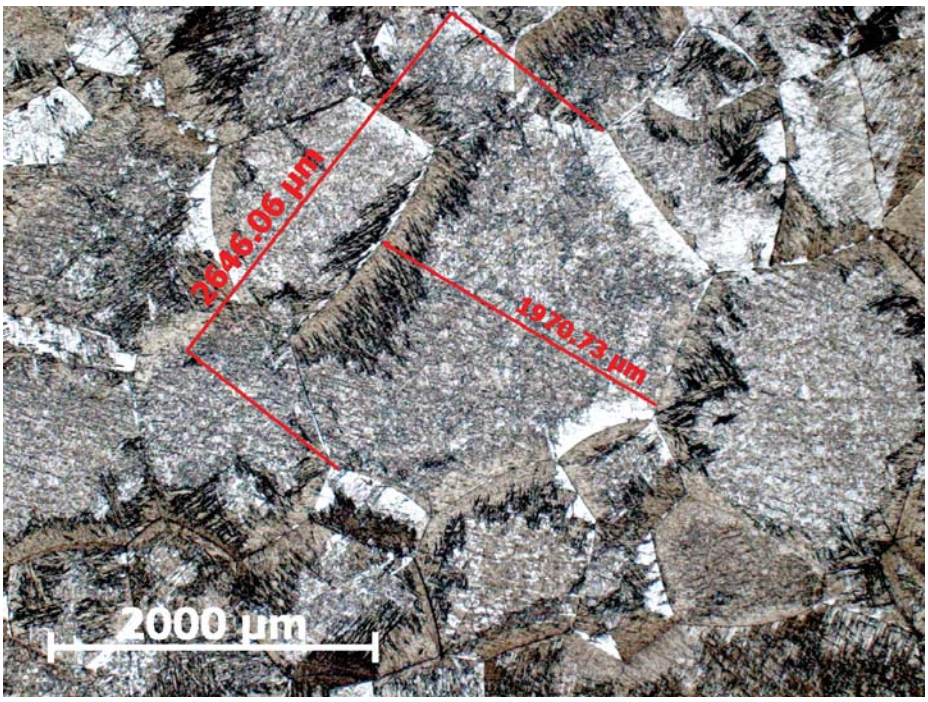

Figure 4.14. Large grains were identified at the center of specimen 8835A and were measured for comparison to average grain size.

4.2.1.2 Sidepressing Forging 8836 - 955 °C Initial Furnace Temperature - 8.5 $\frac{mm}{s}$ Ram Speed - 65% Reduction

Specimen A through C results for forging 8836 are shown in Figure 4.15. This forging was conducted with 955 °C initial furnace temperature, 8.5 $\frac{mm}{s}$ ram speed, 65% reduction in height, and β annealed in air and air cooled. Forging conditions for this test represent high furnace temperature and low ram speed. The material flow prediction for these conditions is very similar to as-forged result shown in specimen B.

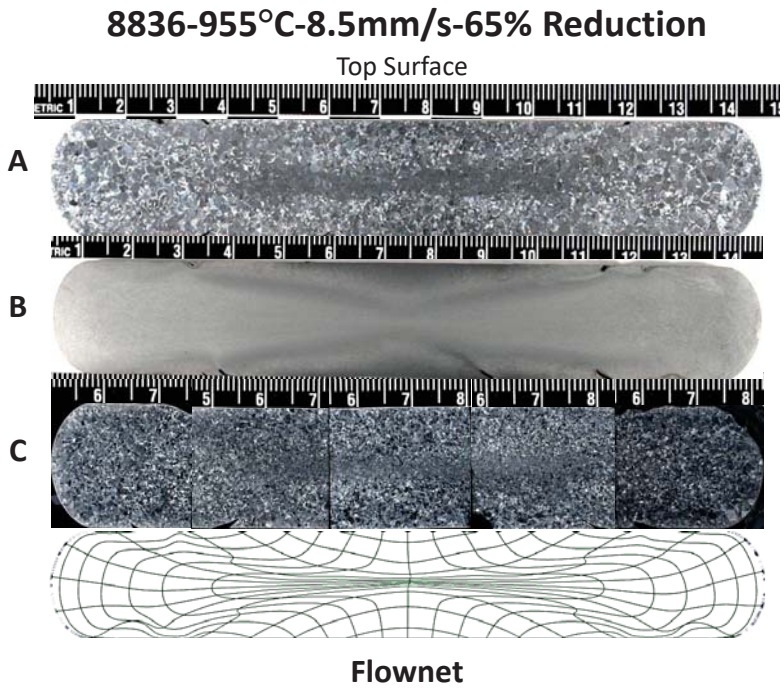

Figure 4.15. Side-by-side comparison on forging 8836 specimen A, B, and C. The material flow prediction is also included for comparison with specimen B. Scale bar: cm

Further analysis of specimen A is shown in Figure 4.16 with regions of interest labeled with corresponding 2.5x magnification image. Simulations for forging test did not predict exceeding β transus. Despite being forged at high temperature, strain induced by deformation was not large enough to result in significant deformation heating. Interestingly this resulted in a uniform, coarse grain distribution. Using the lineal intercept method, the grain diameter and area were measured to be approximately 1.136 mm and 1.300 mm. When compared to the other sidepressing forging tests, this specimen has the largest average grain diameter and area.

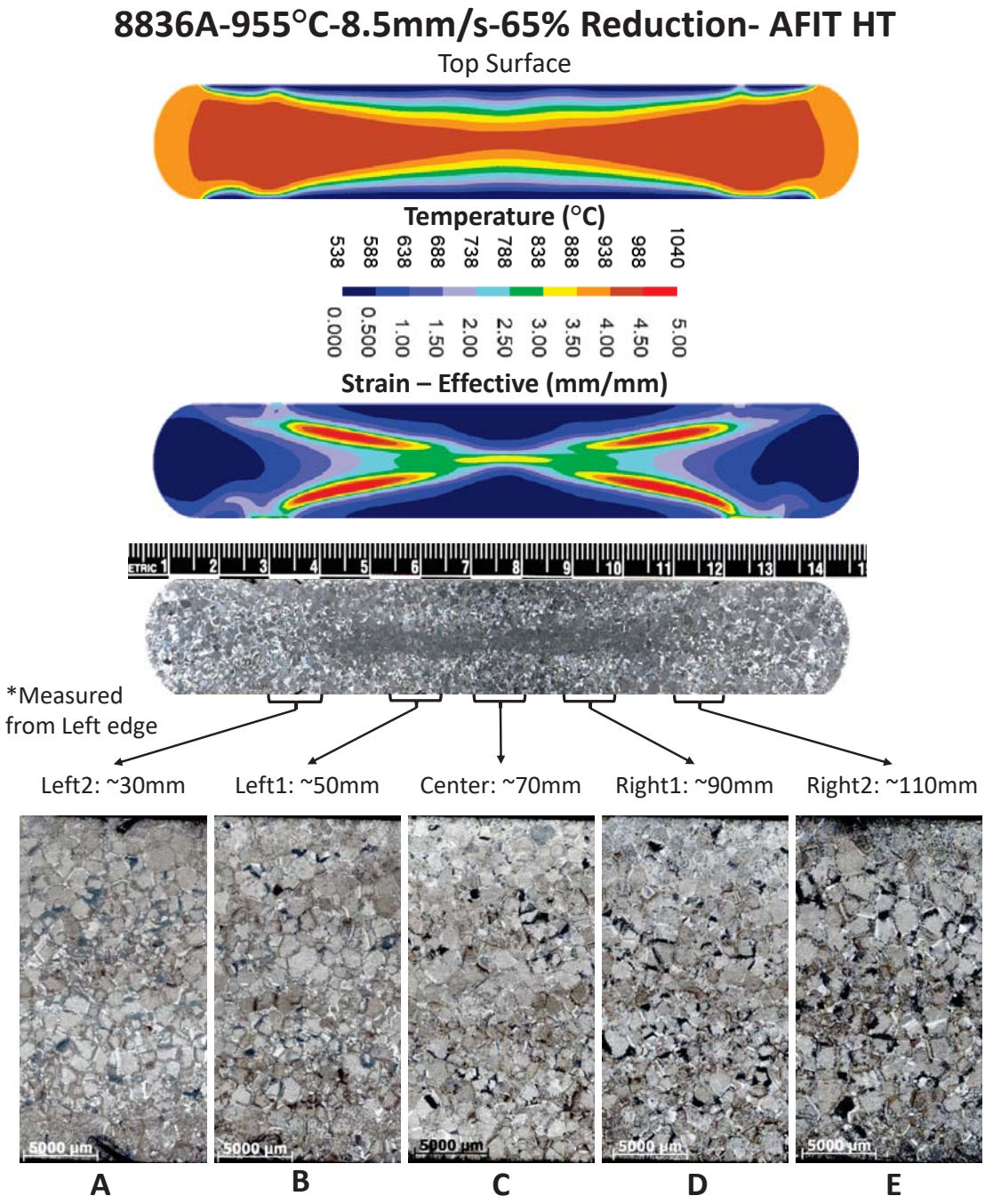

Figure 4.16. Sidepressing forging result at 955 °C, 8.5 $\frac{\text{mm}}{\text{s}}$, 65% reduction in height,and AFIT heat treatment. The macro scale image provides comparison between the predicted strain and temperature contour images. Each region of interest is labeled for closer grain size evaluation. This specimen appears to have a uniform grain size distribution.

Grain size distribution of the specimen was analyzed closer at the center region of interest, C. A 5 mm wide section was optically processed to determine vertical distribution of grain size. The results are shown in Figure 4.17. The distribution shows less variation in grain size across the vertical section of material than forging 8835, however, a grouping of larger grains appears near the center.

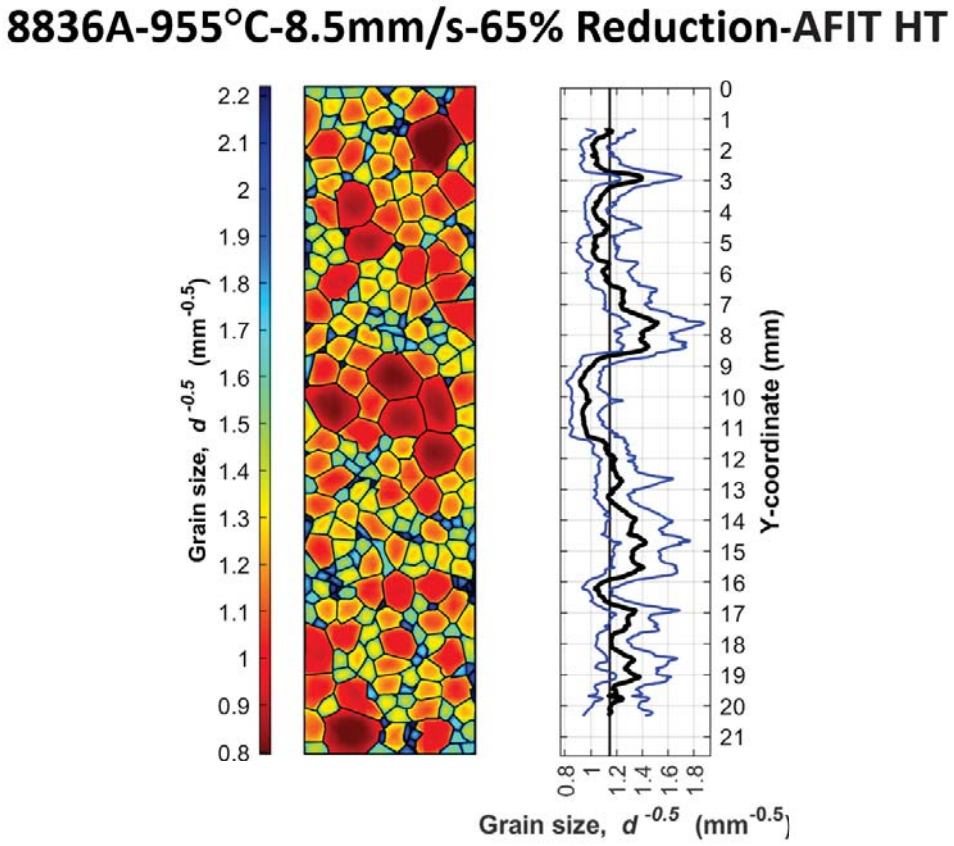

Figure 4.17. Sidepressing grain size heat map and distribution of forging 8836, specimen A, region of interest C. A 5 mm vertical section was optically processed to determine variation in grain size. Values are represented using the Hall-Petch grain size value mentioned in Section 3.8.3.

Additional optical analysis of large grains at the center of the specimen was conducted. Figure 4.18 shows the largest dimensions from each grain, with a maximum measurement of 1.82 mm length. The maximum length measurement is 0.68 mm larger than the average grains size. Additionally, it is 0.804 mm larger than the average lin-

eal intercept length. When compared to the 95% confidence interval of 0.847 mm to 1.179 mm the maximum measured grain length is still 0.638 mm larger. The fact that the maximum grain length exceeds the 95% confidence interval, indicates that this specimen developed AGG.

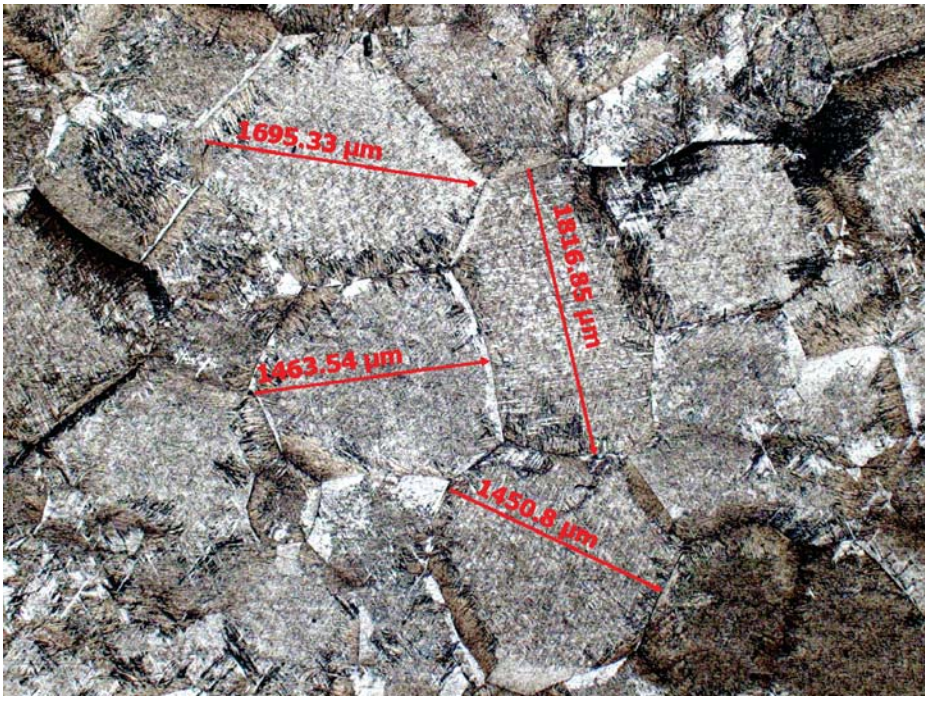

Figure 4.18. Large grains at the center of forging 8836A, dimensioned for comparison to average grain size.

4.2.1.3 Sidepressing Forging 8837 - 913 °C Initial Furnace Temperature - 25.4 $\frac{mm}{s}$ Ram Speed - 65% Reduction

Optical results for specimen A through C from forging 8837 are shown in Figure 4.19. This forging was conducted at 913 °C initial furnace temperature, 38 $\frac{mm}{s}$ ram speed, 65% reduction in height, and β annealed at AFIT in air and air cooled. The forging conditions represent low furnace temperature and moderate ram speed. These specimen were the first processed in this thesis and unfortunately the oxide layer was only partially removed from specimen A and C, making analysis challenging.

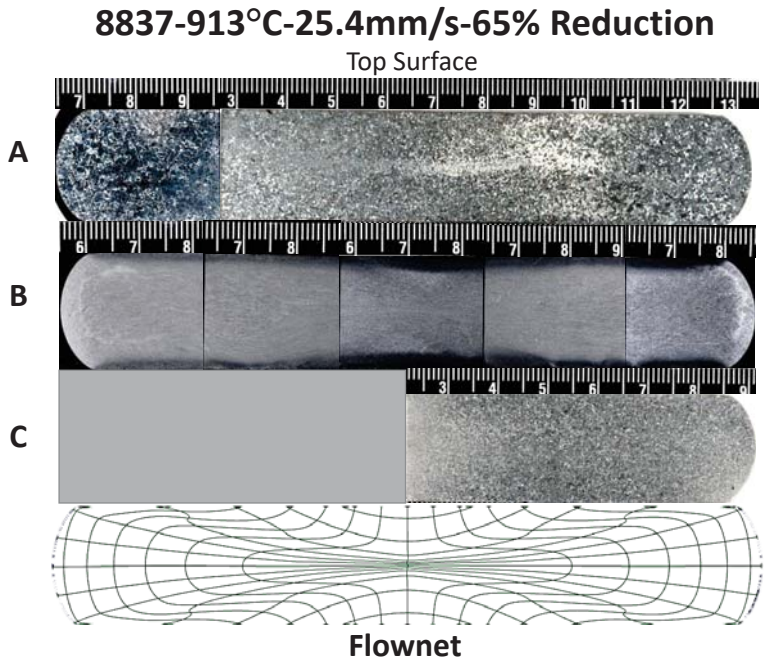

Figure 4.19. Side-by-side comparison on forging 8837 specimen A, B, and C. The material flow prediction is also included for comparison with specimen B. Scale bar: cm

Figure 4.20 shows further optical analysis of specimen A with regions of interest labeled with respective 2.5x magnification images. The images portray mixed clarity of the specimen.

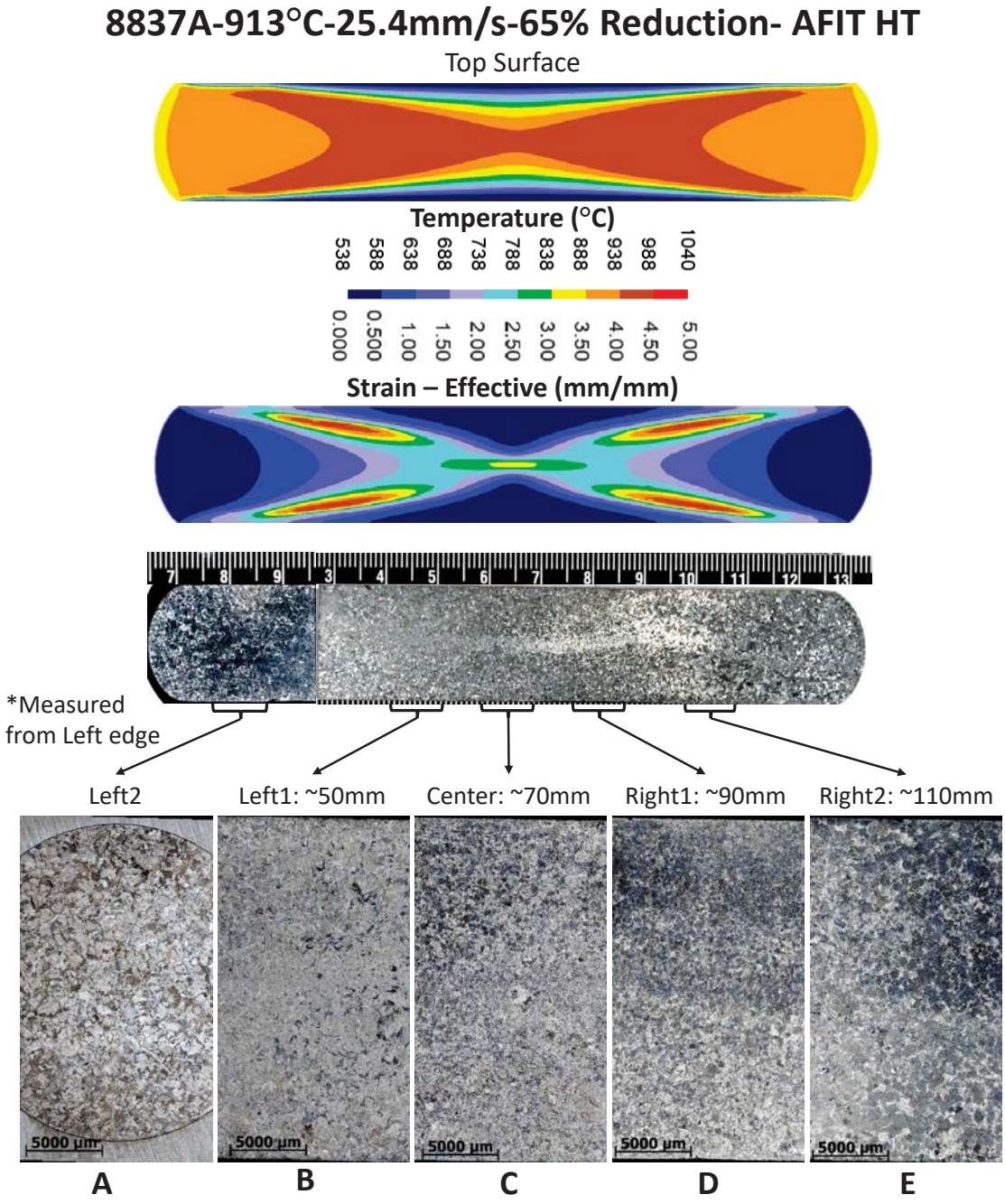

Figure 4.20. Sidepressing forging result at 913 °C, 25.4 $\frac{\text{mm}}{\text{s}}$, 65% reduction in height,and AFIT heat treatment. The macro scale image provides comparison between the predicted strain and temperature contour images. Each region of interest is labeled for closer grain size evaluation. This specimen appears to have a uniform grain size distribution.

Lineal intercept method was attempted and average grain diameter and area are approximately 0.949 mm and 0.833 mm respectively. These values are lower than forging 8835 and 8836 and nothing abnormal can be discerned from the regions of interest. For this reason, poor specimen polish clarity, and the interest of time, a vertical grain distribution and grain size heat map were not produced.

4.2.1.4 Sidepressing Forging 8842 - 955 °C Initial Furnace Temperature - 38 $\frac{mm}{s}$ Ram Speed - 65% Reduction

Results for specimen A through C from forging 8842 are shown in Figure 4.21. This forging was conducted with 955 °C initial furnace temperature, 38 $\frac{mm}{s}$ ram speed, 65% reduction in height, and β annealed at AFIT. Forging conditions for this test represent high furnace temperature and high ram speed. The material flow prediction is also included in the image and appears similar to the as-forged specimen B.

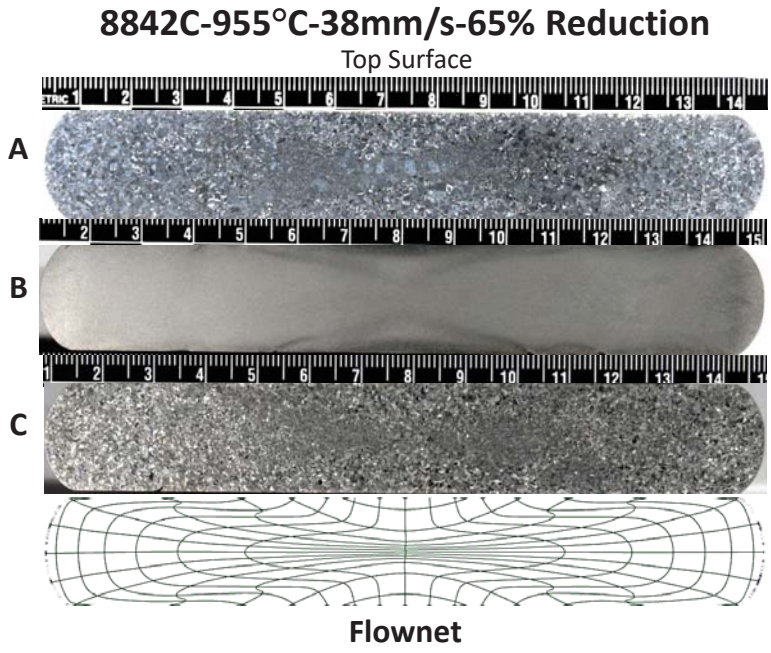

Figure 4.21. Side-by-side comparison of forging 8842 specimen A, B, and C. Material flow prediction is included for comparison with specimen B. Scale bar: cm

Further analysis of specimen A is shown in Figure 4.22. Using the lineal intercept method, the average grain diameter and area are approximately 0.871 mm and 0.731 mm. This specimen represents the smallest average grain size for the sidepressing test. This forging test was conducted at the higher temperature and with highest forging speed. As seen from the simulation contour images, it is predicted to exceed the β transus in the regions of high strain. The specimen shows a similar, yet more pronounced, grain size distribution as found on specimen 8835. Two regions of smaller grains exist in image B and C, while the outer edges (A and E) maintain their appearance of uniformly coarse grains. Again, the center image shows large grains that appear to be developing out of the regions of smaller grains. When optically compared with temperature simulation results, it appears that the large grains correspond with a portion of the predicted β transus region at the core of the specimen. This may indicate a correlation between the simulation temperature predictions and the location abnormal grains. Further analysis of the image is required to show variation in grain size across specimen height.

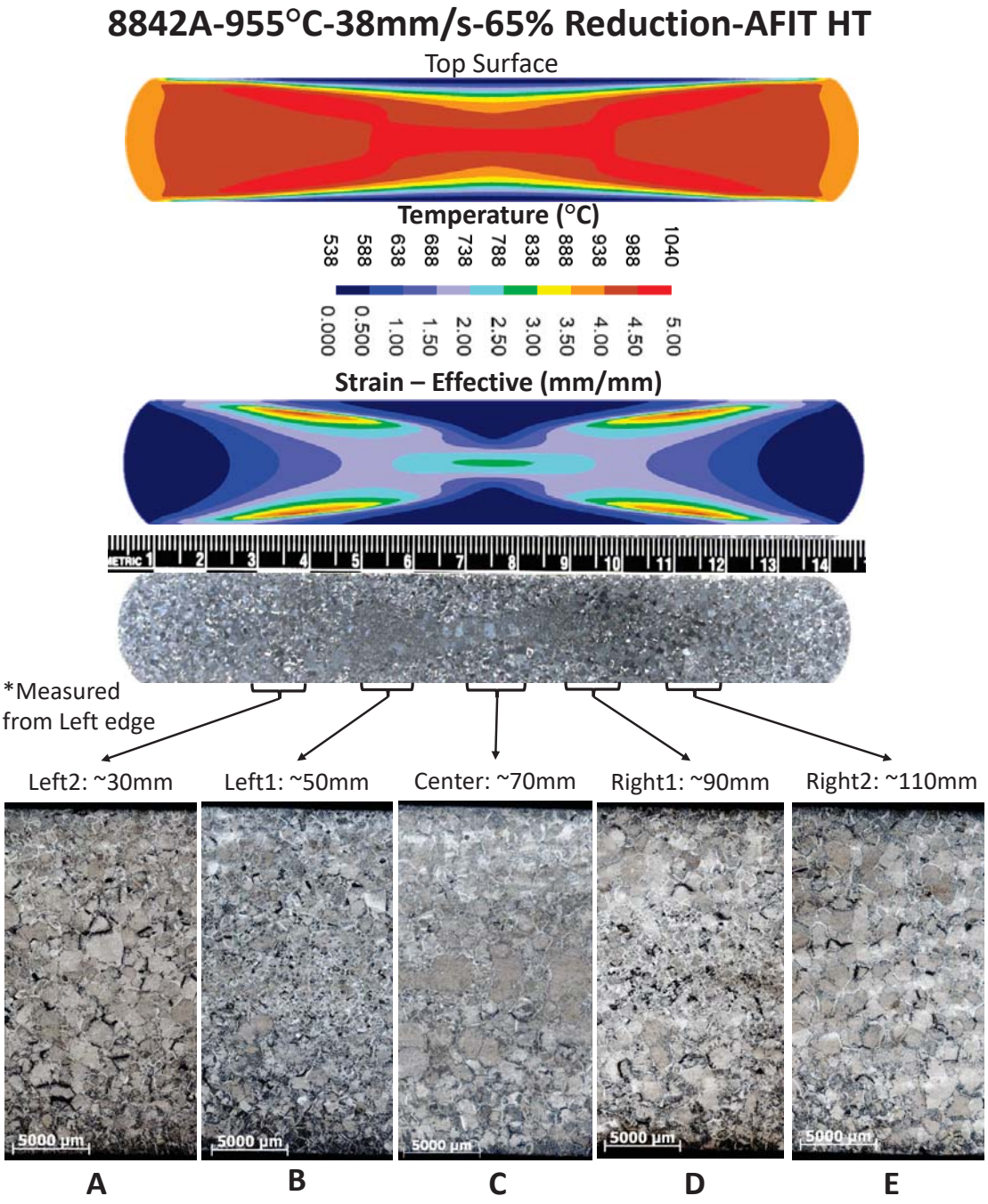

Figure 4.22. Sidepressing forging result at $955\,^{\circ}\mathrm{C}$, $38\,\frac{\mathrm{mm}}{\mathrm{s}}$, 65% reduction in height,and AFIT heat treatment. The macro scale image provides comparison between the predicted strain and temperature contour images. Each region of interest is labeled for closer grain size evaluation. This specimen developed notable coarse grains in the center and on the left and right edges with lobes of smaller grains between.

Figure 4.23 shows the grain size distribution across a 5 mm wide section of image C. The results from this distribution are noticeable. A trend exists where the center of the specimen has significantly larger grain size than material approaching the top and bottom surfaces. Again, this matches a portion of the simulation prediction of β transus temperature in the specimen.

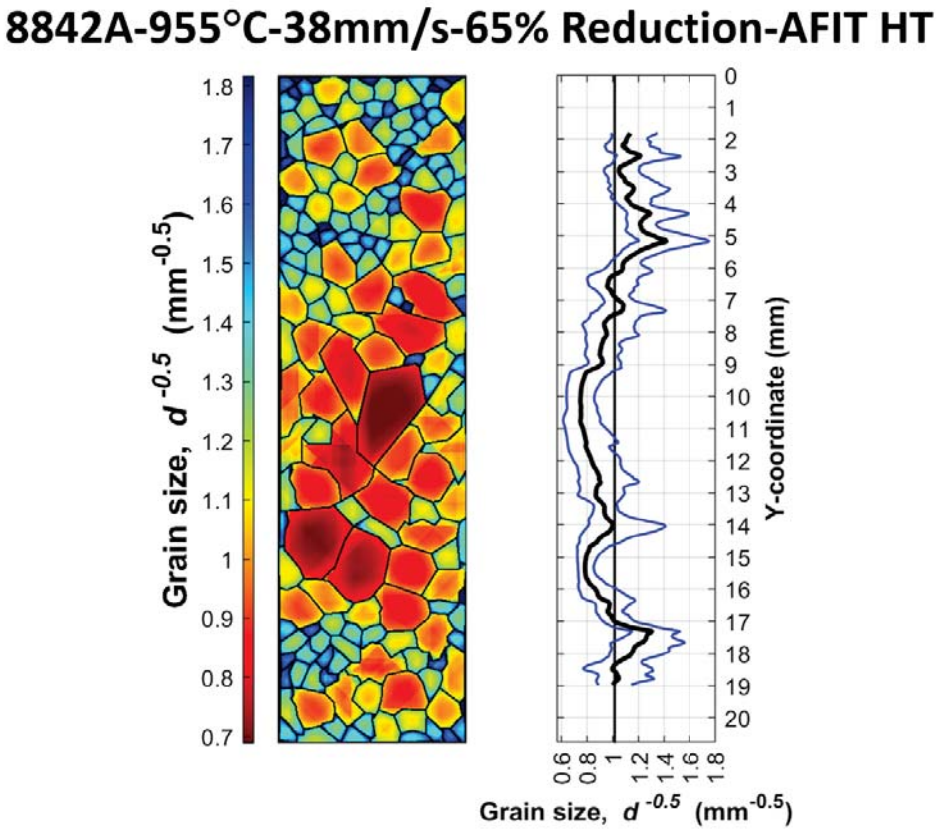

Figure 4.23. Sidepressing grain size heat map and distribution of forging 8842, specimen A, region of interest C. A 5 mm vertical section was optically processed to determine variation in grain size. Values are represented using the Hall-Petch grain size value mentioned in Section 3.8.3.

Further analysis of the grain size in this region shows the largest grain to be approximately 3.52 mm in length. An image of this grain is shown in Figure 4.24. This value is 2.65 mm larger than the average grain size of the specimen. Additionally, the max grain length is 2.763 mm larger than the average lineal intercept length. Furthermore, it is 2.604 mm larger than the 95% confidence interval of 0.598 mm to

0.916 mm. The max lineal grain measurement far exceeds the 95% confidence interval for lineal intercept lengths in this specimen. For this reason it is clear that AGG has developed.

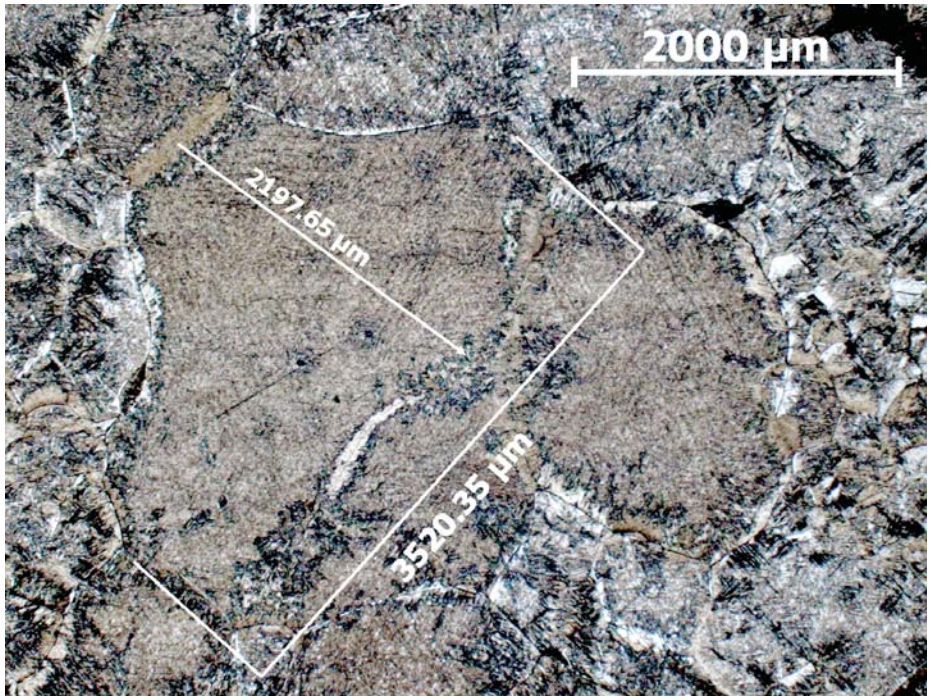

Figure 4.24. The largest grain at the center of specimen 8842A had a maximum length of 3.52 mm

The results further indicates a relationship between the FEM simulation temperature predictions and the location of abnormal grains. However, many additional abnormal grains would be expected based on the temperature simulation contour image prediction of β transus temperature in the material. One explanation for development at the center of the specimen is that the two-dimensional simulation is over-predicting the amount of deformation heat generated in the simulation. Even still, the center of the specimen would be expected to be the hottest location in the workpiece during forging. Therefore, if the simulation is over-predicting, it is still close enough to show regions of the material at the most risk for exceeding the β transus temperature. This relationship between simulations and forgings could have

large impacts on industry and the identification of AGG in sidepressing type forgings.

4.2.2 Sidepressing Summary

Four sidepressing forging conditions were tested based on simulation results showing deformation heating from high strain regions. The forging tests were evaluated for grain size and distribution to determine if potential pre-exposure to β transus temperature would effect grain growth. The increase in ram speed across sidepressings with an initial furnace temperature of 955 °C showed the development of abnormal grain size near the center of the material. The location of AGG development in each specimen was consistent with the predicted hottest regions from the simulations. When compared, the simulations showed usefulness in predicting the location of AGG development in sidepressing forgings.

A summary of the measurements gathered using the lineal intercept method are shown in Table 4.4 by forging number. Additionally, a side-by-side comparison of the vertical distribution of the evaluated specimen is shown in Figure 4.25

Table 4.2. Summary of average grain size measurements via lineal intercept method

Forging no.	mean lineal intercept (mm)	Std. Dev. (mm)	95% C.I. (mm)	% Relative Accuracy	ASTM Grain Size no.	Average Diameter (mm)	Average Area (mm^2)	Max grain length (mm)
8835	0.827	0.094	0.117	14.118	10.545	0.976	0.868	2.646
8836	1.013	0.134	0.166	16.391	9.962	1.136	1.300	1.817
8837	0.809	0.072	0.090	11.085	10.612	0.949	0.833	N/A
8842	0.757	0.138	0.159	21.0239	10.802	0.871	0.731	3.520

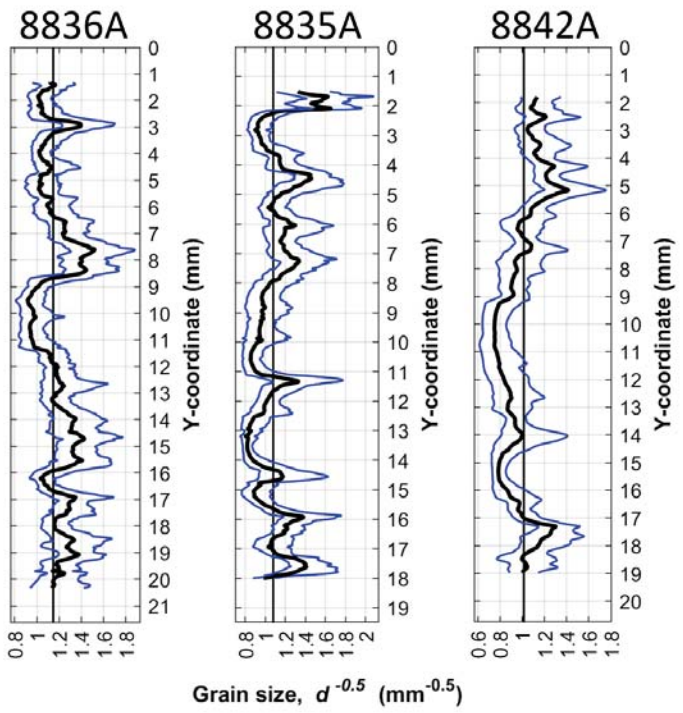

Figure 4.25. Sidepressing grain size distribution of forging 8835, 8836, and 8842 at region of interest C.

4.3 Upsetting Simulation Results

Upsetting was the other forging test conducted in this thesis. As an axial forming operation, this test was easier to simulate and process due to workpiece symmetry. Additionally, the results and experience gained from sidepressing simulations and forgings facilitated upsetting research. Developing an upsetting simulation was simple due to shared forging characteristics between the two tests. The simulations used similar material models and simulation settings based on those conducted in the sidepressing test. In all, twelve simulations were conducted with two sets of reductions in height analyzed, and three forgings trials conducted and evaluated.

4.3.1 Simulation Results Overview

Upsetting forging simulations were easier to conduct due to workpiece symmetry. Three dimensional simulations would not provide any additional information because the workpiece is represented as a uniform cylinder being deformed axially. Therefore, only an axisymmetric two dimensional simulation was designed and tested for each forging condition. The simplification of these simulations dropped average computational time significantly from approximately 15 hours to 30 minutes. Analysis of these simulations were conducted at two different reductions in height and the results used to guide the selection of conditions for forging trials.

4.3.1.1 2-D Upsetting Temperature Results

Figures 4.26 and 4.27 show temperature results for two dimensional upsetting simulations conducted at 65% reduction in height. Additionally, Figures 4.28 and 4.29 shows temperature results for 80% reduction in height. The figures are aligned in the same manner as they were presented in Section 4.2.

Temperature Results show a similar trend to those of the sidepressing test. As ram speed increases, more deformation heat is generated raising the temperature at the core of the workpiece beyond the initial furnace temperature. This is evident in both reductions in height and can be seen clearly in the plots at the line of symmetry and 38.1 mm radial offset as shown in Figures 4.27 and 4.29. Five simulations show signs of exceeding the β transus and potentially pre-exposing material to β phase.

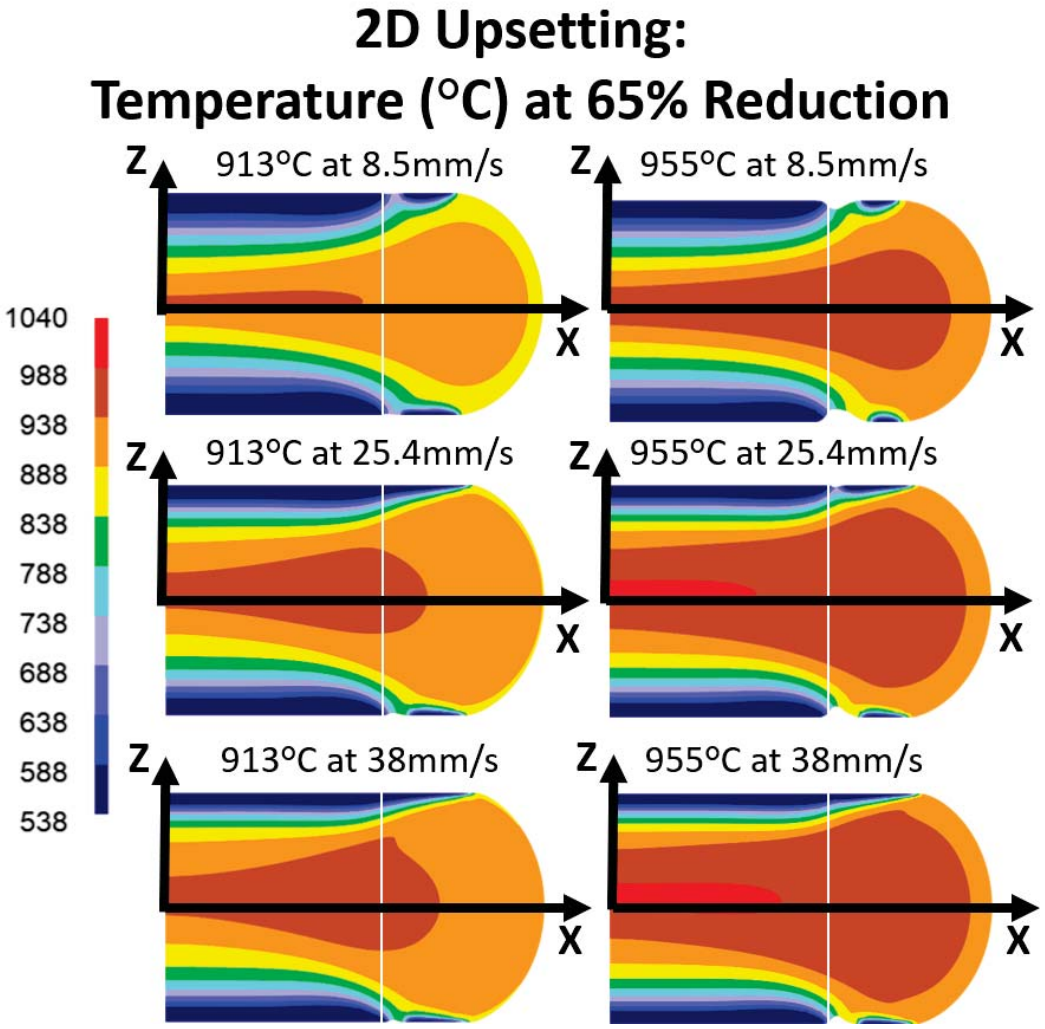

Figure 4.26. **Axisymmetric two-dimensional upsetting results conducted at 65% reduction in height. The images are organized into two columns for each temperature and three rows for each ram speed. Faster ram speed resulted in greater internal heat generation causing some regions to exceed the β transus(993 °C).**

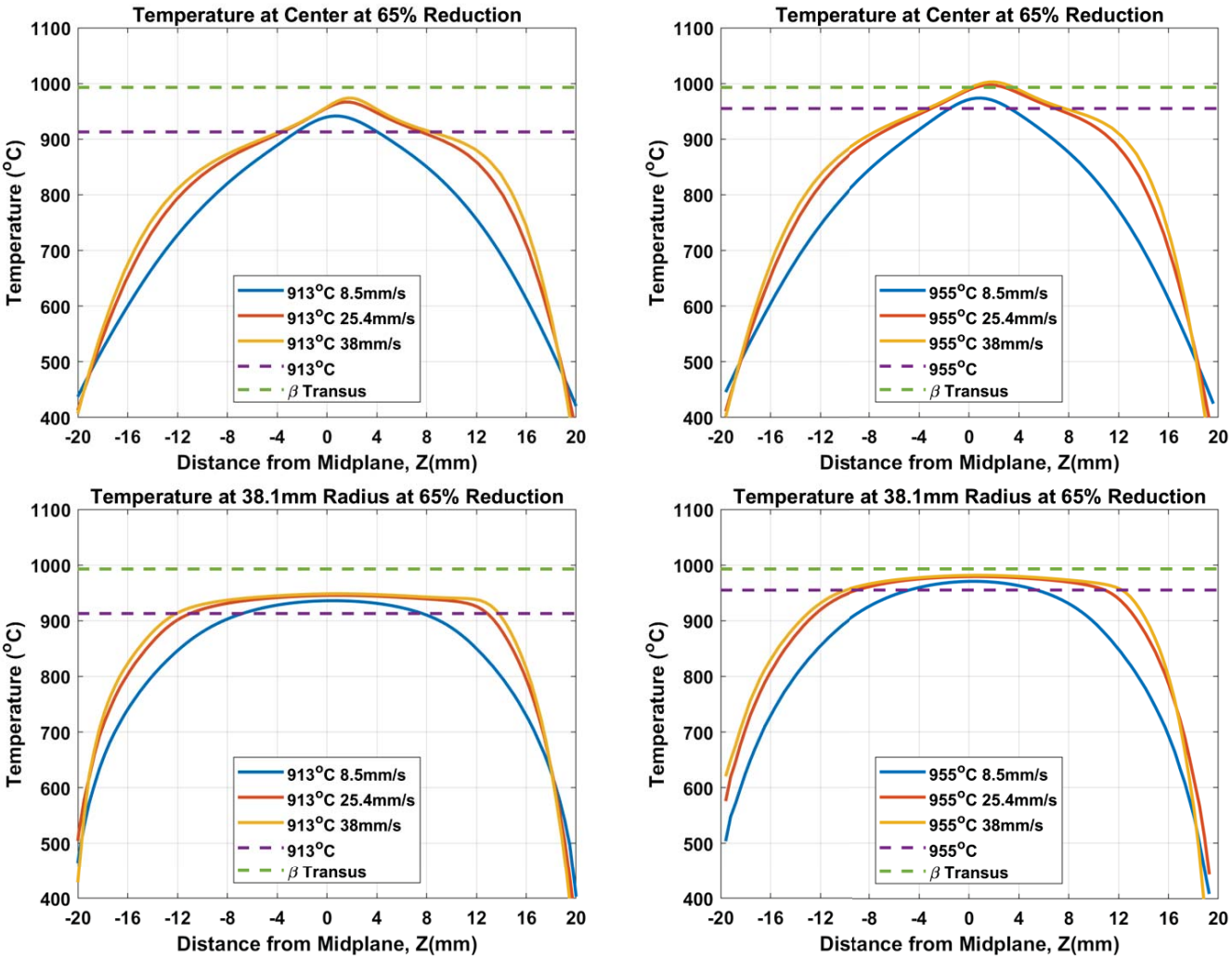

Figure 4.27. The plots depict temperature distribution of each simulation from Figure 4.26. The left column shows results from 913 °C simulations and the right from 955 °C simulations. The top row depicts temperature data from the line of symmetry along the z-axis, while the bottom row depicts temperature data from a vertical line 38.1 mm from the line of symmetry. The location of this data is represented in Figure 4.26 by a vertical white line. Initial furnace temperature and β transus are plotted for reference.

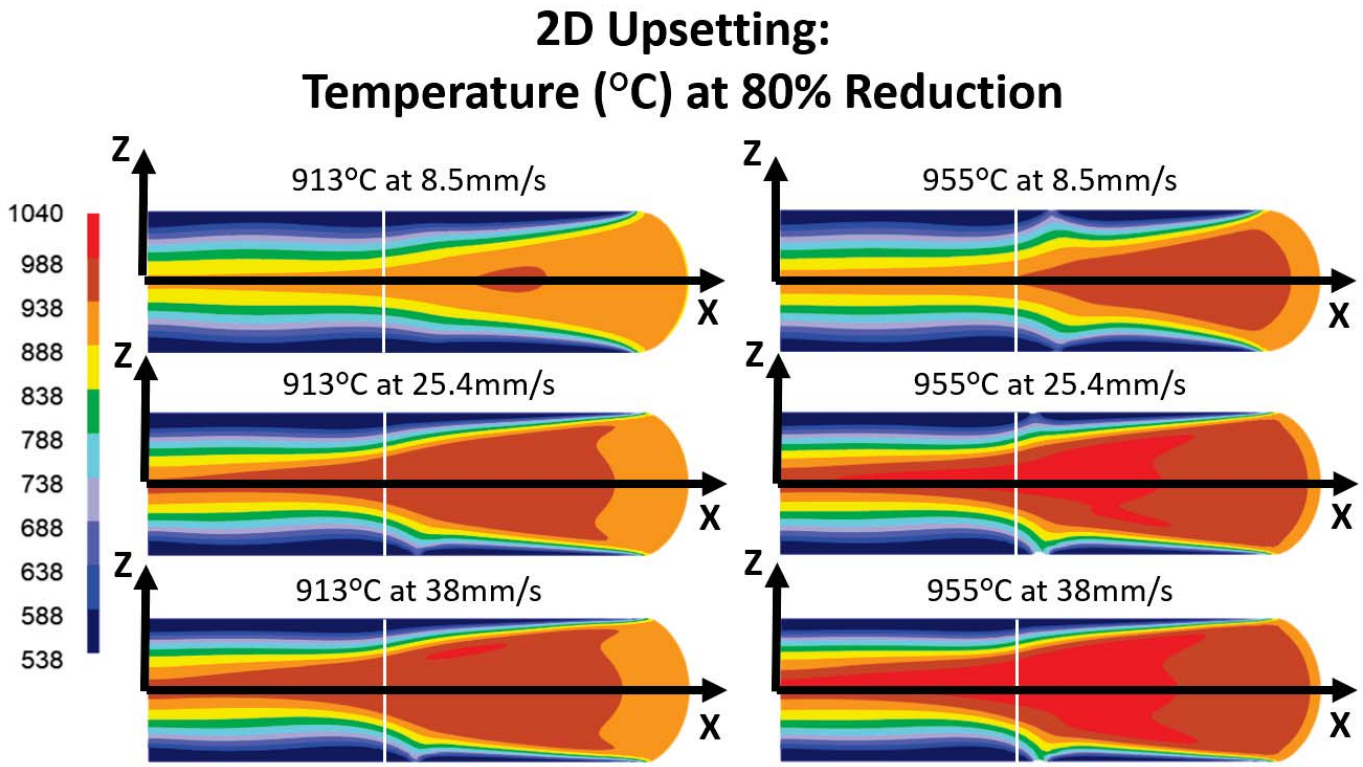

Figure 4.28. Axisymmetric two-dimensional upsetting results conducted at 80% reduction. The images are organized into two columns for each temperature and three rows for each ram speed. Faster ram speed resulted in greater internal heat generation between both sets of temperature with some exceeding the β transus(993 °C).

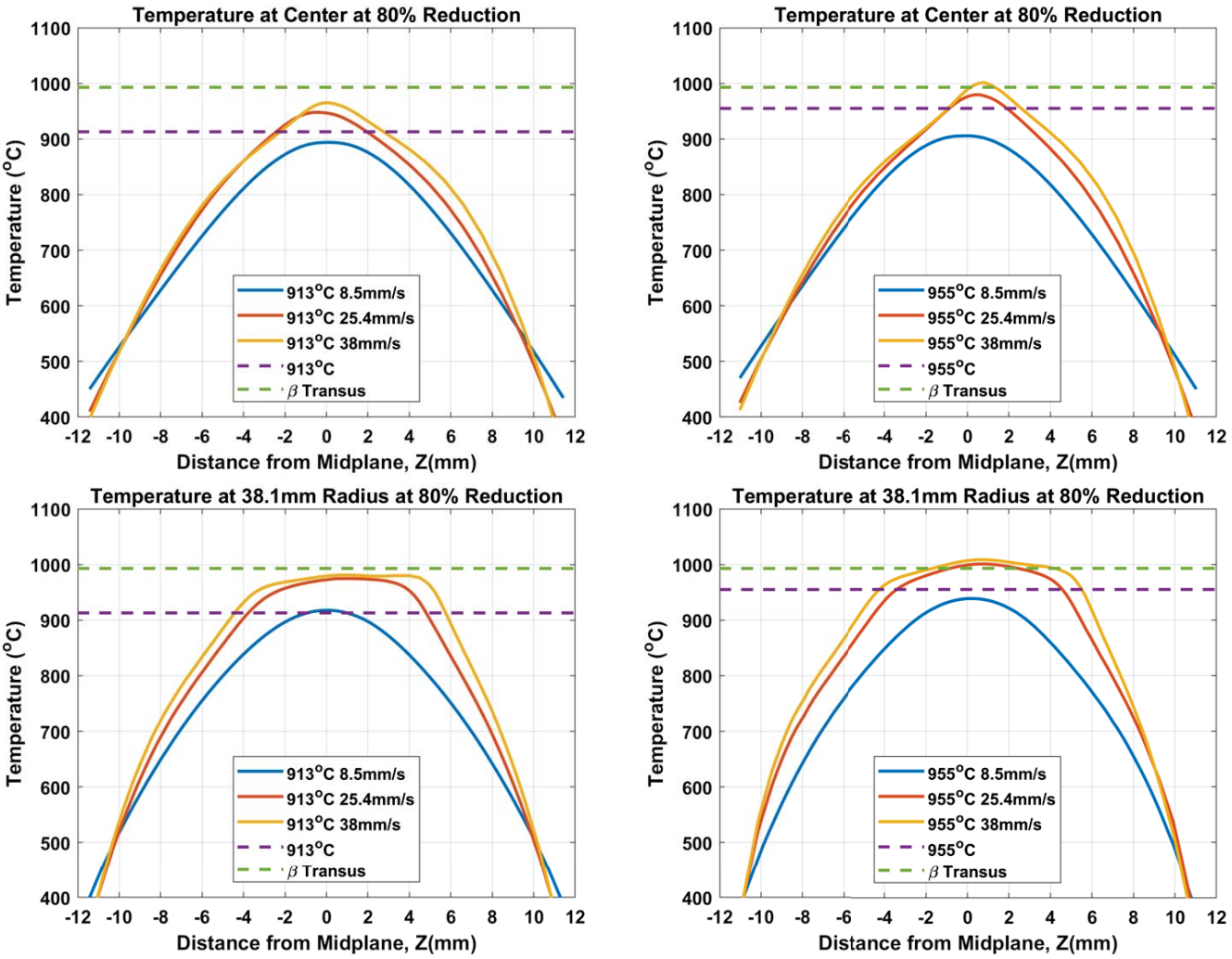

Figure 4.29. The plots depict temperature distribution of each simulation from Figure 4.28. The left column shows results from 913 °C simulations and the right from 955 °C simulations. The top row depicts temperature data from the line of symmetry, while the bottom row depicts temperature data from a vertical line 38.1 mm from the line of symmetry. The location of this data is represented in Figure 4.28 by a vertical white line. Initial furnace temperature and β transus are plotted for reference.

Die chill effects have a similar trend to sidepressing as well. Dead zones produced by die chill decrease in size as ram speed increases. This is the result of shorter forging times and less time for heat transfer. Therefore, faster forgings maintain higher workpiece temperature throughout the forging process. The 80% reduction is a continuation of the 65% reduction simulations and provide insight to workpiece changes with additional deformation. The primary differences between the two sets of simulations are the size of the chilled zones and the increase in deformation heat. As seen in the plots, the temperature near the top and bottom surfaces decreases as heat transfer continues with the forging process. What was a broad temperature curve at 65% becomes more of a peak at 80%. Additionally, deformation heat continues to be generated as reduction increases. For this reason, simulations at 955 °C with 25.4 $\frac{\text{mm}}{\text{s}}$ and 38 $\frac{\text{mm}}{\text{s}}$ were selected for forging trials because they clearly exceed the β transus. As a measure of due diligence, the simulation at 913 °C with 38 $\frac{\text{mm}}{\text{s}}$ was also selected because it showed a temperature localization near β transus and no other lower temperature simulations were selected for forging trials.

4.3.1.2 Strain Results

Figures 4.30 and 4.31 show strain results for 65% reduction in height. Additionally, Figures 4.32 and 4.33 show the results for 80%. As would be expected, strains are larger at higher reductions with more prominent localizations. A strain pattern developed at both distribution locations shown in Figures 4.31 and 4.33. At the line of symmetry a single strain peak developed near the midplane while a three peak curve developed at the radial location. The single peak is shown in the top plots of Figures 4.31 and 4.33 and are related to the dead zones produced from die chill. This peak exists at the location where the dead zones contact and are forced to deform. Cooler material resists deformation more than hotter material and therefore results in

higher strain. The strain curve at the radial locations, shown in the bottom plots of Figures 4.31 and 4.33, represents the development of three strain localizations. The more prominent the peaks, the greater the localization in the material. The strain pattern is beginning to form at 65% reduction, shown in Figure 4.31, with greater localization developing at faster ram speeds. Three distinct localizations are formed at 80% reduction in height, shown in Figure 4.33 with the highest strain associated with moderate ram speed at this location. The large strain shown at 80% reduction further justified the decision to forge the previously mentioned simulations.

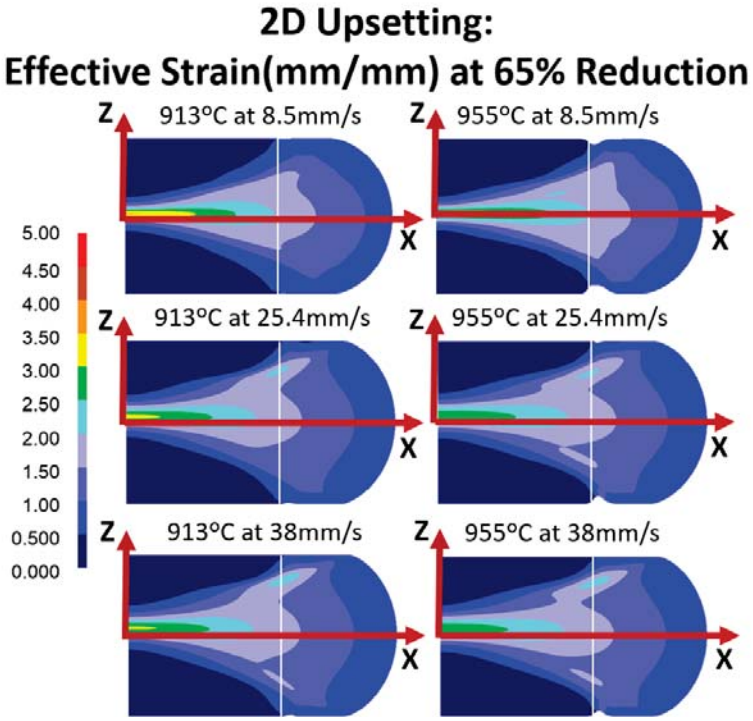

Figure 4.30. Axisymmetric two-dimensional upsetting results conducted at 65% reduction. The images are organized into two columns for each temperature and three rows for each ram speed. Faster ram speed generally resulted in more strain localization, but less overall strain due to less time for heat transfer and die chilling effects.

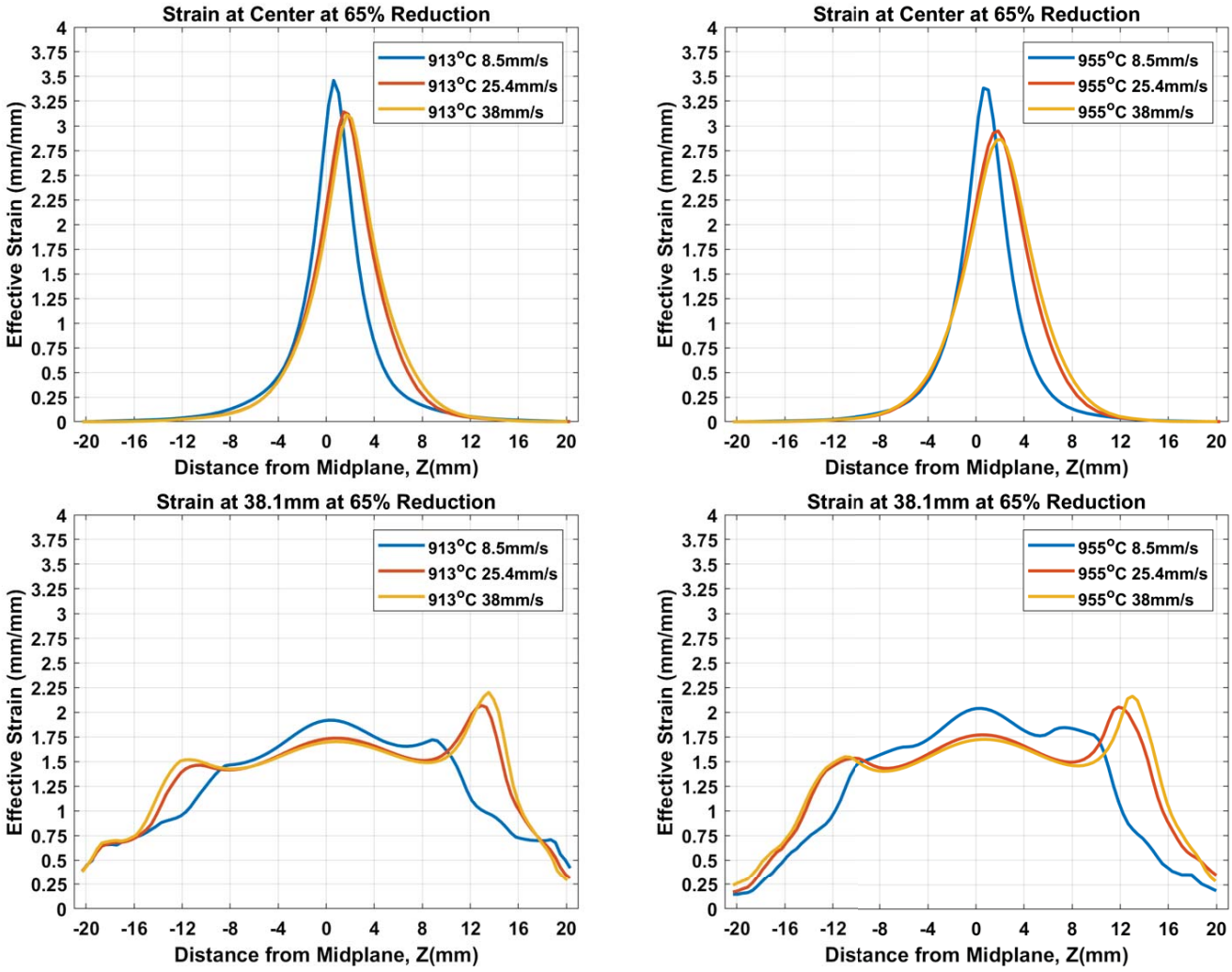

Figure 4.31. The plots depict strain distribution of each simulation from Figure 4.30. The left column shows results from 913 °C simulations and the right from 955 °C simulations. The top row depicts strain data from the line of symmetry, while the bottom row depicts strain data from a vertical line 38.1 mm from the line of symmetry. The location of this data is represented in Figure 4.30 by a vertical white line.

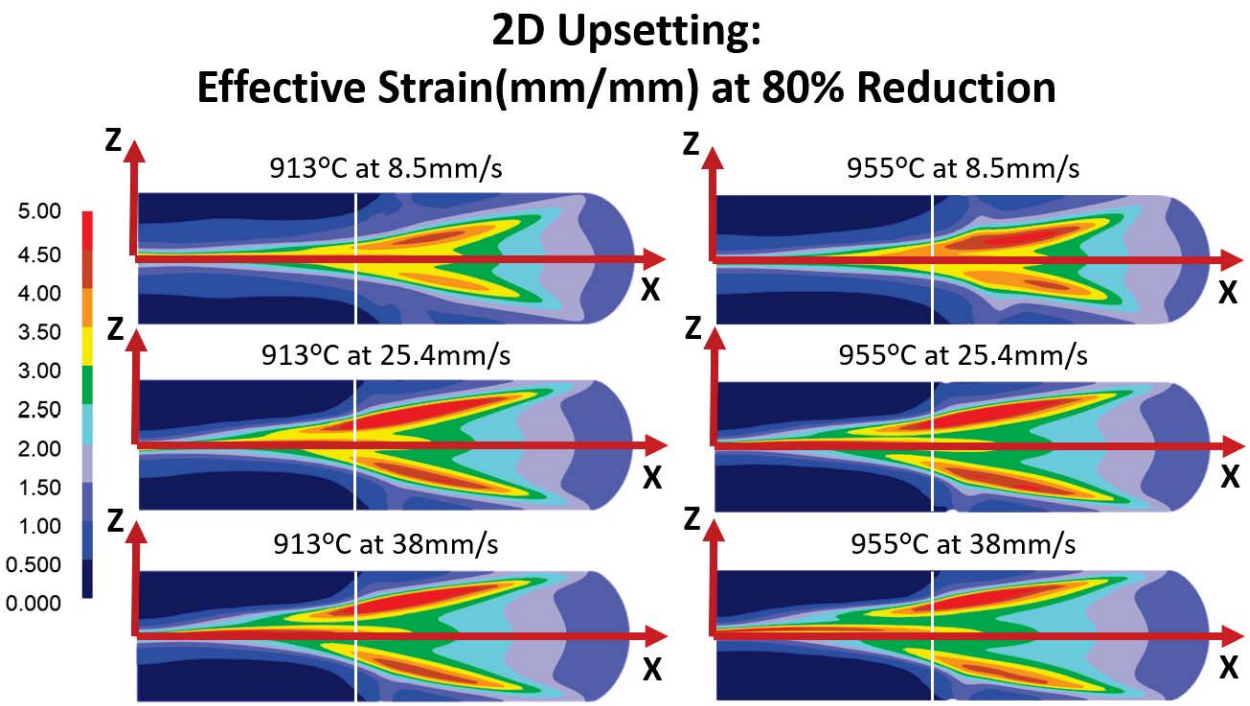

Figure 4.32. Axisymmetric two-dimensional upsetting results conducted at 80% reduction. The images are organized into two columns for each temperature and three rows for each ram speed. Faster ram speed generally resulted in greater strain localization and greater overall strain in the material.

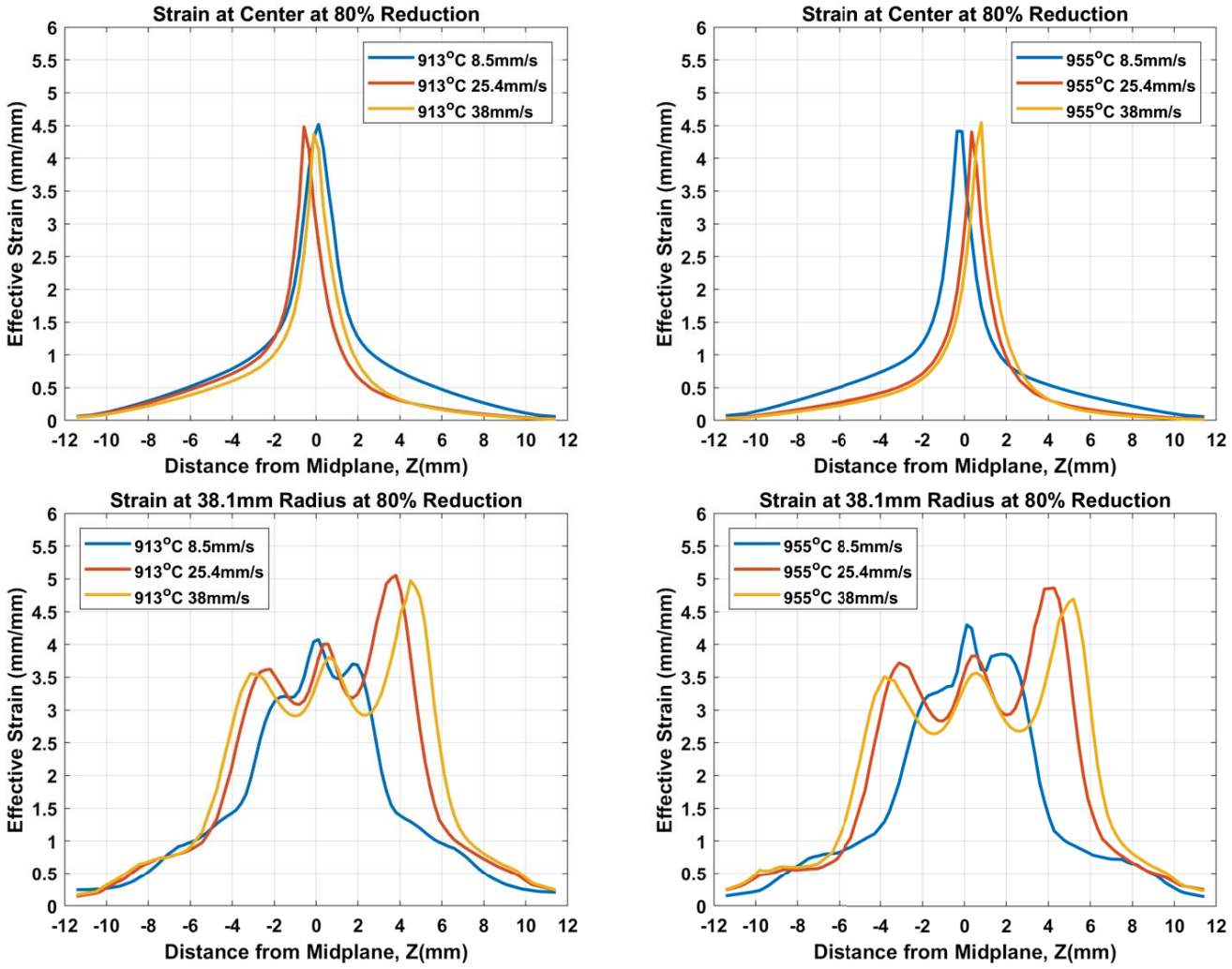

Figure 4.33. The plots depict strain distribution of each simulation from Figure 4.32. The left column shows results from 913 °C simulations and the right from 955 °C simulations. The top row depicts strain data from the line of symmetry, while the bottom row depicts strain data from a vertical line 38.1 mm from the line of symmetry. The location of this data is represented in Figure 4.32 by a vertical white line.

4.3.1.3 2-D Upsetting Flow Results

Figures 4.34 and 4.35 show material flow patterns for both sets of simulation reductions using flownet in DEFORM. Each simulation reduction appears to share very similar material flow patterns with only subtle differences observable between normal and shear strain. Specifically, edge defects begin to form on high temperature, slow ram speed simulations. The defect appears to be the development of material fold where a small section of material does not make contact with the die. This is particularly observable at 955 °C with 8.5 $\frac{\text{mm}}{\text{s}}$. Despite the possible edge effect, material flow did not have a large influence on the selection of simulations for forging trials.

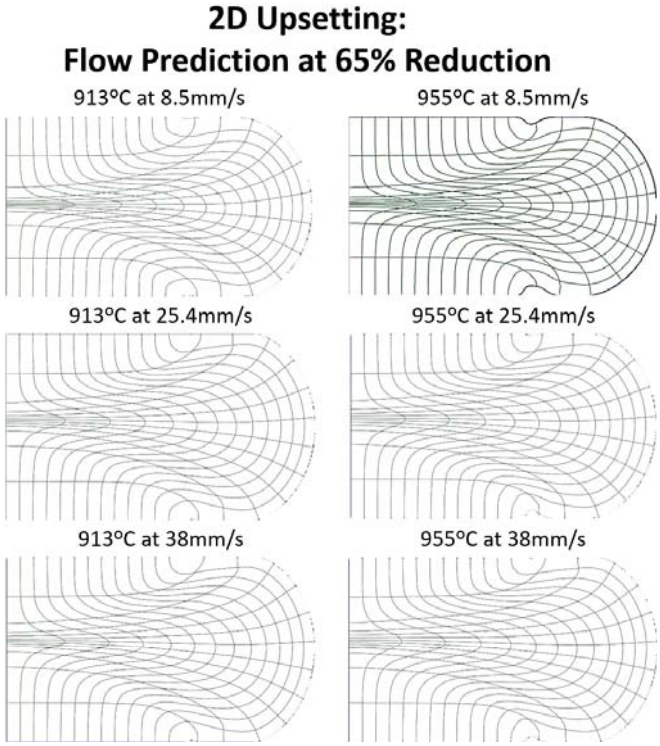

Figure 4.34. The two-dimensional upsetting results conducted at 65% reduction are shown from the line of symmetry of the workpiece. The images are organized into two columns for temperature and three rows for ram speed.

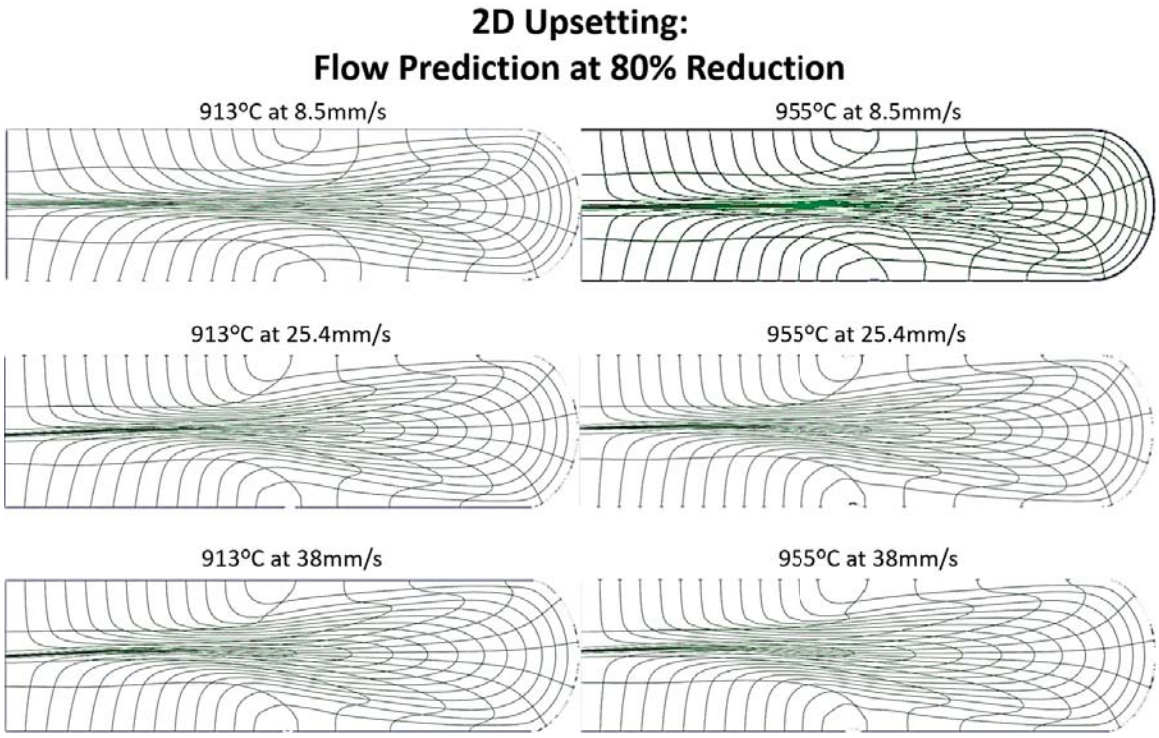

Figure 4.35. The two-dimensional upsetting results conducted at 80% reduction are shown from the line symmetry of the workpiece. The images are organized into two columns for temperature and three rows for ram speed.

4.3.2 Upsetting Simulation Findings

Simulations selected for forging trials include 913 °C with 38 $\frac{\text{mm}}{\text{s}}$ and 955 °C with 25.4 $\frac{\text{mm}}{\text{s}}$ and 38 $\frac{\text{mm}}{\text{s}}$ all at 80% reduction in height. These conditions were selected based on the previous hypothesis that larger grains will develop from regions pre-exposed to β transus temperatures during forging operations. Additionally, even if this hypothesis was proved invalid, these conditions, particularly 80% reduction in height, still represented more extreme conditions believed to produce large or abnormal grain size. In particular, strain contours of the selected simulations represent the largest strains from both sets of 60 and 80% reductions in height, shown in Figures 4.30 and 4.32. Also, material flow shows the greatest severity of shearing in the 80% reduction tests shown in Figure 4.35. For these reasons, the three most extreme upsetting forging conditions were selected for testing. A summary of upsetting

simulation conditions for forging tests are shown in Table 4.3.

Table 4.3. Selected Upsetting forging test conditions based on simulation predictions

Forging No.	Temperature (°C)	Ram Speed ($\frac{mm}{s}$)	% Reduction	Signs of AGG
8843	955	38	80	No
8844	955	25.4	80	No
8845	913	38	80	No

4.3.3 Upsetting Forging Results

Three sets of forging conditions were selected and tested in upsetting forgings. Similar to sidepressing, these conditions were selected based on the hypothesis that deformation heating a workpiece above β transus will pre-expose the material to β phase and result in abnormal grain growth during β annealing.

Prior to evaluating each forging, the simulation load-stroke data is compared against the data compiled from the forging press. The data is compared in Figure 4.36. Overall the simulations follow the same loading pattern as the forging press. At low stroke values below about 70 mm the simulation under predicts deformation loads, while at above this value the simulation overpredicts. While it is clear that the simulation derived from the sidepressing model is not perfect, it still provides a sufficient degree of predictive capacity for forging analysis.

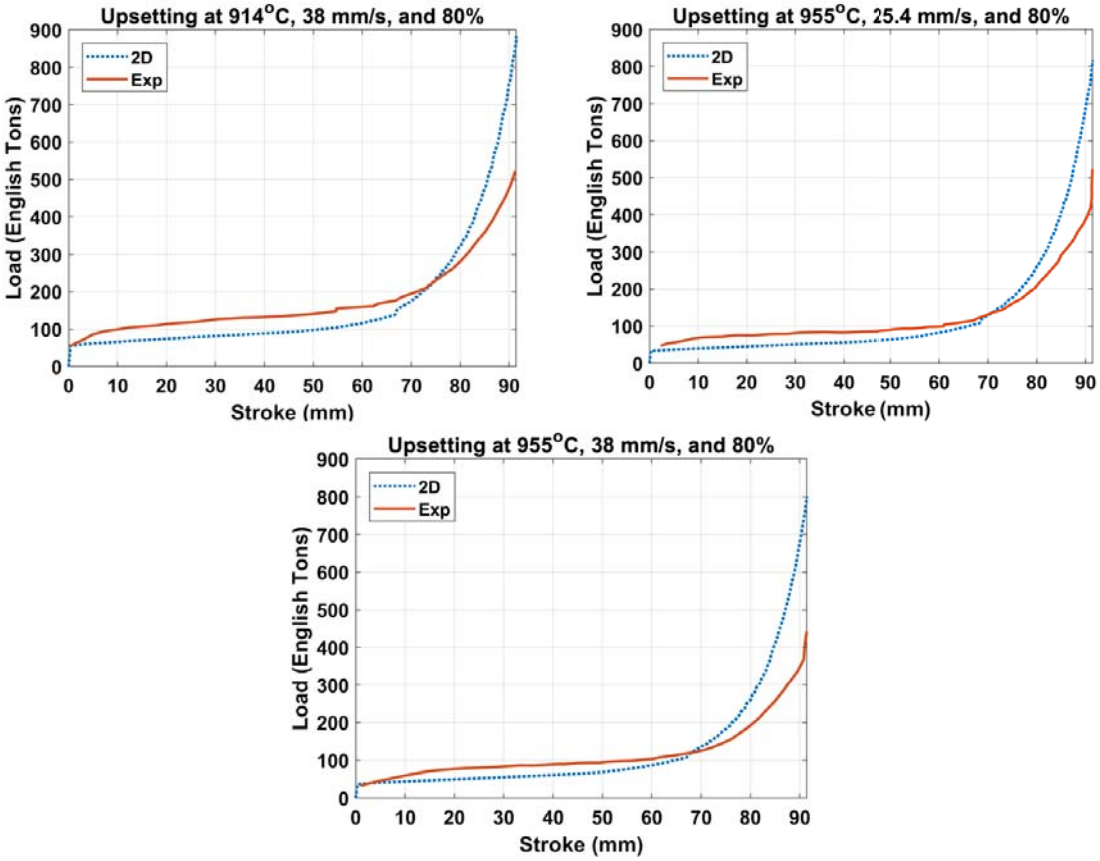

Figure 4.36. Load-Stroke plots for each forging trial are shown comparing two dimensional simulation results against experimental forging results. The simulations generally underpredict the low 70 mm reductions, except for the 955 °C and 8.5 $\frac{\text{mm}}{\text{s}}$ condition. This condition is represented well by the two dimensional simulation.

The following subsections go into detail evaluating the results from each forging trial. As was mentioned in the Section 4.2.1, Winston β annealed parts will not be evaluated in this thesis due to small grain boundaries and grains as compared to AFIT β annealed specimen. Optical results from these specimen are shown in Chapter B.

4.3.3.1 Upsetting Forging 8845 - 913 °C Initial Furnace Temperature - 38 $\frac{\text{mm}}{\text{s}}$ Ram Speed - 80% Reduction

Forging 8845 was conducted with an initial furnace temperature of 913 °C, ram speed of 38 $\frac{\text{mm}}{\text{s}}$, an 80% reduction in height, and air annealed/air cooled at AFIT. From the test matrix, these conditions represent a low forging temperature with high

ram speed and high reduction in height. Similar to the sidepressing forging tests, specimen A was β annealed at AFIT and specimen B represents the as-forged condition to show metal flow behavior. Figure 4.37 shows specimen B and the surfaces that were evaluated. Additionally, it compares the specimen to the flownet prediction generated through DEFORM. By optical examination, it is clear a qualitative correlation can be observed that the simulation is similar to the forging result.

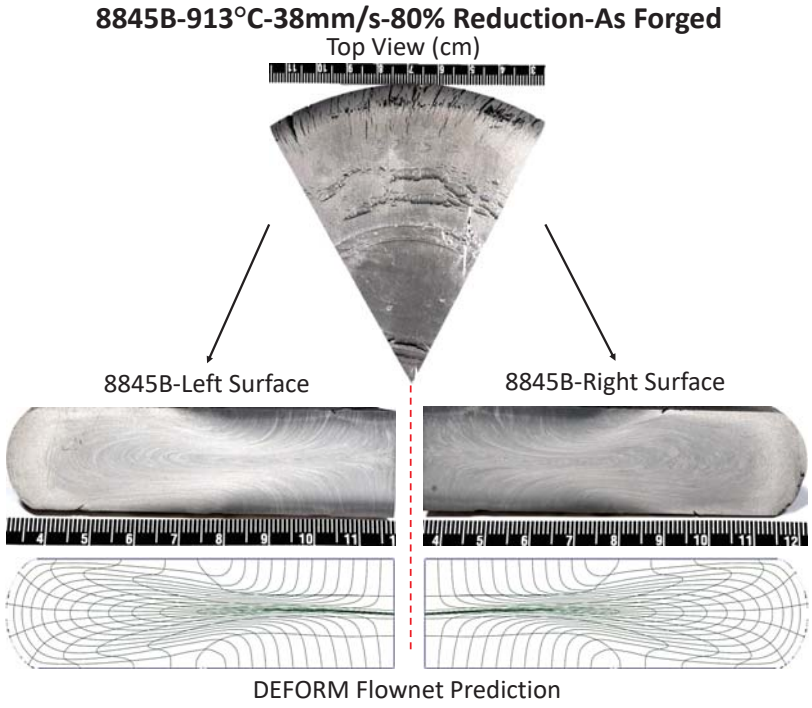

Figure 4.37. Upsetting forging result at 913 °C, 38 $\frac{mm}{s}$, 80% reduction in height in the as-forged condition compared against the DEFORM flownet prediction. Prediction show very similar metal flow patterns.

Simulation and metallography results from specimen A are shown in Figure 4.38. This figure is laid out to provide a visual comparison between the simulation and forging results. Both sides of the specimen were evaluated in order to provide more fields of view. This forging test was selected because the simulation showed a small region of material may exceed the β transus during deformation. The condition represented in this forging test, however, is of the lower temperature. Despite a fast ram speed,

the material was likely mot hot enough at time of forging for deformation heat to raise the internal temperature above transus. There are no clear AGG grain size trends or patterns in the material by optical analysis of the regions of interest. Using the lineal intercept method, average grain size and area were determined to be approximately 0.823 mm and 0.668 mm^2, respectively. When compared to sidepressing, this forging has the smallest average grains size. Without any obvious grain patterns or abnormal grain sizes, this specimen appears mostly uniformly distributed with small average grain size.

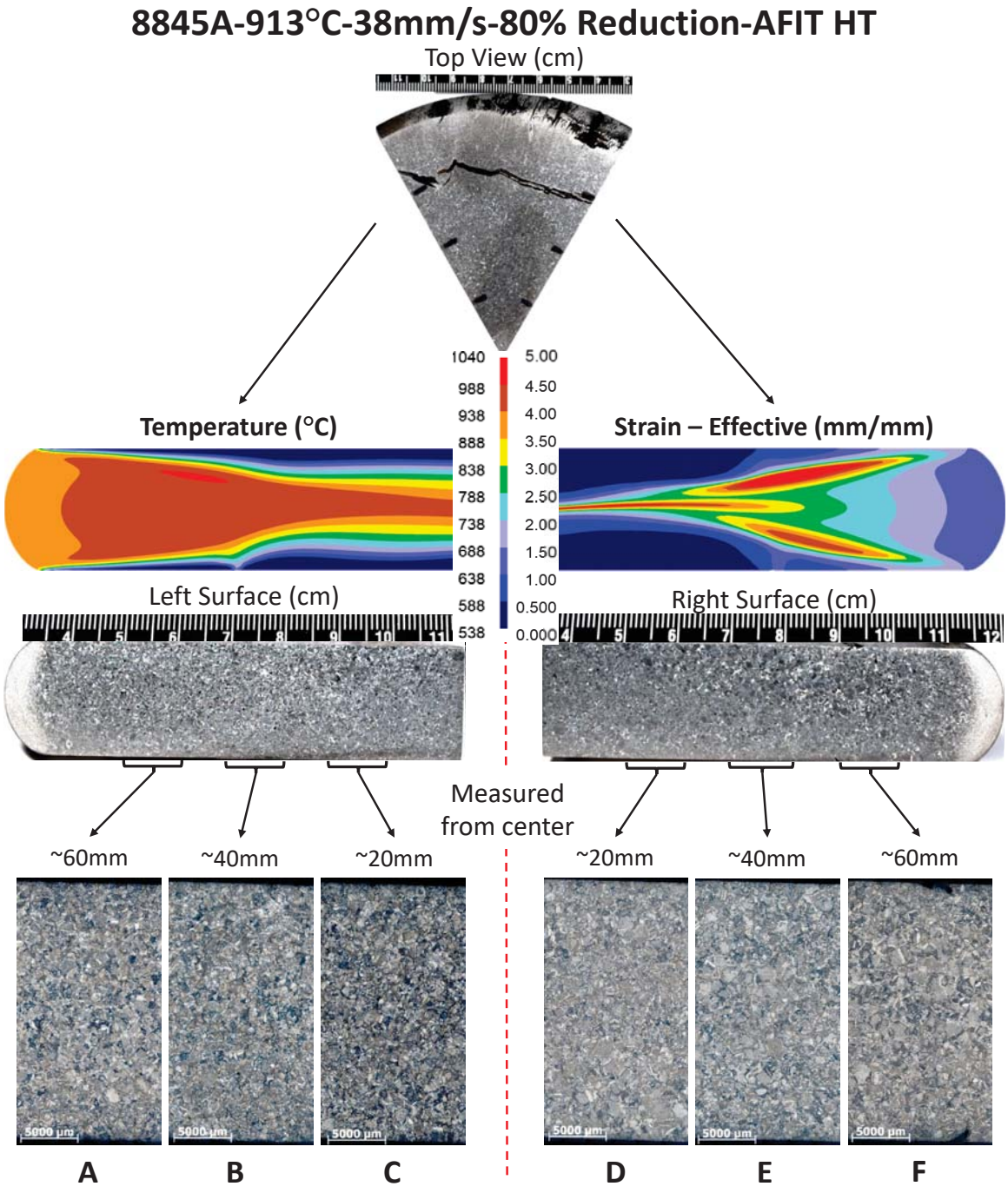

Figure 4.38. Upsetting forging result at 913 °C initial furnace temperature, 38 $\frac{\text{mm}}{\text{s}}$ ram speed, 80% reduction in height, and AFIT heat treatment. The macro scale forging images provide comparison between the predicted strain and temperature contour images. Each region of interest is labeled for closer grain size evaluation.

Even still, for the sake of comparison, a vertical section of region B was analyzed to evaluate grain distribution. The results are shown in Figure 4.39. The grain distribution appears uniform, with the larges grains observed near the bottom surface of the material. The largest grain measures approximately 1.23 mm making it only about 0.4 mm larger than the average grain.

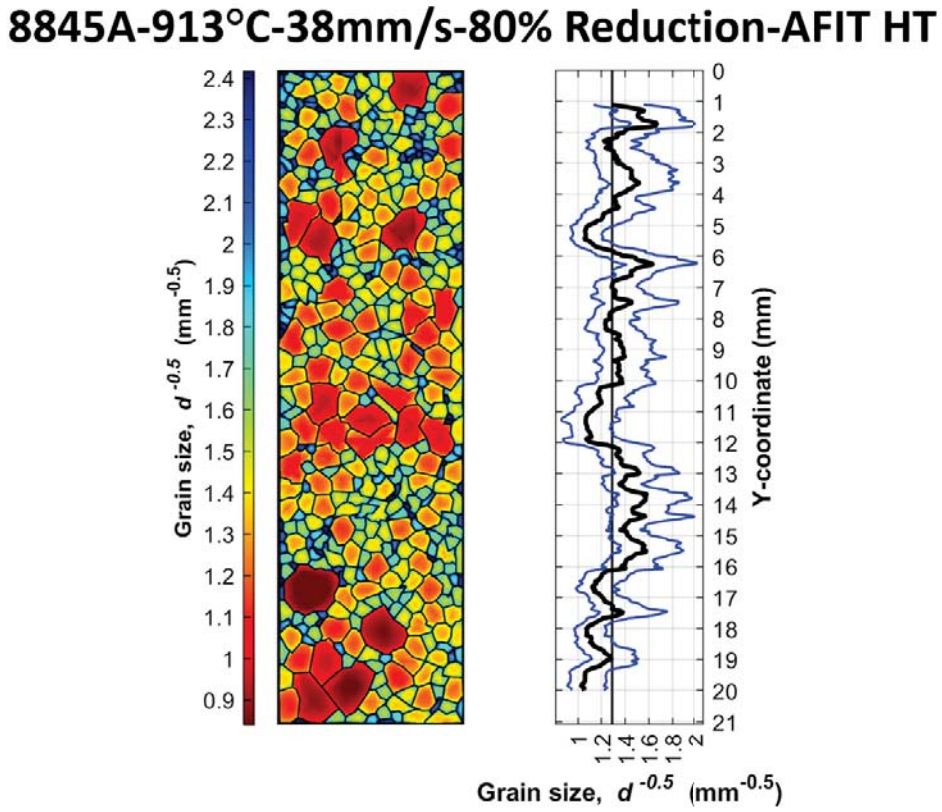

Figure 4.39. Sidepressing grain size heat map and distribution of forging 8845, specimen A, region of interest B. A 5 mm vertical section was optically processed to determine variation in grain size. Values are represented using the Hall-Petch grain size value mentioned in Section 3.8.3.

4.3.3.2 Upsetting Forging 8844 - 955 °C Initial Furnace Temperature - 25.4 $\frac{\text{mm}}{\text{s}}$ Ram Speed - 80% Reduction

Forging 8844 was conducted at 955 °C initial furnace temperature, 25.4 $\frac{\text{mm}}{\text{s}}$ ram speed, 80% reduction in height, and was β annealed in air/air cooled at AFIT. These

parameters represent a high furnace temperature and moderate ram speed. Figure 4.40 compares the as-forged results from specimen B to the material flow prediction from DEFORM. The simulation appears very similar to the forging results despite differences from the load-stroke data.

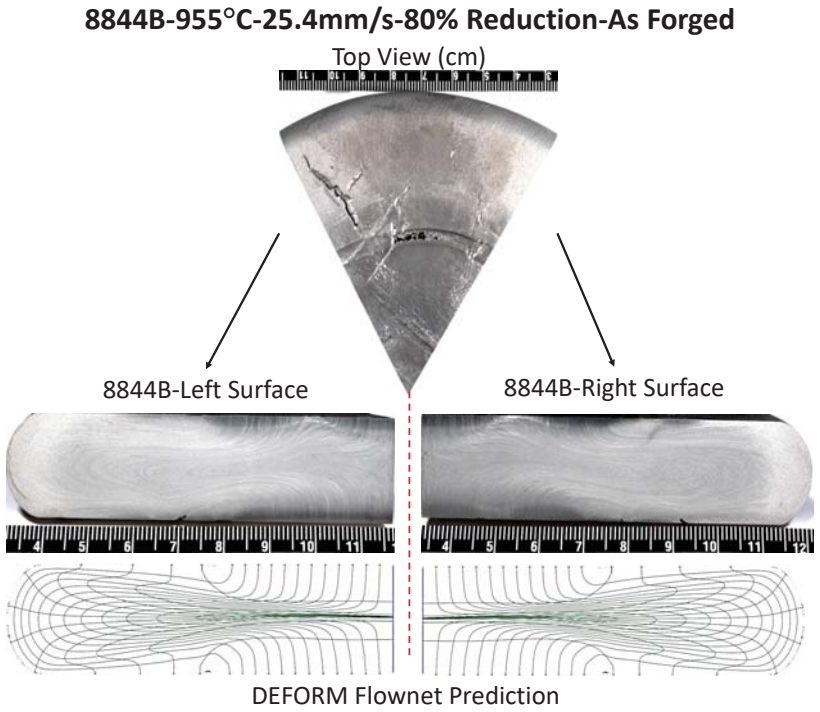

Figure 4.40. Upsetting forging result at 955 °C, 25.4 $\frac{\text{mm}}{\text{s}}$, 80% reduction in height in the as-forged condition compared against the DEFORM flownet prediction. Prediction show very similar metal flow patterns.

Optical results from specimen A are shown in Figure 4.41. The simulations for this forging test showed greater internal heat generation due large reduction in height, high initial furnace temperature, and large strain localizations. Despite lack of grain patterns, the specimen does have observably coarser grains than forging 8845. Additionally, there is greater resolution of grain boundaries making it easier to use image processing techniques. Using the lineal intercept method, the average grain diameter and area were determined to be approximately 0.853 mm and 0.707 mm^2, respectively. Still, the average grain size is smaller than observed in sidepressing tests.

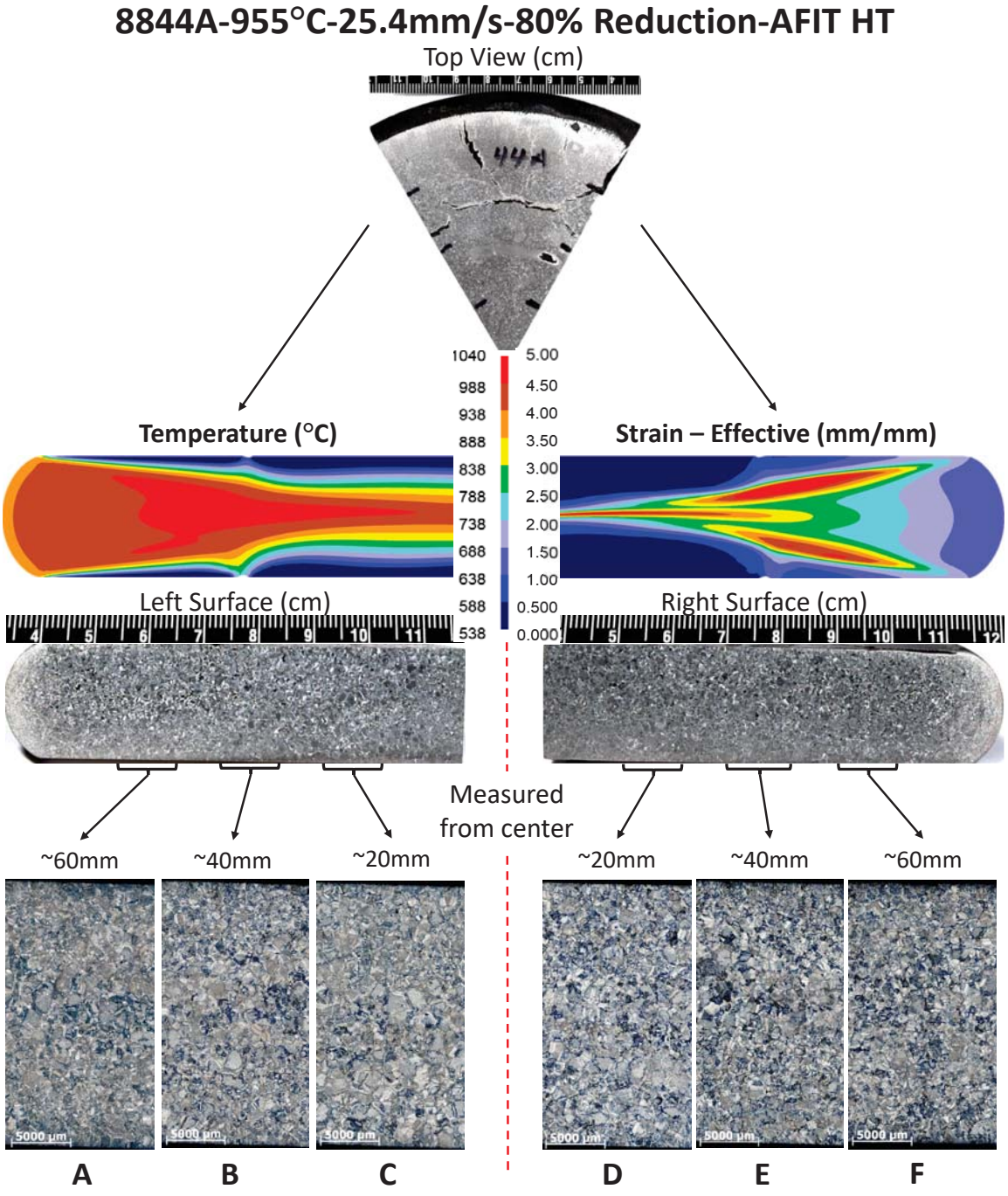

Figure 4.41. Upsetting forging result at 955 °C initial furnace temperature, 25.4 $\frac{\text{mm}}{\text{s}}$ ram speed, 80% reduction in height,and AFIT heat treatment. The macro scale forging images provide comparison between the predicted strain and temperature contour images. Each region of interest is labeled for closer grain size evaluation.

A grain size distribution analysis was conducted in the same region as forging 8845 for comparison. The results are shown in Figure 4.42. Overall, the grain size in the region appears larger than forging 8845. Additionally, the large sized grains in the region appear close to the bottom surface, but are closer to the center than those of forging 8845. The maximum grain size estimated in the distribution is approximately 1.56 mm and is almost twice the size of the specimen's average grain diameter. Regions of abnormal grain growth do not appear obvious with this forging condition, but it is clear that grain size is increasing between specimen.

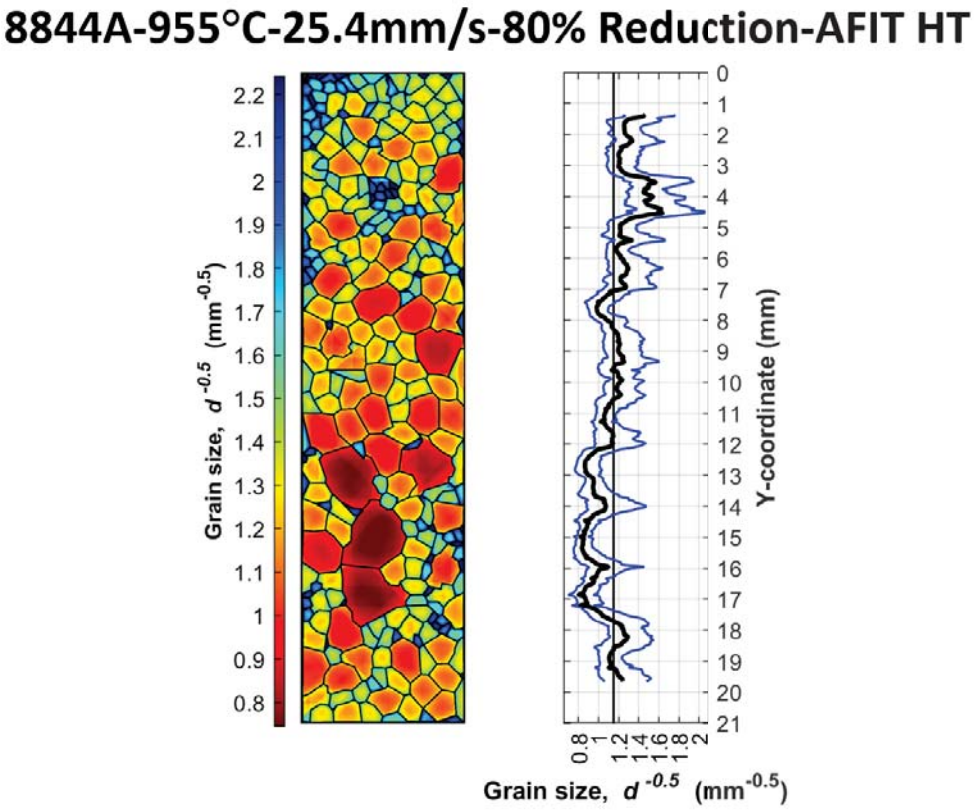

Figure 4.42. Sidepressing grain size heat map and distribution of forging 8844, specimen A, region of interest B. A 5 mm vertical section was optically processed to determine variation in grain size. Values are represented using the Hall-Petch grain size value mentioned in Section 3.8.3.

4.3.3.3 Upsetting Forging 8843 - 955 °C Initial Furnace Temperature - 38 $\frac{mm}{s}$ Ram Speed - 80% Reduction

Forging 8844 was conducted at 955 °C initial furnace temperature, 38 $\frac{mm}{s}$ ram speed, 80% reduction in height, and was β annealed at AFIT. These parameters represent a high furnace temperature and fast ram speed. Figure 4.43 compares the as-forged results from specimen B to the material flow prediction from DEFORM. Even with fast forging speed and high reduction in height, the simulation still appears very similar to the forging results.

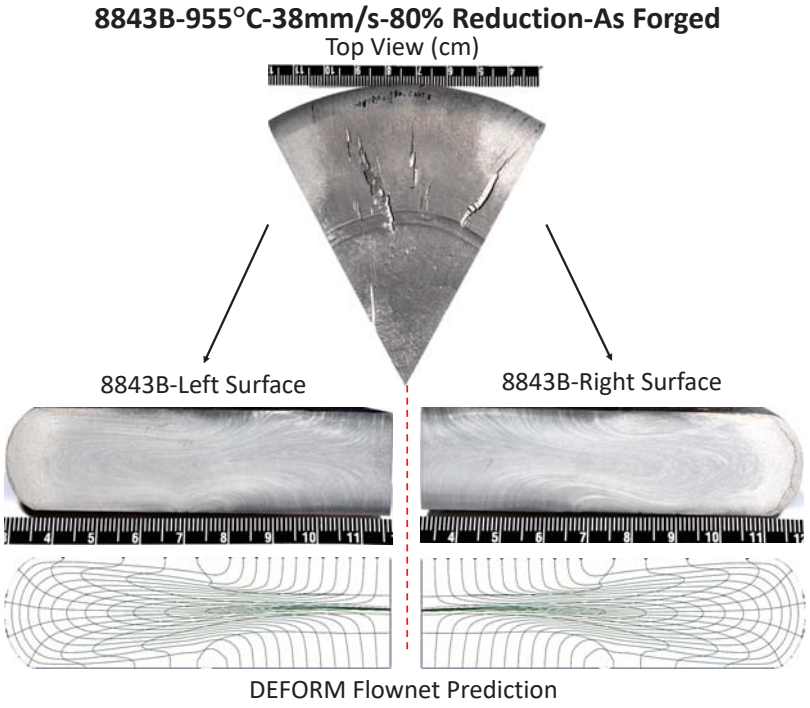

Figure 4.43. Upsetting forging result at 955 °C initial furnace temperature, 38 $\frac{mm}{s}$ ram speed, 80% reduction in height in the as-forged condition compared against the DEFORM flownet prediction. Prediction show very similar metal flow patterns.

Optical results for specimen A are shown in Figure 4.44 and are compared against simulation results. This forging test represents the most extreme parameters in the test matrix. Simulations also predicted it would achieve the highest internal temperature and remain above β transus for approximately two seconds after forging had

ceased. Additionally, due to high reduction in height, this condition also has high strain localizations that help portray the regions that may result in the highest temperatures. Still, no optical grain patterns or trends are discernible. However, grain size is notably larger than the previous forgings. Using the lineal intercept method, the average grain size and area were estimated to be approximately 1.05 mm and 1.056 mm^2, respectively. This is the largest average compared to the other upsetting forging tests. A proportional relationship seems to exist between change in grain size and forging ram speed in upsetting forgings.

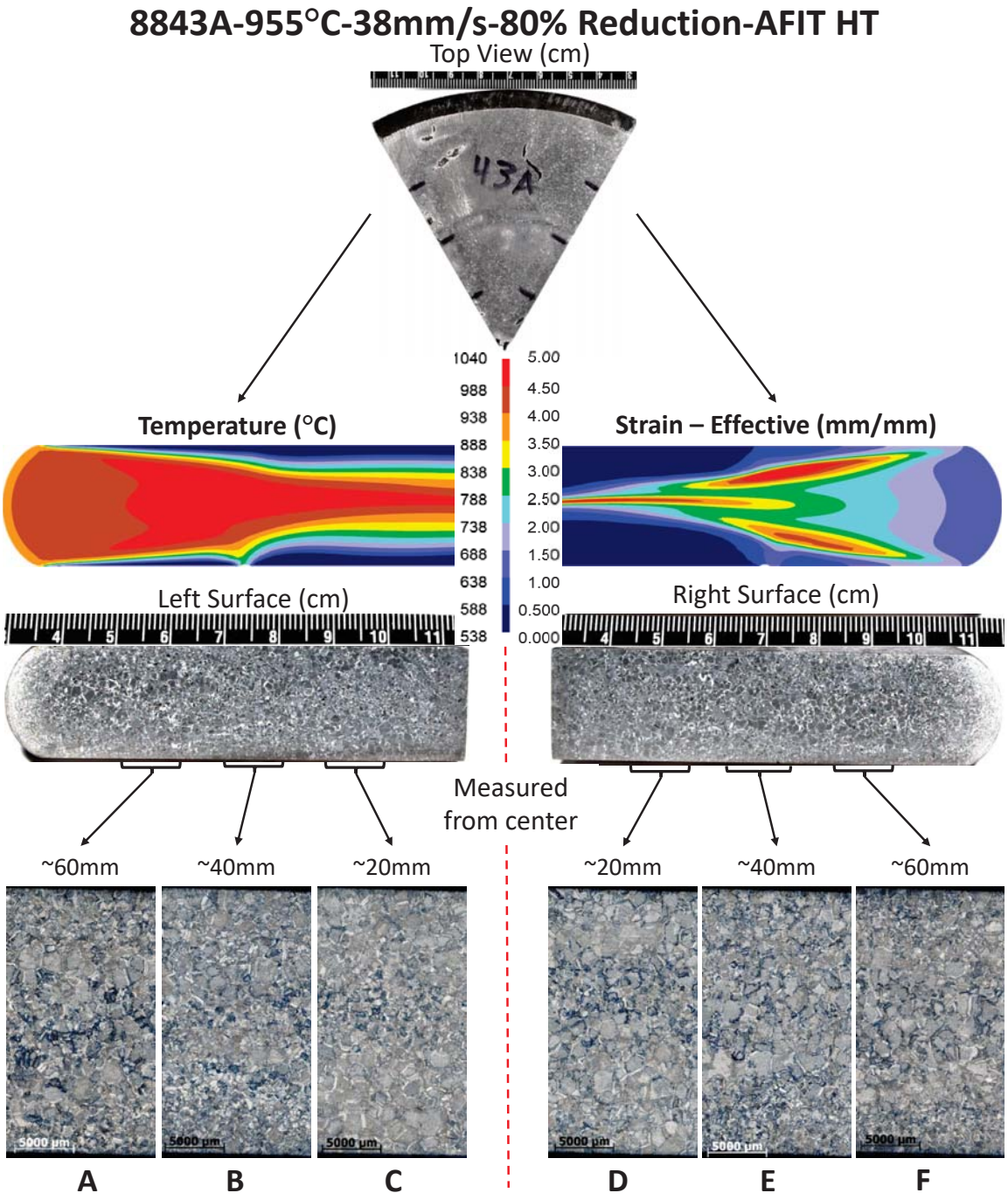

Figure 4.44. Upsetting forging result at 955 °C initial furnace temperature, 38 $\frac{\text{mm}}{\text{s}}$ ram speed, 80% reduction in height,and AFIT heat treatment. The macro scale forging images provide comparison between the predicted strain and temperature contour images. Each region of interest is labeled for closer grain size evaluation.

A grain size distribution analysis was conducted to evaluate potential abnormal grain growth. The results for this forging are shown in Figure 4.45. The maximum grain size in the distribution is similar to that of forging 8844, but the locations are different. The large grains are no longer near the bottom surface, but a grouping now forms just above the center. This group migration with ram speed may be simple coincidence, but warrants additional attention for later research. Additionally, the distribution of grains surrounding the large grains appear more dramatic. Though abnormal grain growth is not evident in the upsetting specimen, it appears as though the tested forging conditions do result in larger grains with faster forging speeds, a relationship that appears opposite to sidepressing specimen.

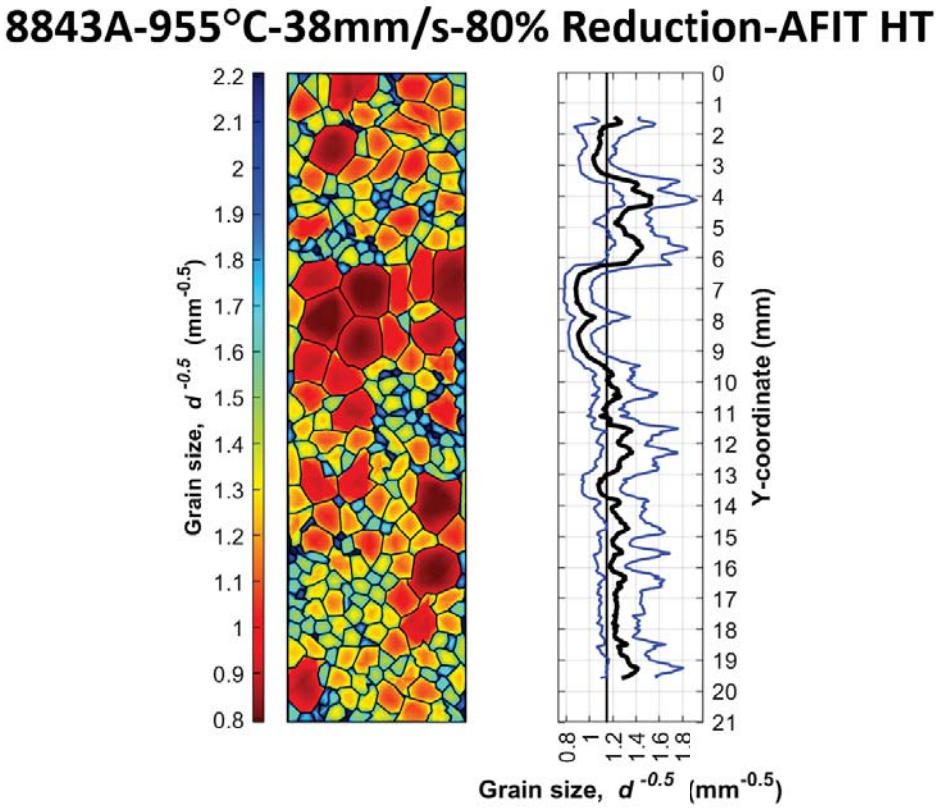

Figure 4.45. Sidepressing grain size heat map and distribution of forging 8843, specimen A, region of interest B. A 5 mm vertical section was optically processed to determine variation in grain size. Values are represented using the Hall-Petch grain size value mentioned in Section 3.8.3.

4.3.4 Upsetting Summary

Three upsetting forging conditions were tested based on simulation results showing deformation heating from high strain regions. The forging tests were evaluated for grain size and distribution to determine if pre-exposure to β transus would effect grain growth. The increase forging conditions tested showed that large grain size is effected by the initial furnace temperature and ram speed. Test showed a drastic difference in average grain size between specimen of different temperature with all other conditions being the same. Similarly, a large difference was seen between specimen of similar temperature, but different ram speeds.

A summary of the measurements gathered using the lineal intercept method are shown in Table 4.4 by forging number. Additionally, a side-by-side comparison of the vertical distribution of the evaluated specimen is shown in Figure 4.25

Table 4.4. Summary of average grain size measurements via lineal intercept method

Forging no.	Mean lineal intercept (mm)	Std. Dev. (mm)	95% C.I. (mm)	% Relative Accuracy	ASTM Grain Size no.	Average Diameter (mm)	Average Area (mm^2)
8843	0.908	0.081	0.100	11.018	10.277	1.05	1.056
8844	0.744	0.043	0.054	7.197	10.853	0.853	0.707
8845	0.725	0.076	0.094	13.015	10.928	0.823	0.668

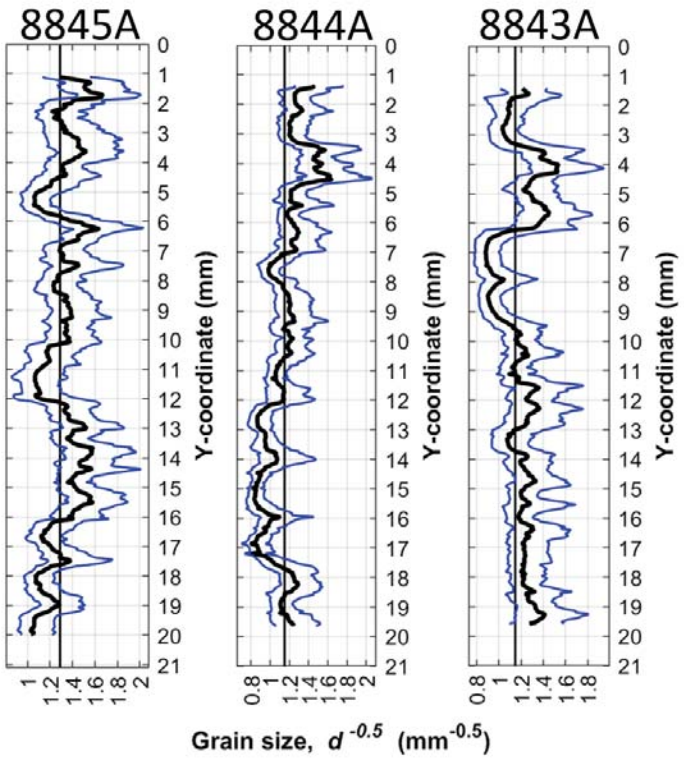

Figure 4.46. Upsetting grain size distribution plot comparison between forging 8843, 8844, and 8845.

4.4 Summary

In summary, this thesis has shown that simulations can be used to assist in predicting development of AGG in Ti-6Al-4V. Two sets of twelve simulations were conducted based on standard forging conditions between idealized sidepressing and upsetting processes. Based on these results, temperature and strain localizations were identified to select parameters most likely to result in AGG. Through this analysis, the hypothesis that unintentionally pre-exposing material to β transus temperature, was developed. Simulations were selected based on high temperature localizations and tested to determine resulting grain size.

Sidepressing results showed an inverse relationship with average grain size and ram speed. As ram speed increases, average grain size decreases. However, the reduction

in average grain size is compensated by the development of abnormally large grains. As mentioned in Section 2.3.7, AGG is the growth of a small number of grains at a rate greater than the average grain size. Despite producing large average grain sizes, slow ram speed sidepressings resulted in uniform distribution of grain size throughout the specimen. In contrast, upsetting forgings did not produce any noticeable abnormal grain growth. Instead it was shown that increasing initial furnace temperature and increasing ram speed resulted in larger average grain size.

There are a lot variables with large effects on forging processes. Despite an inverse in the effects of ram speed between sidepressing and upsetting processes, it is clear that temperature has a large effect on grain size. All forgings with the same ram speed but higher initial furnace conditions resulted in larger average grain size than its counterpart. This alone shows forging sensitivity to temperature. Furthermore, it is clear through sidepressing, that exceeding the β transus also has an effect on AGG development during forging.

V. Conclusions and Recommendations

5.1 Summary

The goal of this thesis was to use Finite Element Method (FEM) as a tool to predict the development of Abnormal Grain Growth (AGG) in forging specimens. Initial furnace temperature, ram speed, and reduction in height were parameters selected for analysis because of their effects on temperature and strain during forging. Two forging operations, sidepressing and upsetting, were selected as idealized processes to evaluate because of their common use in industry. From these processes a series of simulations were developed to predict the results furnace temperature, ram speed, and reduction in height have on strain and temperature in the material. These simulations were used to guide the selection of conditions for forging tests based on localizations generated in the workpiece. In particular, conditions resulting in deformation heat during forging causing internal temperature to exceed the β transus temperature, were selected.

Forging tests were conducted and evaluated to determine the effects of forging parameters on the development of grain size. Optical microscopy, lineal intercept method, and point intercept method were used to evaluate the material for grain size and distribution. Additionally, the tests were used to compare forging results with simulation results to determine their validity. Comparison of load-stroke data, workpiece dimensions, and material flow were key metrics for validating results. Forgings were then compared against each other to determine relationships between varying parameters and to determine if AGG had occurred.

5.2 Conclusions

Several conclusions were drawn from this work. FEM is a powerful tool that is capable of predicting useful results representative of physical operations. By evaluating temperature generated through deformation, it is possible to identify forgings at risk of exceeding β transus temperature. Sidepressing forgings predicted to exceed the transus temperature were forged, evaluated, and discovered to lead to AGG when high initial furnace temperature, fast ram speeds, moderate reduction in height, and air annealing and cooling conditions were applied. In contrast, sidepressing forgings of the same parameters, but with slow ram speed were found to develop smaller AGG and have a larger more uniformly distributed average grain size.

When the same conditions were applied to upsetting forgings, it was found that fast ram speeds at high initial furnace temperatures develop large/coarse grains, while lower initial furnace temperatures or lower ram speeds produce finer average grain size. The difference in results might be attributable to either reduction in height or type of forging operation. Reduction in height might have an effect on the distribution of grain size throughout the material. The possibility exists that a large reduction in height, as seen in the upsetting forgings, may cause excessive deformation that results in an even distribution of grain sizes. An alternative thought, is that axial stress from upsetting forgings versus plane strain from sidepressing forgings respond differently to forging parameters. When upsetting and sidepressing simulations were compared, the strain and temperature patterns predicted through simulations were different and their effect on grain size was not clear.

In all cases, initial furnace temperature had a notable effect on grain size. When forgings of the same ram speed, reduction in height, geometry, and annealing processes are compared, the specimen with the higher initial furnace temperature developed larger average grain size. This makes sense because more energy is being introduced

to the material when the initial furnace temperature is higher. In contrast, with all other parameters being the same, small average grain size developed when vacuum annealing with Nitrogen quench was used instead of air annealing and cooling. Based on the differences in annealing processes, limiting exposure above the β transus after annealing will result in smaller grain size because the material does not linger around the β transus temperature as it does with slow cooling rates.

In addition, sidepressing tests appeared more sensitive to the development of AGG. In sidepressing tests it was shown that ram speed effects the development of AGG by causing deformation heat increasing temperature localizations in the material beyond the β transus temperature. In contrast, upsetting forgings under the same conditions, but greater reduction in height, did not result in AGG. Also notable, the center/core localization with the highest predicted temperature in sidepressing simulations was shown to correspond to the development of AGG in the physical sidepressing tests. The use of Design Environment for Forming (DEFORM) to predict the location of AGG in a forging has profound impacts in the Air Force and Industry.

The research conducted was sufficient to adequately answer the research questions presented in Section 1.3. It was identified that ram speed in combination with high initial furnace temperature contributed the most to the development of AGG in Ti-6Al-4V sidepressings by increasing deformation heat generated in the material to cause it to be pre-exposed to the β transus temperature. Sidepressing tests were also discovered to be more sensitive to ram speed and the development of AGG than upsetting tests with the same conditions, but greater reduction in height. In sidepressing tests the forging parameters that most likely result in AGG were high initial furnace temperature (about 50 °C below β transus temperature), Fast ram speed greater than 25.4 $\frac{\text{mm}}{\text{s}}$, and moderate reduction in height at 65%. The parameters that result in AGG in upsetting forgings are not yet fully understood. Additional

research is required to determine these values.

5.3 Recommendations

In industry it is recognized that near net forgings reduce the number of forging steps, use fewer resources, and lower costs. It is possible that the deformation and the consequent heat generated in these forgings may result in the material exceeding and being pre-exposed to the β transus temperature. By applying this research to industry it is recommended that forging facilities use an FEM solver to simulate their forging processes to evaluate temperature localizations during the deformation. These simulations can be used to determine if the material is predicted to exceed the β transus temperature. If so, then the forging design would be re-worked to relieve the cause of deformation heat. In the case of near net forgings, an additional forging step may be required.

Impacts extend to the Air Force as parts with AGG continue to be discovered throughout the fleet. The effects of AGG on the mechanical properties of these parts is not well understood and therefore it is desired that the parts be removed and quarantined. Based on this research it is recommended that the Air Force use these findings to develop specimen with AGG for mechanical testing to begin quantifying the impact AGG has on affected parts. Additionally, affected program offices should work with part suppliers to develop forging FEM simulations representative of existing forging processes to determine if they are at risk of exceeding the β transus temperature. By doing so, they will also determine the location most likely to develop AGG, which can be used to develop more targets and efficient aircraft inspections.

5.4 Future Work

Additional testing is required to further separate the effects of ram speed from reduction in height. Air Force Research Laboratory (AFRL) has additional preforms available for forging work and analysis. Future work should focus on simulation refinement and additional sidepressing and upsetting tests. These results have shown that the developed simulation tends to over predict deformation loads. Additional simulation refinement should be conducted with data gathered from the forging tests conducted in this thesis. Deformation profiles and material flow are represented well in the current simulations, but loading data requires further refinement. With data generated from the forging press, it should now be possible to iterate through the simulations to produces more representative loading, strain, and temperature predictions.

Two sidepressing preforms remain available for additional testing. Based on the results from this thesis, a forging test at 955 °C initial furnace temperature , 38 $\frac{\text{mm}}{\text{s}}$, and 75-80% reduction in height would provide additional insight into the effects of reduction in height on the development of abnormal grains. Additionally, the same parameters, but at a lower reduction in height around 45-50 % may provide an indication of when AGG begins to develop through reduction in height and temperature generation.

Three upsetting preforms remain available for testing as well. Further analysis on the effects of reduction in height and deformation heat generation should also be evaluated for this process. It seems intuitive that upsetting processes are more sensitive to the effects of reduction in height because their preforms are longer in the direction of deformation. Therefore a percentage reduction will result in more material deformation than that of a sidepressing process. Testing with a reduction in height around 50% seems large enough to produce deformation heat, but small

enough not to over deform the workpiece. Unlike sidepressing, a grain size pattern could not be distinguished in the 80% reduction upsetting tests. Lower deformation may retain a grain pattern that could lead to further insight into the development of AGG by means of ram speed and reduction in height.

The peculiarity of AGG in titanium forgings has plagued the development of next generation aircraft. The uncertainty of its material effects presents safety issues resulting in additional man power costs for continuous part inspections. AGG has been so elusive that material scientists have not been able to reproduce it in specimens for testing. The first step to understanding the effects of this microstructural phenomenon is to understand the forging parameters that produce it. Once reproducibility is established, then testing can be accomplished with representative specimen. Until then, the Air Force will be flying blindly with a potential structural issue on some of the most advance aircraft in the world. This research takes the first directed step towards reproducing and understanding the cause of AGG in Ti-6Al-4V.

Appendix A. Two-Dimensional Convergence Studies

Convergence studies were conducted for both two-dimensional sidepressing and upsetting simulations.

A.1 Sidepressing Convergence Study

The image in Figure A.1 shows the locations of specific points used to track simulation convergence throughout the full range of deformation. Images in Figures A.2 to A.5 show convergence of temperature values while Figures A.6 to A.9 shows convergence of strain values. Convergence occurs at 8,000 elements with a step ratio of 0.01 seconds/step.

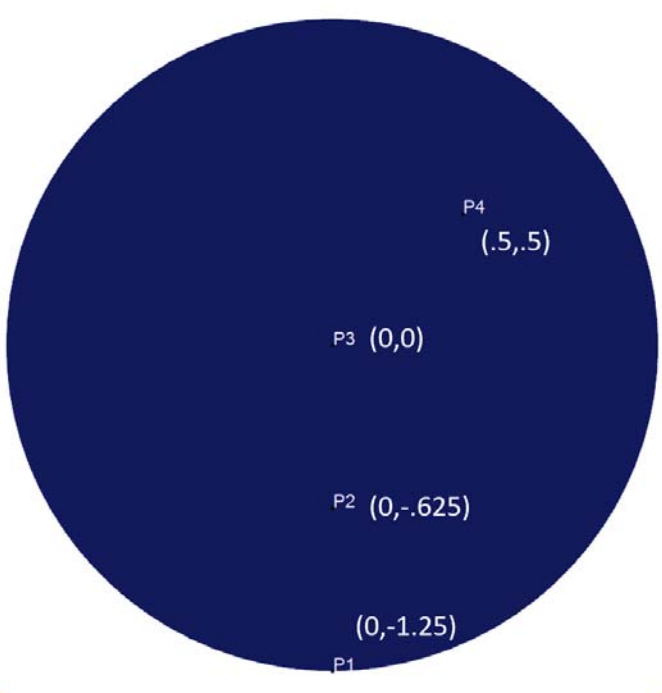

Figure A.1. Two-dimensional sidepressing preform with points labeled for convergence tracking.

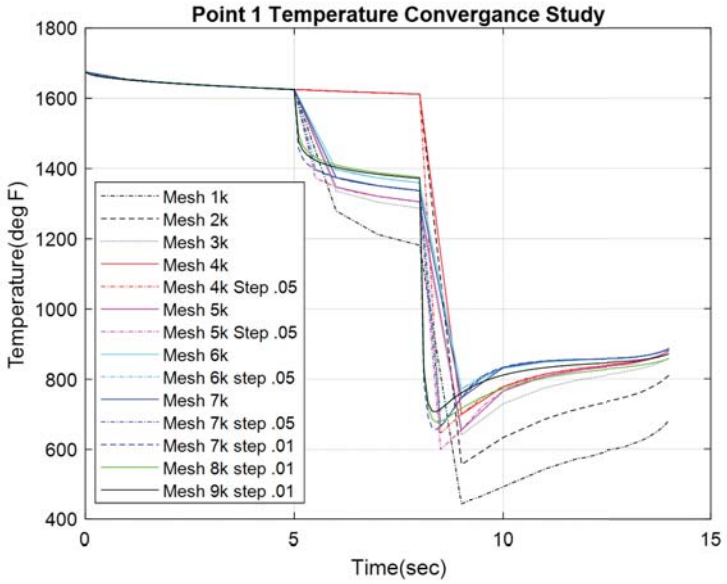

Figure A.2. Two-dimensional sidepressing temperature convergence plot of a point at (0,-1.25) inches on the preform.

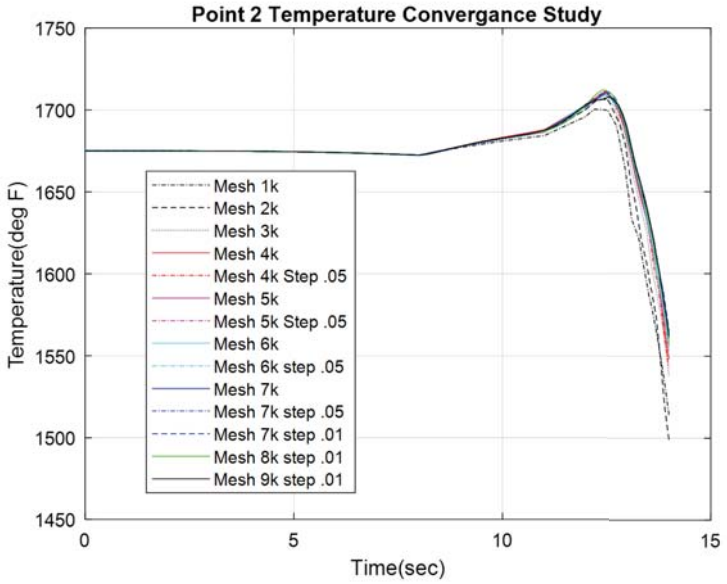

Figure A.3. Two-dimensional sidepressing temperature convergence plot of a point at (0,-0.625) inches on the preform.

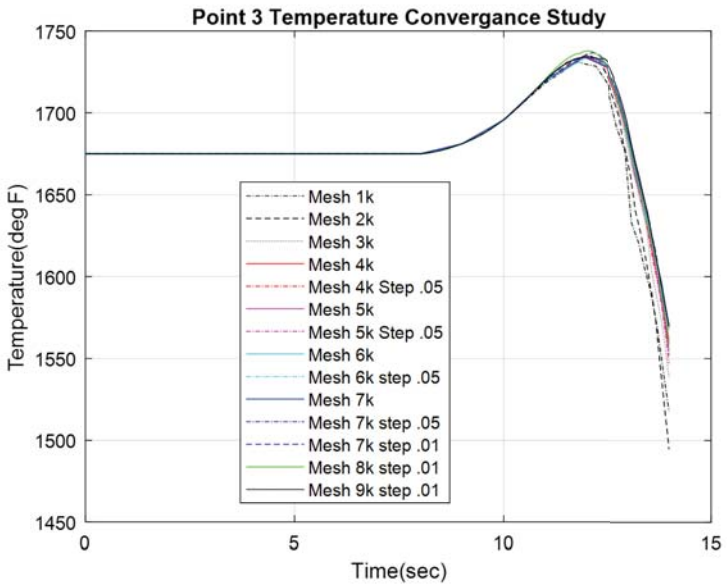

Figure A.4. Two-dimensional sidepressing convergence plot of a point at (0,0) inches on the preform.

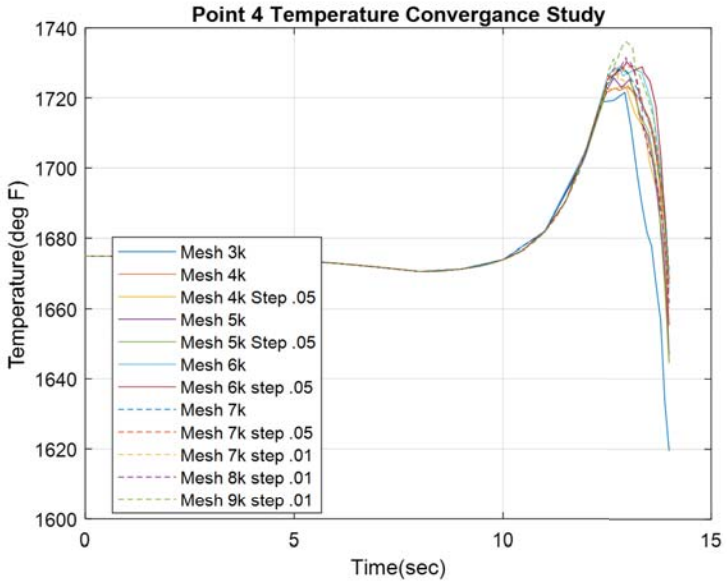

Figure A.5. Two-dimensional sidepressing temperature convergence plot of a point at (0.5,0.5) inches on the preform.

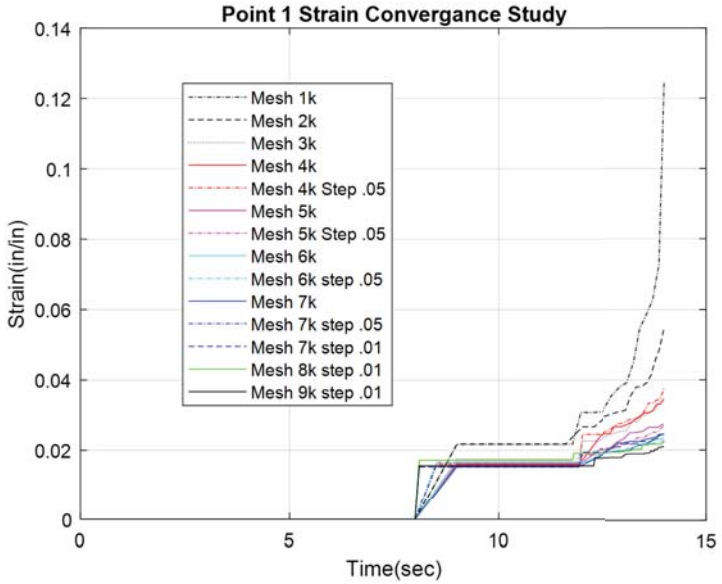

Figure A.6. Two-dimensional sidepressing strain convergence plot of a point at (0,-1.25) inches on the preform.

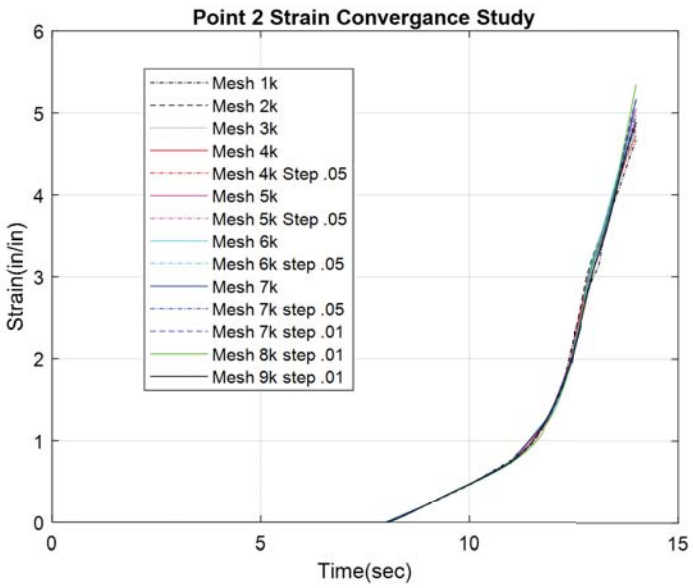

Figure A.7. Two-dimensional sidepressing strain convergence plot of a point at (0,-0.625) inches on the preform.

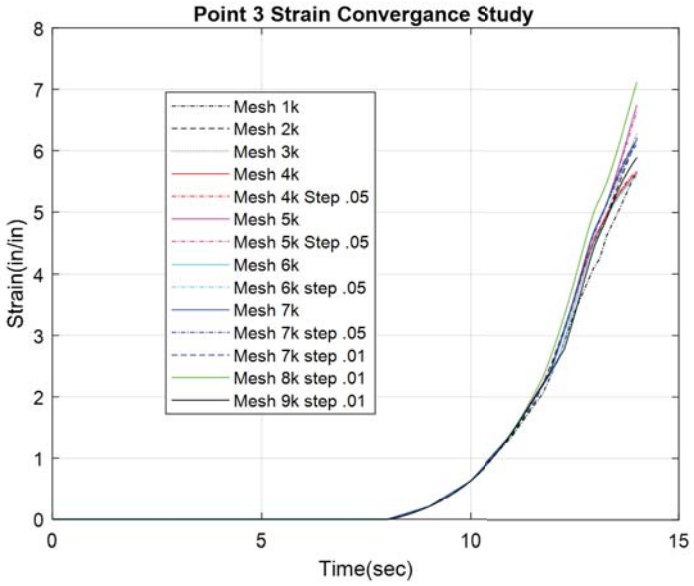

Figure A.8. Two-dimensional sidepressing strain convergence plot of a point at (0,0) inches on the preform.

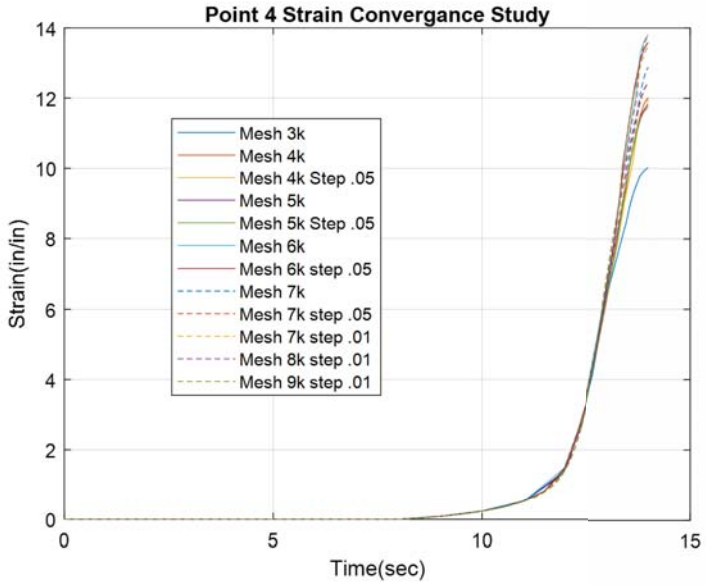

Figure A.9. Two-dimensional sidepressing strain convergence plot of a point at (0.5,0.5) inches on the preform.

A.2 Upsetting Convergence Study

Figure A.10 shows the location of a point used to evaluate convergence in the two-dimensional upsetting simulation. The point is located at (0.25, 2.25) inches from the origin. The stimulation converges quickly with as few as 1,000 elements as shown in Figures A.11 and A.12. As a measure of safety, 4,000 elements were used for this simulation because computational time remained low at about 15 minutes per simulation run.

Figure A.10. Two-dimensional upsetting preform with a point labeled for convergence tracking.

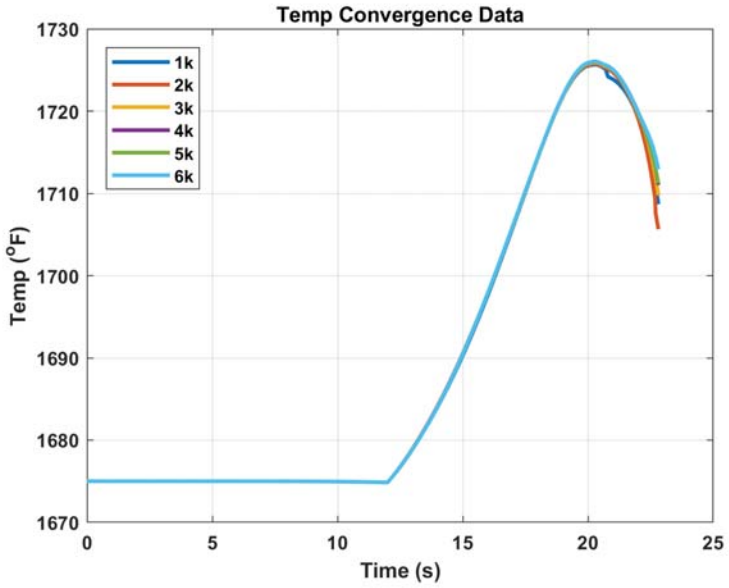

Figure A.11. Two-dimensional upsetting temperature convergence plot of a point at (0.25,2.25) inches on the preform.

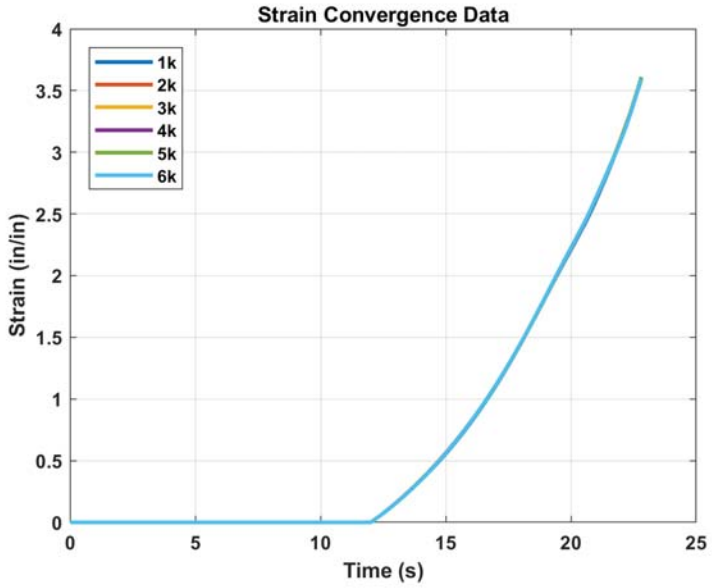

Figure A.12. Two-dimensional upsetting strain convergence plot of a point at (0.25,2.25) inches on the preform.

Appendix B. Winston Heat Treatment Optical Results

This appendix provides additional optical results for specimen C of each forging operation. Specimen C was annealed at Winston Heat Treating in a vacuum and cooled with a nitrogen quench. The controlled atmosphere and fast cooling rate resulted in a fine microstructure and fewer precipitates in the grain boundaries. Although this process is well controlled and exceeds industry standards, it is also very challenging to evaluate optically. Furthermore, grain size is noticeably smaller than the specimen annealed in open air. These results are provided as a supplement for further/future analysis of this work.

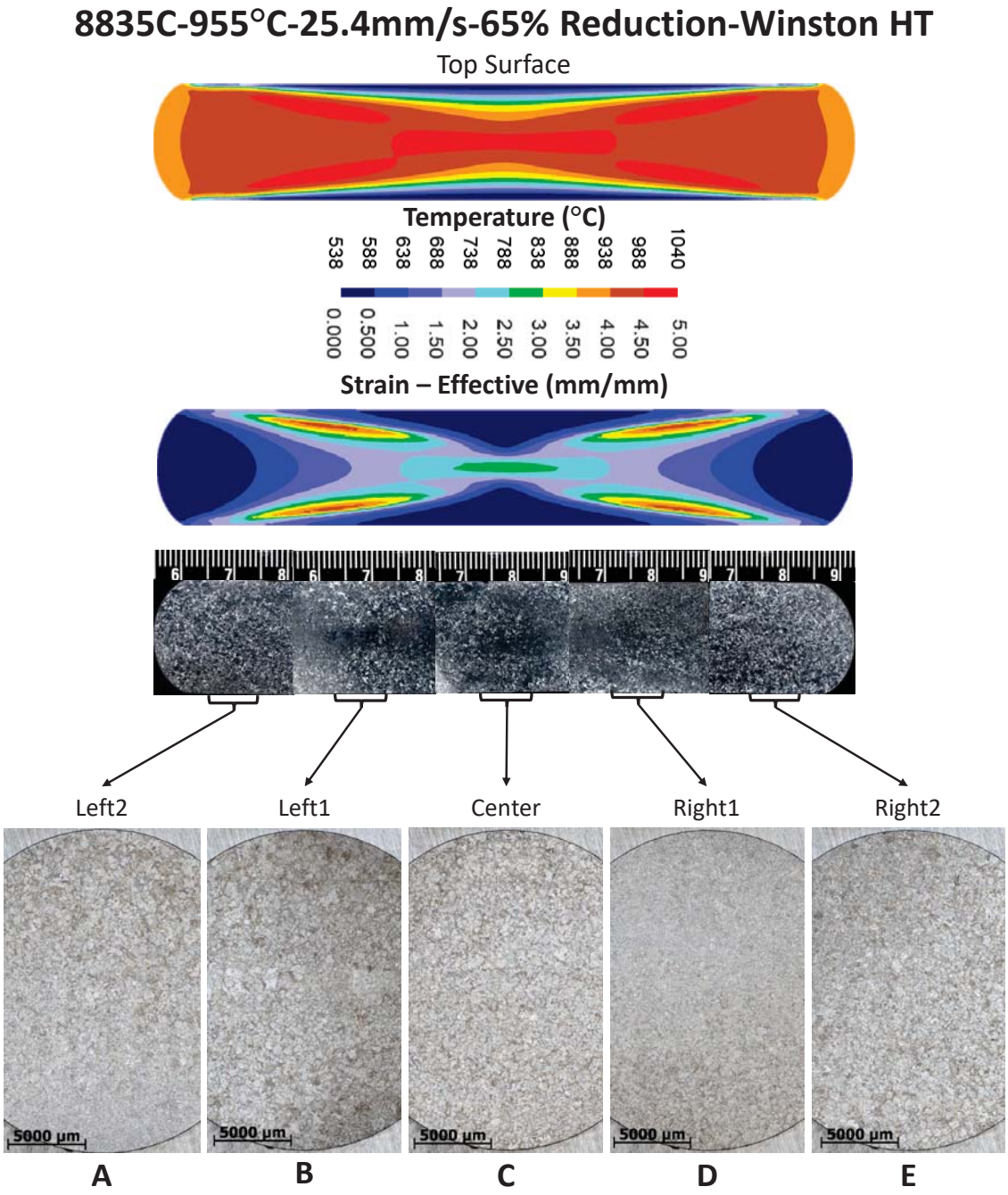

Figure B.1. Sidepressing forging result at 955 °C, 25.4 $\frac{\text{mm}}{\text{s}}$, 65% reduction in height,and Winston heat treatment. The macro scale image provides comparison between the predicted strain and temperature contour images. Each region of interest is labeled for closer grain size evaluation. This specimen appears to be developing coarse grains in the center and on the left and right edges with lobes of smaller grains in between.

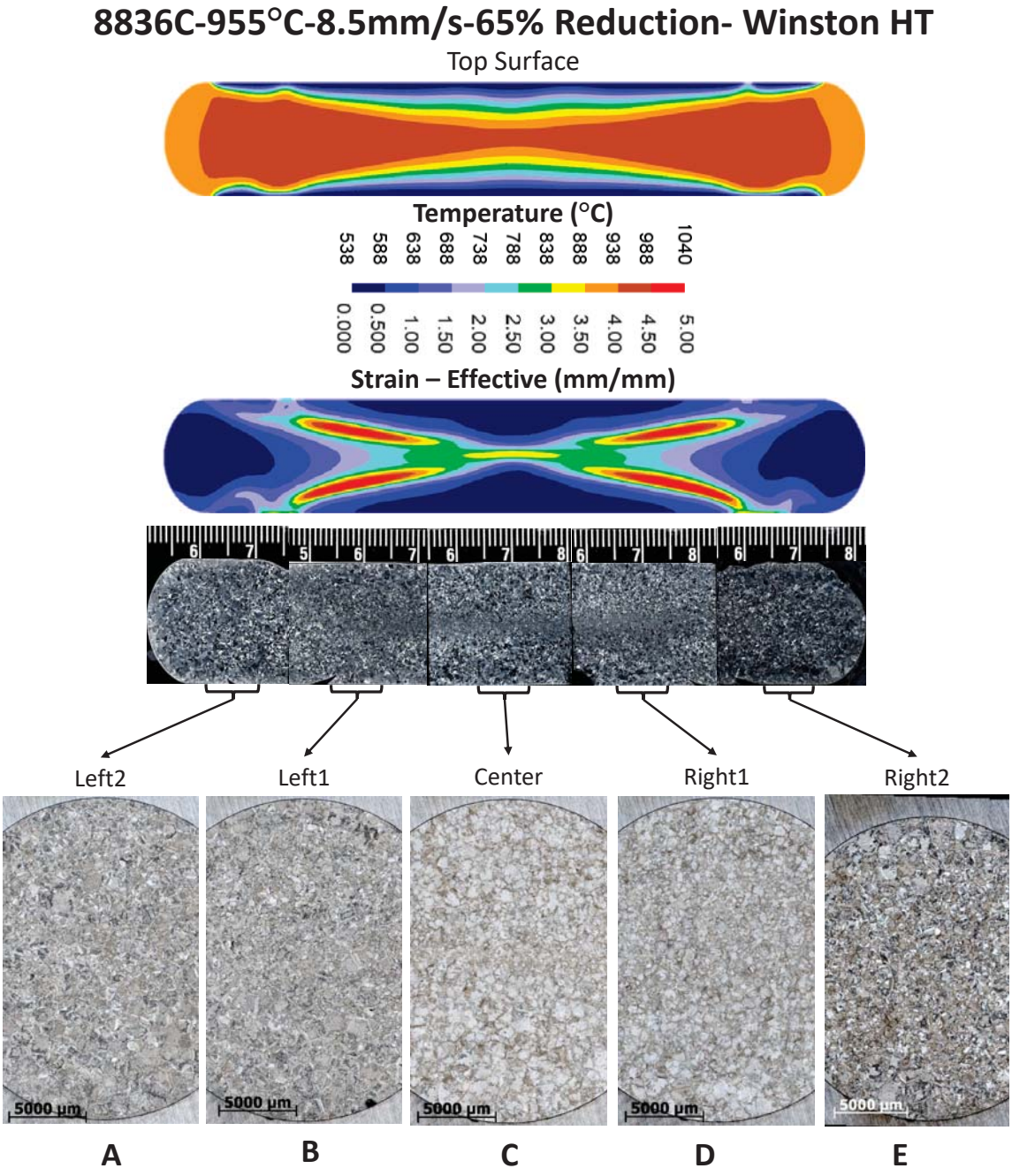

Figure B.2. Sidepressing forging result at 955 °C, 8.5 $\frac{\text{mm}}{\text{s}}$, 65% reduction in height,and Winston heat treatment. The macro scale image provides comparison between the predicted strain and temperature contour images. Each region of interest is labeled for closer grain size evaluation. This specimen appears to have a uniform grain size distribution.

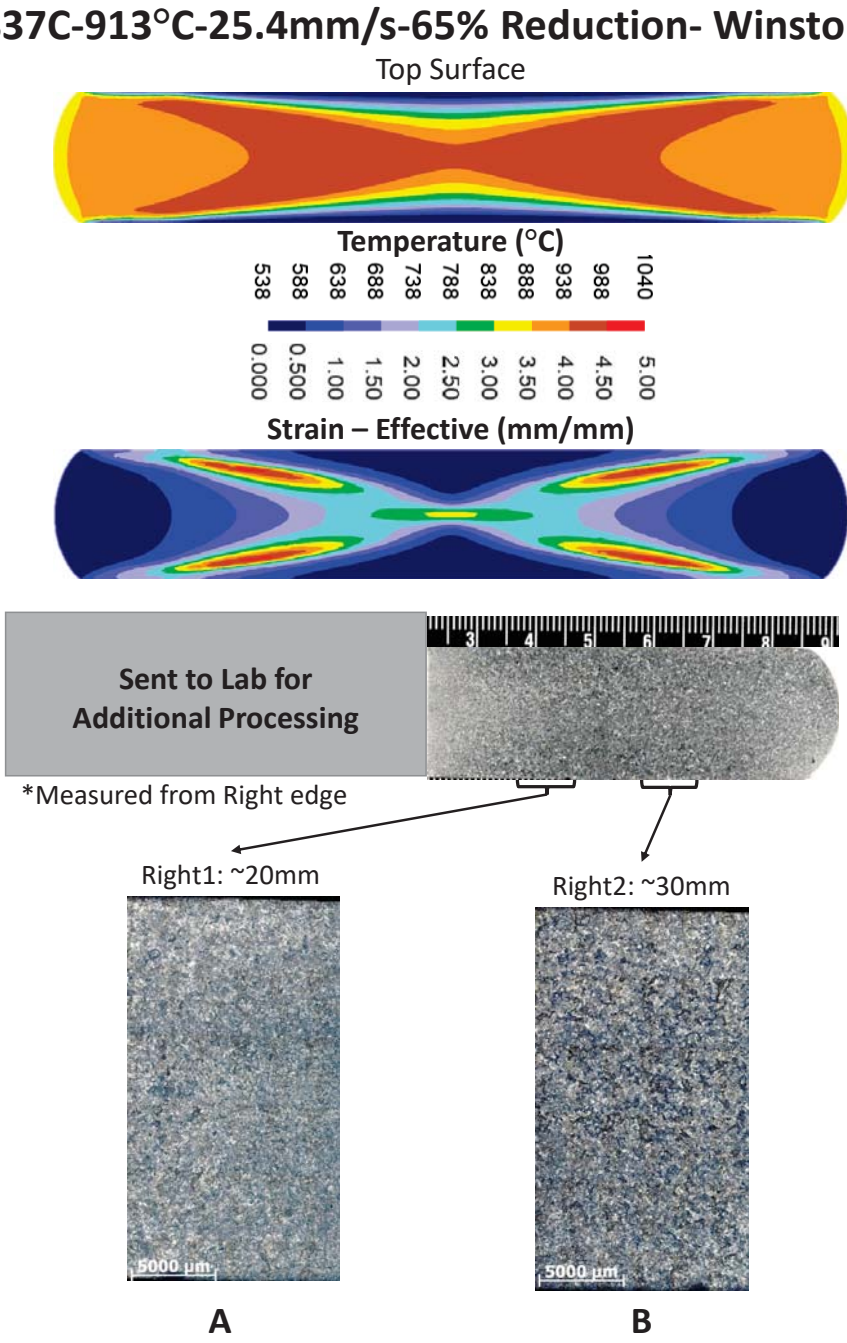

Figure B.3. Sidepressing forging result at 913 °C, 25.4 $\frac{\text{mm}}{\text{s}}$, 65% reduction in height,and Winston heat treatment. The macro scale image provides comparison between the predicted strain and temperature contour images. Each region of interest is labeled for closer grain size evaluation. This specimen appears to have a uniform grain size distribution.

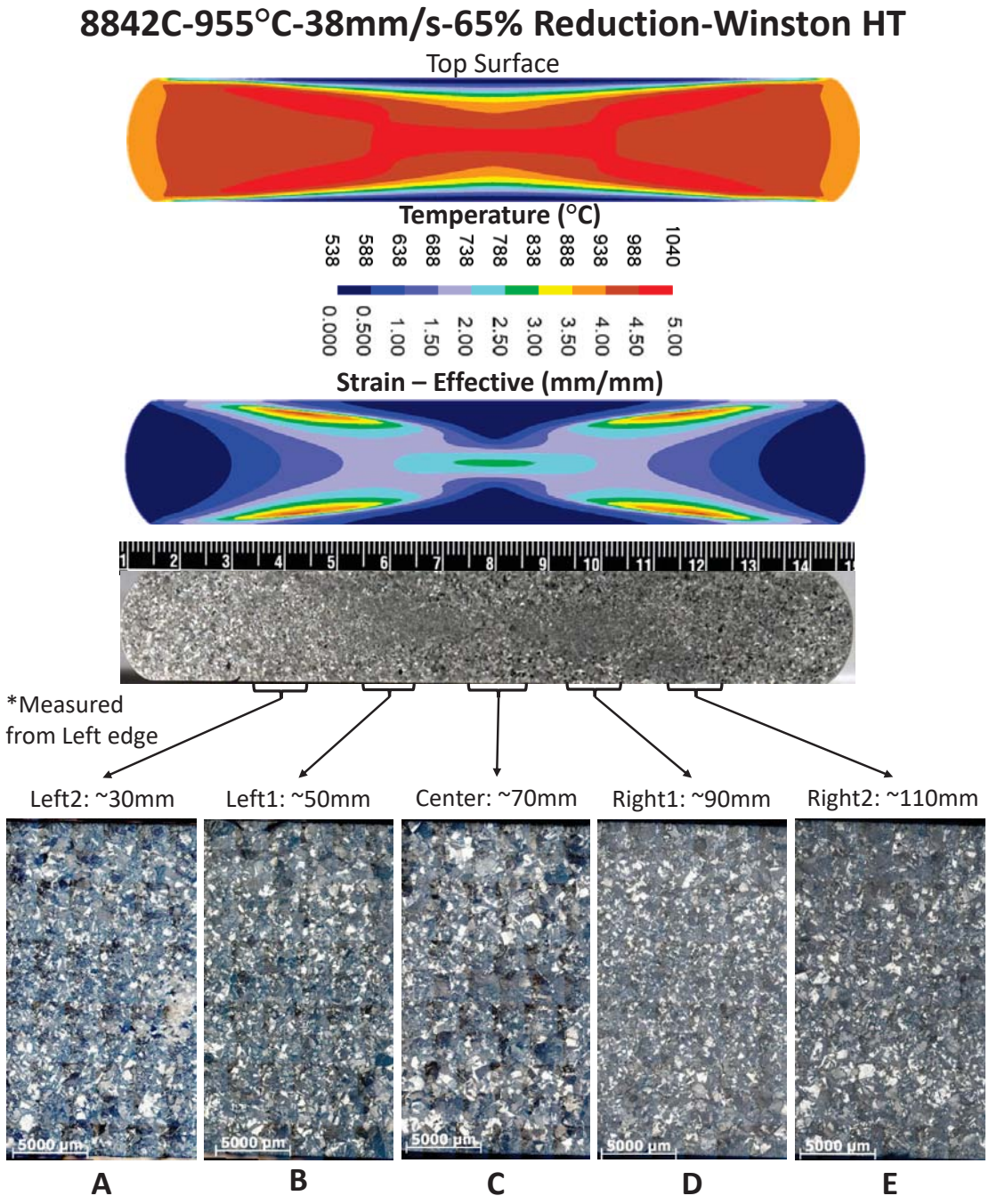

Figure B.4. Sidepressing forging result at 955 °C, 38 $\frac{\text{mm}}{\text{s}}$, 65% reduction in height,and Winston heat treatment. The macro scale image provides comparison between the predicted strain and temperature contour images. Each region of interest is labeled for closer grain size evaluation. This specimen developed notable coarse grains in the center and on the left and right edges with lobes of smaller grains between.

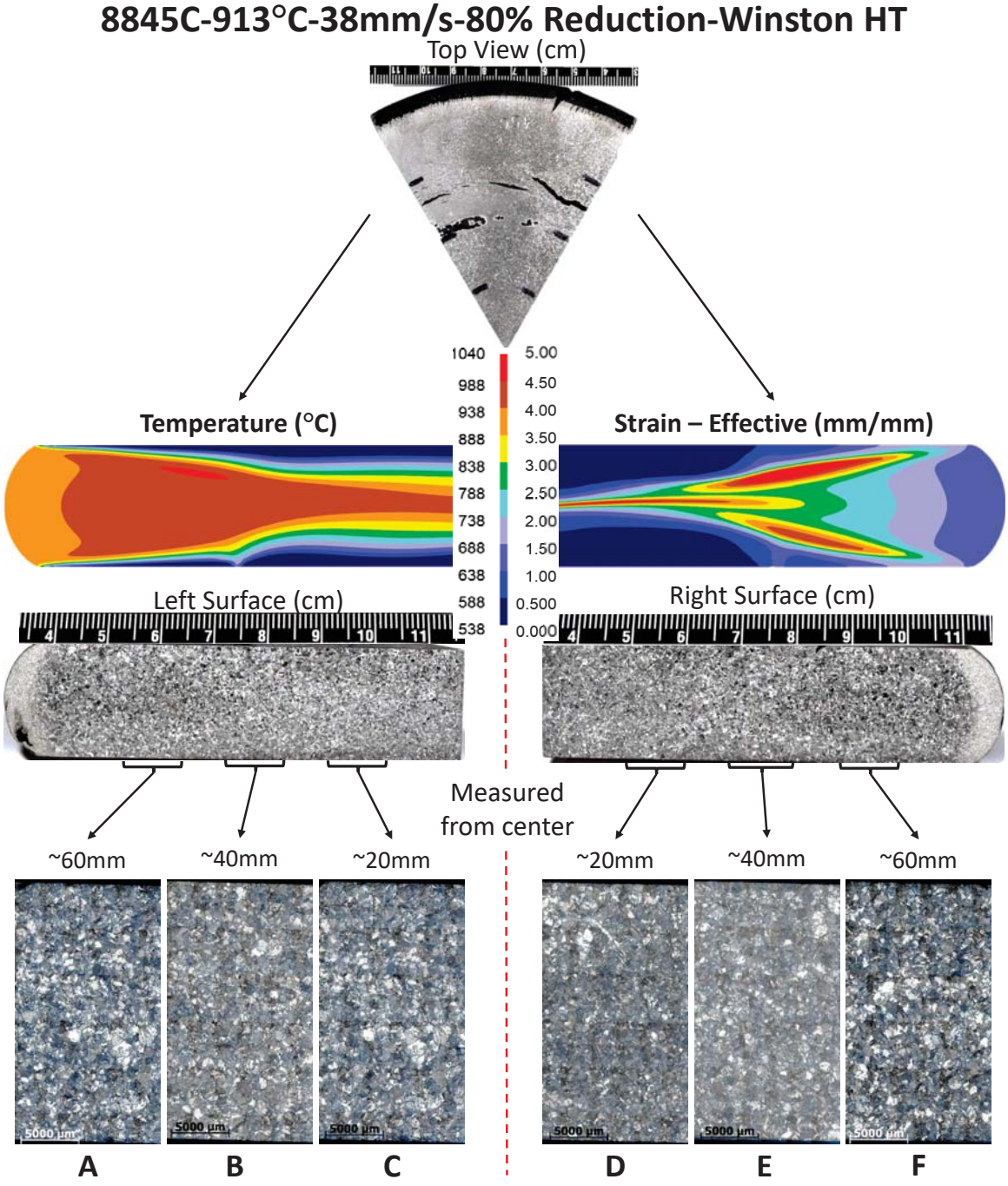

Figure B.5. Upsetting forging result at 913 °C initial furnace temperature, 38 $\frac{\text{mm}}{\text{s}}$ ram speed, 80% reduction in height,and Winston heat treatment. The macro scale forging images provide comparison between the predicted strain and temperature contour images. Each region of interest is labeled for closer grain size evaluation.

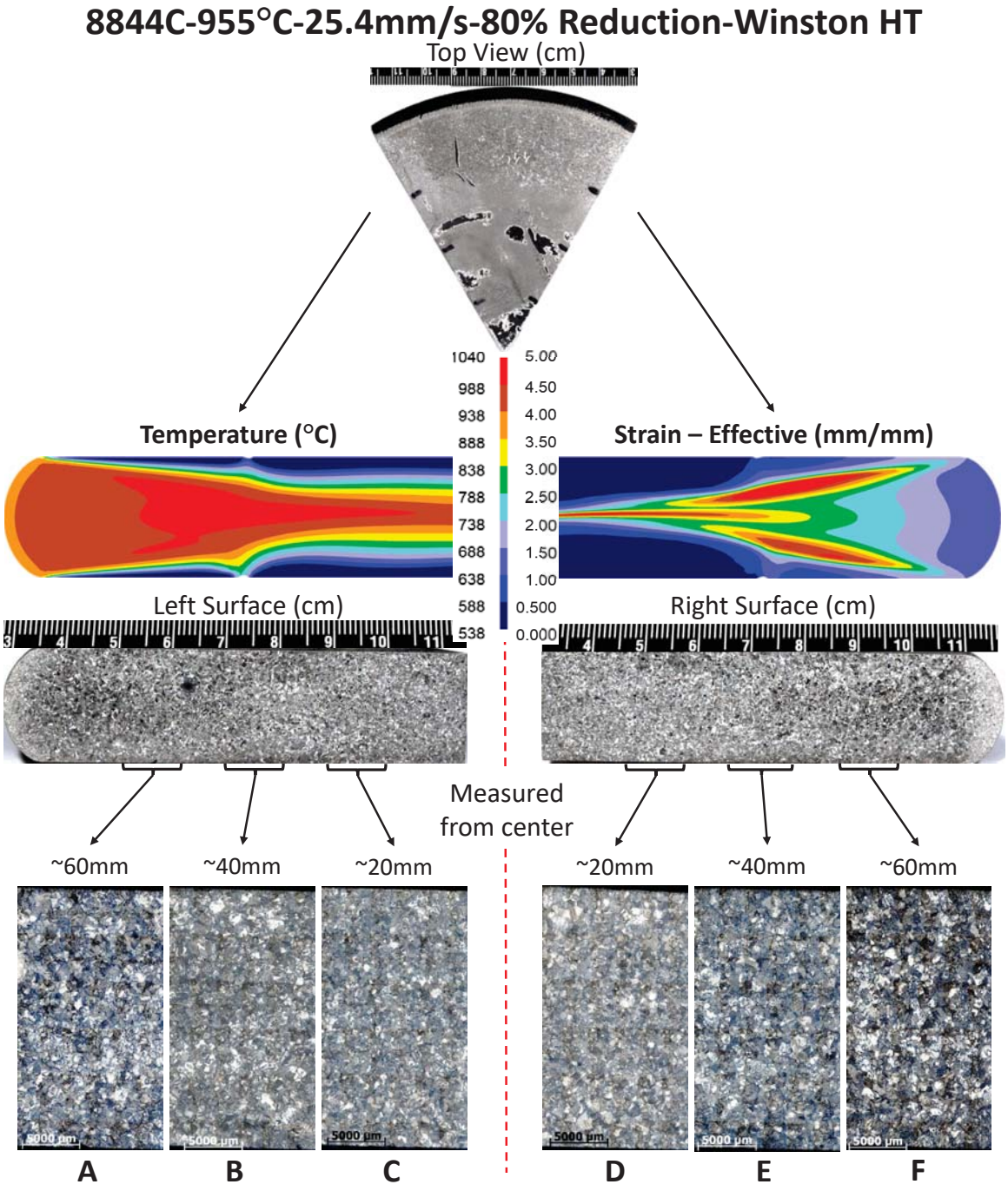

Figure B.6. Upsetting forging result at 955 °C initial furnace temperature, 25.4 $\frac{\text{mm}}{\text{s}}$ ram speed, 80% reduction in height,and Winston heat treatment. The macro scale forging images provide comparison between the predicted strain and temperature contour images. Each region of interest is labeled for closer grain size evaluation.

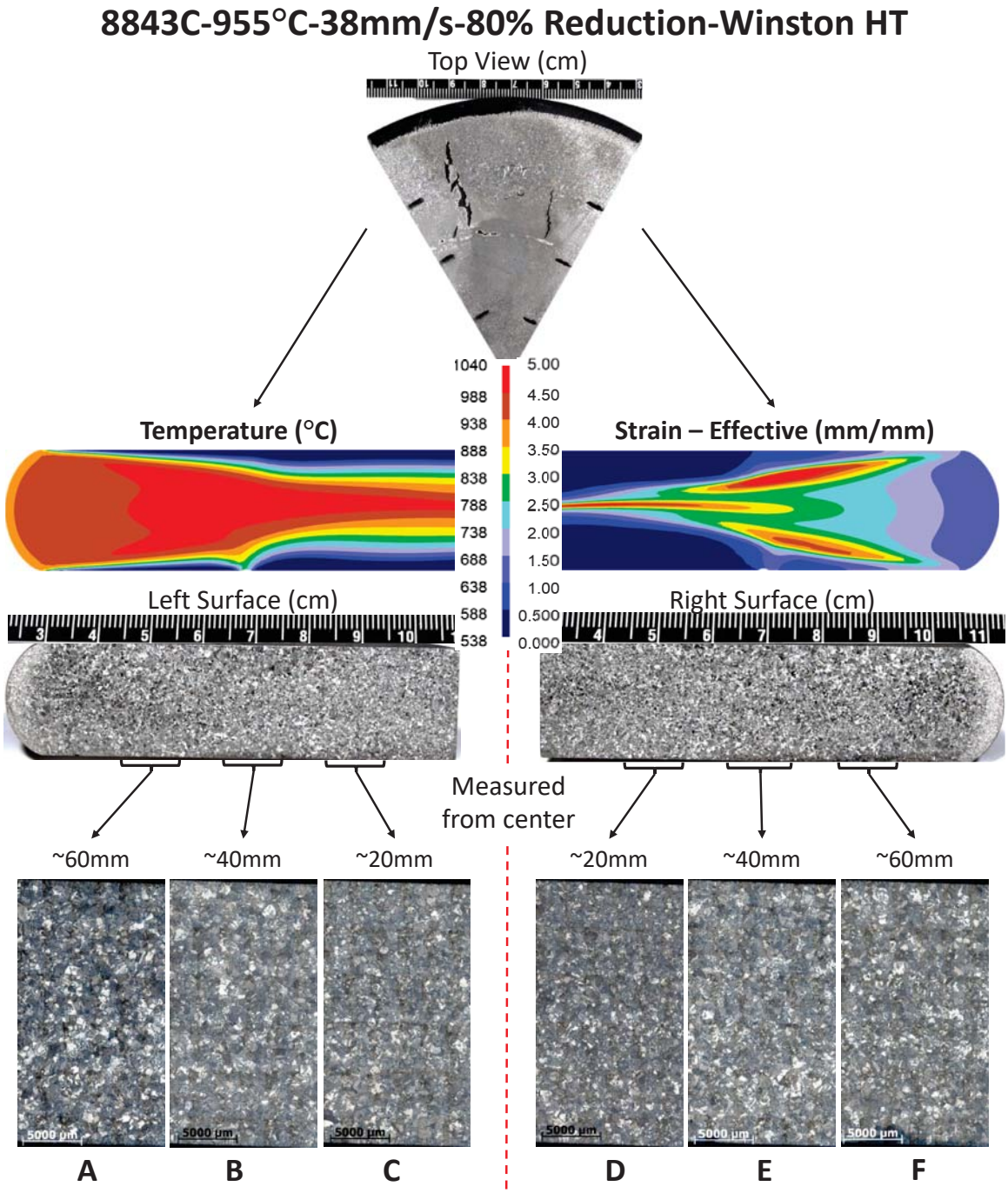

Figure B.7. Upsetting forging result at $955\,^{\circ}\mathrm{C}$ initial furnace temperature, $38\,\frac{\mathrm{mm}}{\mathrm{s}}$ ram speed, 80% reduction in height,and Winston heat treatment. The macro scale forging images provide comparison between the predicted strain and temperature contour images. Each region of interest is labeled for closer grain size evaluation.

Bibliography

[1] G. Lutjering and J. C. Williams, *Titanium*, 2nd ed., B. Derby, Ed. Heidelberg: Springer-Verlag, 2007.

[2] M. Kukuryk, "Analysis of deformation and microstructural evolution in the hot forging of the Ti-6Al-4V alloy," *Archives of Metallurgy and Materials*, vol. 60, no. 2A, pp. 597–604, 2015.

[3] P. K. Chaudbury and D. Zhao, "Atlas of Formability: Ti-6Al-4V ELI," National Center for Excellence in Metalworking Technology, Johnstown, Tech. Rep., 1992.

[4] P. M. Souza *et al.*, "Constitutive analysis of hot deformation behavior of a Ti6Al4V alloy using physical based model," *Materials Science and Engineering A*, vol. 648, pp. 265–273, 2015. [Online]. Available: http://dx.doi.org/10.1016/j.msea.2015.09.055

[5] S. L. Semiatin and D. U. Furrer, "Modeling of Microstructure Evolution During the Thermomechanical Processing of Titanium Alloys (Preprint)," *Processing*, vol. 22, no. July, p. 73, 2008.

[6] Z. X. Zhang *et al.*, "Achieving grain refinement and enhanced mechanical properties in Ti-6Al-4V alloy produced by multidirectional isothermal forging," *Materials Science and Engineering A*, vol. 692, no. March, pp. 127–138, 2017.

[7] C. Leyens and M. Peters, *Titanium an Titanium Alloys*, 2003.

[8] R. Pederson, "Microstructure and Phase Transformation of Ti-6Al-4V," pp. 27–30, 2002.

[9] P. Flowers *et al.*, *Chemistry*. OpenStax CNX, 2016. [Online]. Available: http://cnx.org/contents/85abf193-2bd2-4908-8563-90b8a7ac8df6@9.311

[10] Y. Wang, "Fundamentals of Recrystallization in Titanium Thesis," Ph.D. dissertation, 2014.

[11] S. L. Semiatin *et al.*, "Hot workability of titanium and titanium aluminide alloysan overview," *Materials Science and Engineering A243*, pp. 1–24, 1998.

[12] S. L. Semiatin, "Workability in Forging," in *Handbook of Workability and Process Design*, 2nd ed., G. E. Dieter *et al.*, Eds. Materials Park: ASM International, 2003, ch. 13, pp. 187–207.

[13] R. Shean Lee and H. Chang Lin, "Process design based on the deformation mechanism for the non-isothermal forging of Ti6Al4V alloy," *Journal of Materials Processing Technology*, vol. 79, no. 1-3, pp. 224–235, 1998.

[14] N. K. Park *et al.*, "Characterization of deformation stability in hot forging of conventional Ti-6Al-4V using processing maps," in *Journal of Materials Processing Technology*, vol. 130-131, 2002, pp. 540–545.

[15] P. R. D. M. D. o. G. Burte *et al.*, "An Investigation of the Heat Transfer and Friction in Hot Forging of 304 Stainless and Ti-6A1-4V," 1990.

[16] S. Semiatin and J. Jonas, *Formability & Workability of Metals: Plastic Instability & Flow Localization*, H. L. Gegel, Ed., Materials Park, 1984.

[17] L. M. Gammon *et al.*, "Metallography and Microstructures of Titanium and its Alloys," *Materials Park, OH: ASM International, 2004.*, vol. 9, pp. 899–917, 2004.

[18] R. D. Doherty *et al.*, "Current issues in recrystallization: A review," *Materials Science and Engineering A*, vol. 238, no. 2, pp. 219–274, 1997.

[19] J. Burke and D. Turnbull, "Recrystallization and grain growth," *Progress in Metal Physics*, vol. 3, pp. 220–292, 1952. [Online]. Available: http://linkinghub.elsevier.com/retrieve/pii/0502820552900099

[20] G. Grest *et al.*, "Abnormal Grain Growth in Three Dimensions," *Scripta Metallurgica et Materialia*, vol. 24, pp. 661–665, 1990.

[21] S. R. Thompson, "Fatigue Crack Growth-Microstructural Relationship of Ti-6Al-4V," 1989.

[22] Astm Standard, "E112-12:Standard Test Methods for Determining Average Grain Size," *ASTM International*, vol. E112-12, pp. 1–27, 2012.

[23] Y. Prasad and T. Seshacharyulu, "Processing maps for hot working of titanium alloys," *Materials Science and Engineering: A*, vol. 243, no. 1-2, pp. 82–88, 1998. [Online]. Available: http://linkinghub.elsevier.com/retrieve/pii/S092150939700782X

[24] Y. W. Kwon and H. Bang, *The Finite Element Method Using Matlab*, 2nd ed. Boca Raton: CRC Press, 2000.

[25] S. F. T. Corporation, "Design Environment for Forming Start Help System v11.2," Columbus, 2017.

[26] J. Henderson and H. Groot, "Thermophysical Properties of Titanium Alloys," vol. 1581, no. 765, 1993.

[27] H. Carslaw and J. Jaeger, *Conduction of Heat in Solids*, 2nd ed. Oxford: Oxford University Press, 1978.

[28] Scientific Forming Technologies Corportation, "DEFORM Manuals," Columbus, 2017.

[29] TIMET Corporation, "Timetal 6-4," 1998.

[30] S. Luo *et al.*, "Effects of friction model on forging process of Ti-6Al-4V turbine blade considering the influence of sliding velocity," *International Journal of Advanced Manufacturing Technology*, vol. 82, no. 9-12, pp. 1993–2002, 2016.

[31] Y. Zhu *et al.*, "Determination of the friction factor of Ti-6Al-4V titanium alloy in hot forging by means of ring-compression test using FEM," *Tribology International*, vol. 44, no. 12, pp. 2074–2080, 2011. [Online]. Available: http://dx.doi.org/10.1016/j.triboint.2011.07.001

[32] S. Forming *et al.*, "The State of the Art ' in Process Simulation," pp. 1–18, 2017.

[33] "Titanium and Titanium Alloy Bars (Rolled of Forged) and Reforging Stock, Aircraft Quality," p. 48497, 1997. [Online]. Available: https://assist.dla.mil

[34] ASTM, "Standard Test Methods for Determining Average Grain Size Using Semiautomatic and Automatic Image Analysis," *ASTM International*, vol. 97, no. Reapproved, pp. 1–24, 2015.

[35] M. Funk and S. Meister, "Grain Size Line Cut Analysis," 2012. [Online]. Available: https://www.mathworks.com/matlabcentral/fileexchange/35203-grain-and-particle-analysis-with-line-intersection-method?s{_}tid=gn{_}loc{_}drop

[36] P. Lehto, "Point-Sampled Intercept Length Measurement Code," Espoo, 2016. [Online]. Available: https://wiki.aalto.fi/display/GSMUM/Grain+size+measurement+using+Matlab

[37] P. Lehto *et al.*, "Characterisation of local grain size variation of welded structural steel," *Welding in the World*, vol. 60, no. 4, pp. 673–688, 2016. [Online]. Available: http://dx.doi.org/10.1007/s40194-016-0318-8

[38] Lehto, Pauli *et al.*, "Influence of grain size distribution on the Hall-Petch relationship of welded structural steel," *Materials Science and Engineering A*, vol. 592, pp. 28–39, 2014. [Online]. Available: http://dx.doi.org/10.1016/j.msea.2013.10.094

REPORT DOCUMENTATION PAGE

Form Approved
OMB No. 0704–0188

1. REPORT DATE *(DD–MM–YYYY)*	2. REPORT TYPE	3. DATES COVERED *(From — To)*
22-03-2018	Master's Thesis	Sept 2017 — 22 March 2018

4. TITLE AND SUBTITLE

Study of Abnormal Grain Growth in Beta Annealed Ti-6Al-4V Forgings

5a. CONTRACT NUMBER

5b. GRANT NUMBER

5c. PROGRAM ELEMENT NUMBER

6. AUTHOR(S)

Morris, Lee R. , Captain

5d. PROJECT NUMBER

5e. TASK NUMBER

5f. WORK UNIT NUMBER

7. PERFORMING ORGANIZATION NAME(S) AND ADDRESS(ES)

Air Force Institute of Technology
Graduate School of Engineering and Management (AFIT/EN)
2950 Hobson Way
WPAFB OH 45433-7765

8. PERFORMING ORGANIZATION REPORT NUMBER

AFIT-ENY-MS-18-M-310

9. SPONSORING / MONITORING AGENCY NAME(S) AND ADDRESS(ES)

AFRL/RX
Att: Dr. S. Lee Semiatin
2230 10th Street
WPAFB OH 45433
sheldon.semiatin@us.af.mil

AFRL/RXSA
Att: Dr. Ryan Morrissey
2230 10th Street
WPAFB OH 45433
ryan.morrissey@us.af.mil

10. SPONSOR/MONITOR'S ACRONYM(S)

AFRL/RX

11. SPONSOR/MONITOR'S REPORT NUMBER(S)

12. DISTRIBUTION / AVAILABILITY STATEMENT

DISTRIBUTION STATEMENT A:
APPROVED FOR PUBLIC RELEASE; DISTRIBUTION UNLIMITED.

13. SUPPLEMENTARY NOTES

14. ABSTRACT

Beta annealed Ti-6Al-4V has been used extensively in current aerospace platforms due to properties such as high strength to weight ratio. Recent inspections during aircraft production have revealed regions of excessive grain sizes, resulting in quarantined parts and excessive time spent on root cause analysis and risk mitigation efforts. Uncertainty surrounding these parts has led to increased costs and may cause future aircraft production delays. Part manufacturers have intermittently reported problems with abnormal grain growth in these alloys for years, but to date no supplier has been able to determine the source of this micro-structural phenomenon. Leveraging common FEM software, sidepressing and upsetting forging processes are simulated to predict internal strain and temperature results for use in identifying regions of localizations effecting grain development. Results were used to guide forging tests in an attempt to reproduce abnormal grain growth in the material. Microscopy and image analysis were used to quantify effects of forging parameters on successful development of coarse grains in sidepressing and upsetting forgings. This work seeks to directly support AFRL's Materials and Manufacturing Directorate in determining cause of this ongoing issue.

15. SUBJECT TERMS

Titanium; Ti-6Al-4V; Forging; Finite Element Analysis; Abnormal Grain Growth

16. SECURITY CLASSIFICATION OF:			17. LIMITATION OF ABSTRACT	18. NUMBER OF PAGES	19a. NAME OF RESPONSIBLE PERSON
a. REPORT	b. ABSTRACT	c. THIS PAGE			Maj Ryan O'Hara, AFIT/ENY
U	U	U	UU	192	19b. TELEPHONE NUMBER *(include area code)* (937)255-3636, x4542; ryan.ohara@afit.edu